



# **Working with MetaCORE<sup>®</sup>**

A Design Guide

**Contributors:**

Shawn Aalto, Emily Brann, Art Evans, Ph.D., Cara Moynihan, Aaron Navan, Jesse Silverberg, Ph.D., Bob Tisdell, Karen Tisdell

**Acknowledgments:**

This work was supported by the NASA Space Technology Mission Directorate (STMD) Small Business Innovation Research Program (SBIR) under contract 80NSSC20C0095 through the NASA Langley Research Center (LaRC). The contributing authors also thank Jacob Putnam for his valuable input throughout all stages of this work.

Version 1.0

November 2022

Multiscale Systems, Inc.  
49 Canterbury St. Suite 500  
Worcester, MA 01610

[multiscalesystems.com](http://multiscalesystems.com)

The information herein is based on technical data Multiscale Systems, Inc. ("Multiscale Systems") believes to be accurate at time of issue. Multiscale Systems reserves the right to update, revise, or modify such information at any time. This data is intended for use by persons with technical skill, and is not a substitute for your own testing of suitability of our products for your particular purpose. Multiscale Systems makes no warranties regarding these materials or information, either express or implied, including without limitation the implied warranties of merchantability and fitness for a particular purpose. Nothing herein is to be taken as a license to operate or a recommendation to infringe on patents.

© 2022 Multiscale Systems, Inc. All rights reserved.

# Contents

- PART 1
- Introduction..... 1**
- 1.1. What is MetaCORE®?..... 2
- 1.2. Geometry matters..... 3
- PART 2
- General information..... 4**
- 2.1. MetaCORE concepts ..... 5
- 2.2. MetaCORE geometry ..... 7
- 2.3. MetaCORE base materials ..... 9
- 2.4. MetaCORE mechanical data ..... 11
- 2.6. MetaCORE in computer models ..... 18
- PART 3
- Practical applications ..... 19**
- 3.1. Composite sandwich panels..... 20
- 3.2. Lightweighting semi-trailers..... 23
- 3.3. Unmanned aerial vehicles..... 25
- 3.4. Battery Boxes ..... 27
- 3.5. Aerial delivery and energy absorbing material..... 29
- PART 4
- Guide for working with MetaCORE ..... 34**
- 4.1. Quick reference fabrication tips ..... 35
- 4.2. Flat surfaces ..... 37
- 4.3. Corners ..... 42
- 4.3. Singly-curved surfaces ..... 48
- 4.4. Compound-curved surfaces..... 56
- PART 5
- Appendices ..... 62**
- Appendix A: A primer on thermoforming ..... 63
- Appendix B: A primer on 3D printing..... 66
- Appendix C: Cellular solids..... 69
- Appendix D: MetaCORE in simulations..... 77
- Appendix E: Sandwich panels ..... 85
- Appendix F: Cylindrical structures ..... 93

PART 1

# Introduction

## 1.1. What is MetaCORE®?

New product development and system integration requires the modern engineer to carefully navigate trade-offs when selecting materials for weight-sensitive applications. Material scientists respond to these challenges by developing advanced materials whose properties exist on fundamentally new performance trade-off curves. These advances shift the boundary of what can be achieved for a wide range of industrial and engineering applications. While the benefits of advanced materials may take time to ripple out, their value is immediately recognizable.

Mechanical metamaterials are still largely a topic of academic research, but these advanced materials are gradually leaving the university lab and taking root in industrial applications. Metamaterials are a class of advanced materials where repeated geometric patterns are embedded in a base material to engineer enhanced performance. This approach to materials engineering opens new routes to develop high-performance properties independent of conventional molecular engineering or chemical compounding. Corrugated and honeycomb geometries are historical precursors of modern mechanical metamaterial design, as both examples rely on periodic structure to reduce weight and maintain stiffness.

One of the historical limiting factors for metamaterial engineering is their manufacturability. Today, the mathematics and physics of paper folding, commonly known as *origami*, is being used to solve this problem. *Origami*-inspired metamaterial design focuses on geometries compatible with common pattern transfer manufacturing methods. Since many stock materials are mass produced as 2D sheets, this approach opens the door to scalable and cost-effective manufacturing.

*Working with MetaCORE®: A Design Guide* is written for the modern engineer interested in working with advanced materials. MetaCORE mechanical metamaterials are optimized for use as a lightweight core material in composite structures (Figure 1). It was specifically designed to overcome the limitations of honeycomb and foam cores in weight-sensitive applications requiring impact absorption, isotropic response, and high shear strength. Customers benefiting from products engineered with MetaCORE reside in a wide variety of markets including transportation, energy, aerospace, and defense. The applications are limited only by the engineer's imagination.

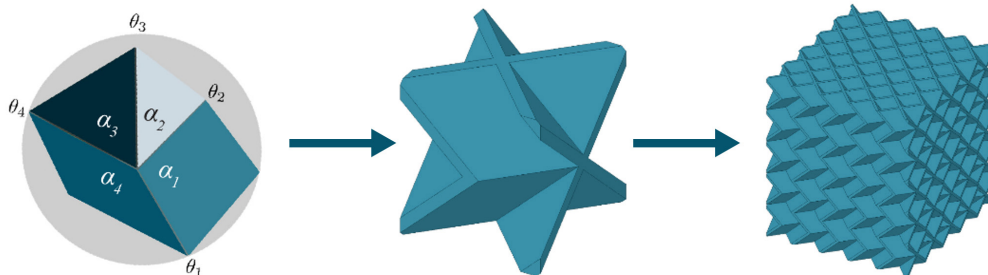


**Figure 1:** MetaCORE was designed using a 3-step process central to all Multiscale Systems' metamaterial technologies.

## 1.2. Geometry matters

When quantifying bulk materials by their stiffness, strength, and density we often think of these metrics as intrinsic to the material's molecular composition. In contrast, mechanical metamaterials like MetaCORE achieve their remarkable properties largely due to their unusual geometry. As a result, the analysis of metamaterial properties is more like the analysis of an I-beam than of an ingot.

For example, consider a standard I-beam (Figure 2). The geometry is simple enough, but small changes have large consequences. The weight per unit length is proportional to the cross-sectional area of the beam:  $BH - 2bh$  whereas the beam stiffness is proportional to these same geometric variables according to:  $BH^3 - 2bh^3$ . Scaling analysis of these equations is approximate but drives the point home. The first equation

scales linearly in beam height while the second scales cubically. The stiffness-to-weight ratio is therefore proportional to  $H^2$ . This quadratic scaling means doubling the beam height quadruples its stiffness-to-weight ratio, while tripling the beam height is nearly a 10-fold improvement.

This I-beam example contains two critical lessons to keep in mind when working with MetaCORE:

1. Conceptually separating material from geometry is how metamaterials are engineered.
2. *Effective* material properties can be engineered by geometry, with increasingly complicated geometries providing access to increasingly remarkable performance.

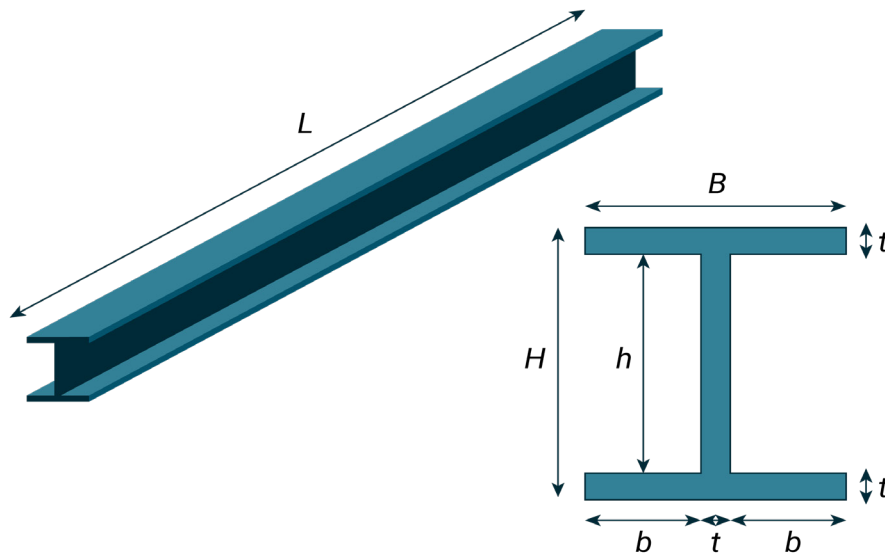


**Figure 2:** A common I-beam is a useful example for explaining why geometry matters. This beam has an envelope defined by height  $H$ , width  $B$ , and length  $L$ . The webbing height  $h$ , and flange width  $b$ , are determined by the thickness  $t$  of the extruded material. To keep the example simple, the wall thickness is assumed everywhere uniform, and corners are  $90^\circ$ .

PART 2

# **General information**

## 2.1. MetaCORE concepts

---

MetaCORE is manufactured by patterning specific geometries into a base material (Figure 3). The effect of the geometry is to promote material properties the base material does not natively exhibit.

During its early stages of development, the MetaCORE geometry was successfully embedded in a variety of polymer, metallic, and natural fiber materials. Metals such as 316L steel, G300 maraging steel, copper, and 6061 aluminum all presented interesting commercial applications. As the technology matured, it became clear that thermoplastics were of special interest. This design guide focuses exclusively on neat and fiber reinforced thermoplastics, which defines both the range of base materials and relevant manufacturing methods.

Manufacturing MetaCORE can be accomplished using a variety of methods, offering important trade-offs in terms of design complexity, lead time, production volume, and cost. Two methods are especially important since they cover the extremes of low-cost commodity mass production, and bespoke on-demand customization. These methods are thermoforming (Appendix A) and 3D printing (Appendix B). Together, they give access to a wide range of material properties and offer a proven track record for MetaCORE products. The appendices on these processes give a deep-dive perspective on how the manufacturing process plays into design considerations.

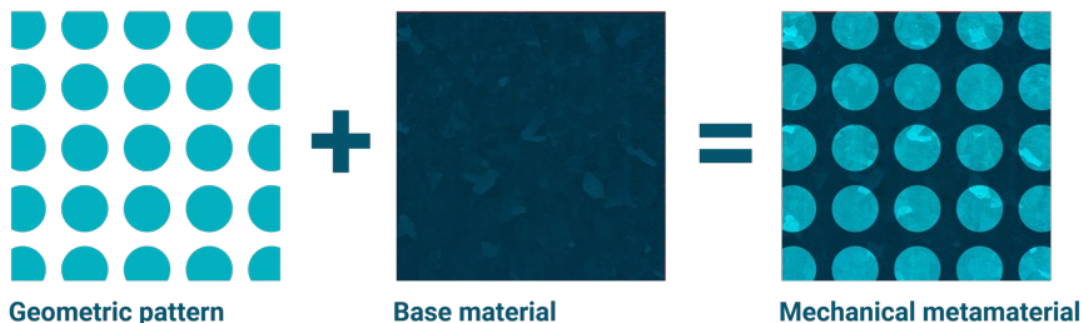


**Figure 3:** Like all mechanical metamaterials, MetaCORE is a combination of a geometric pattern and a base material. In this schematic illustration, manufacturing is the “+” and “=” in the diagram. The geometric pattern conceptually shown here as tessellated circles is typically a complicated 3D geometry. The base material is chosen with the application requirements, end-use, and cost in mind.

For now, it's important to keep in mind:

- Large volume and scaled-up applications require MetaCORE to be produced by thermoforming sheets of thermoplastics. (Figure 4). Working with sheets and integrating them into products requires further processing steps. In Part 4: Guide for working with MetaCORE, numerous tips are offered on how to successfully integrate MetaCORE for maximum effect.
- When producing functional parts with 3D printing, the MetaCORE geometry is integrated directly into the digital design / CAD file. Appendix B addresses specific considerations that arise regarding the anisotropy introduced by most common 3D printing equipment.

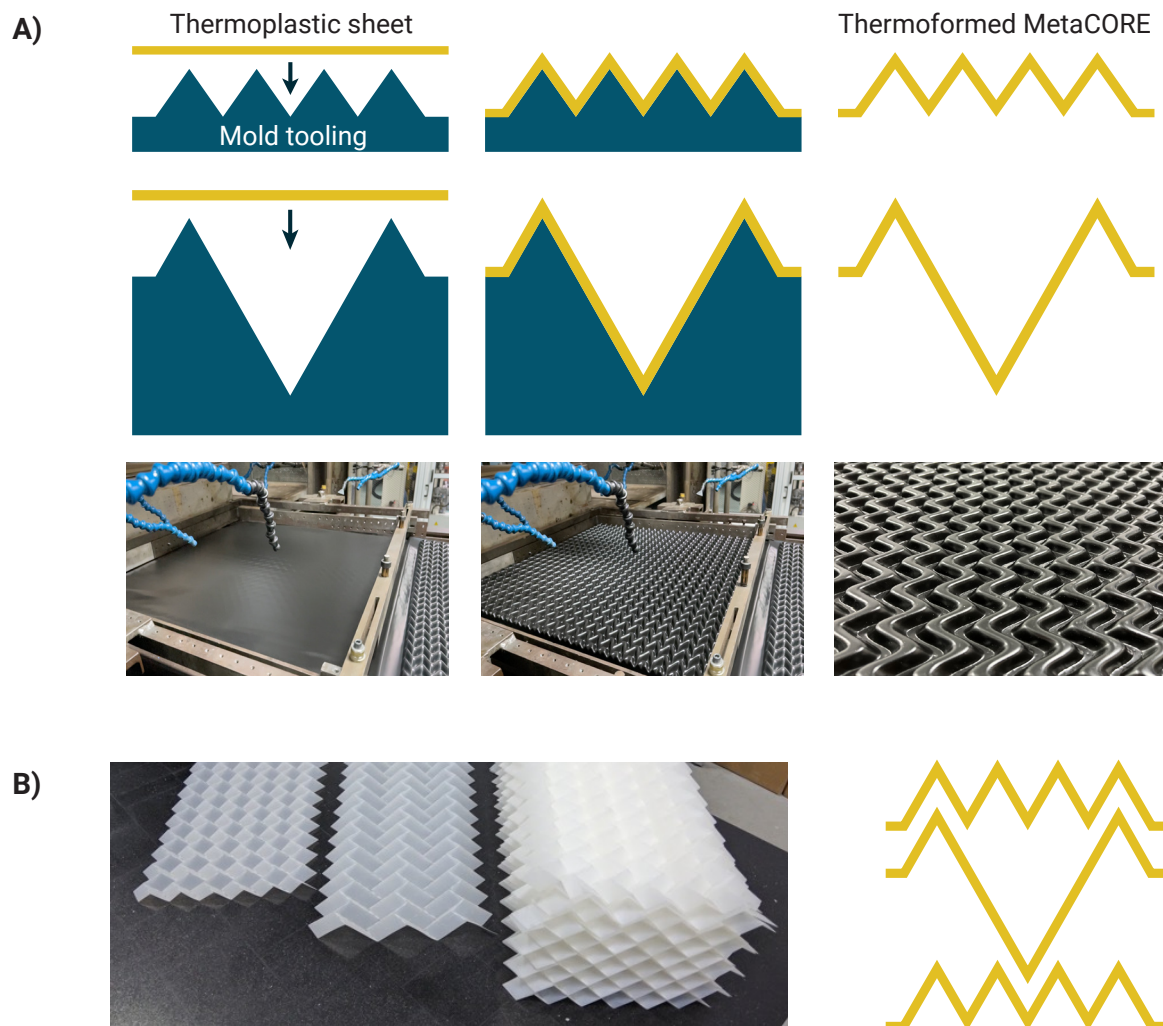


**Figure 4:** Manufacturing MetaCORE with a thermoforming process is an attractive method for scaling up production. (A) The metamaterial geometry is transferred from the mold tool to the thermoplastic, creating a part limited only by the size of the thermoforming machine. (B) Two mold tools produce two distinct, but related, geometries that when stacked together create the full MetaCORE geometry.

## 2.2. MetaCORE geometry

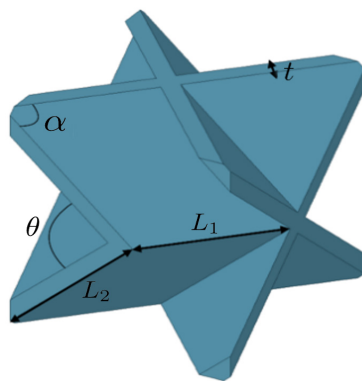
MetaCORE is the trade name for a family of tessellated geometries with a unit cell identifier: [MO]. There are other unit cells covered by the MetaCORE trade name, but MetaCORE [MO] is the most generally useful and easiest to work with.

The [MO] unit cell is characterized by various angles, lengths, and geometric constraint equations. The principal angle variables are the dihedral angle  $\theta$  and the sector angle  $\alpha$  (Figure 5). The principal lengths are  $L_1$ ,  $L_2$ , and a thickness  $t$ . While [MO] has a cuboidal envelope, its dimensions depend on the underlying geometric variables. For very thin walls the unit cell dimensions are given by:

$$X = \frac{2L_1 \cos \alpha}{\sqrt{1 - \sin^2 \alpha \sin^2 \frac{\theta}{2}}}$$

$$Y = 2L_2 \sin \alpha \sin \frac{\theta}{2}$$

$$Z = \frac{2L_1 \sin \alpha \cos \frac{\theta}{2}}{\sqrt{1 - \sin^2 \alpha \sin^2 \frac{\theta}{2}}}$$



With these constraint equations, we can calculate the unit cell volume  $V(\theta, \alpha, L_1, L_2)$  to be:

$$V = \frac{4L_1^2 L_2 \cos \alpha \sin^2 \alpha \sin \theta}{1 - \sin^2 \alpha \sin^2 \frac{\theta}{2}}$$

In typical applications, the dimensions  $X$ ,  $Y$ , and  $Z$  are anywhere between a few millimeters and a few centimeters. Lab tests seeking to determine the limits of mechanical metamaterial design have gone down to the submillimeter scale with edges  $\approx 100 \mu\text{m}$ , as well as up to the macro scale with edges  $\approx 1 \text{ m}$  long. In both extremes, the theoretical underpinnings of metamaterial engineering held, demonstrating the degree to which metamaterial geometry can be treated independently from the base material.

The [MO] design promotes isotropic impact absorption through a collapsible bellows-like mechanical behavior. The facets transmit

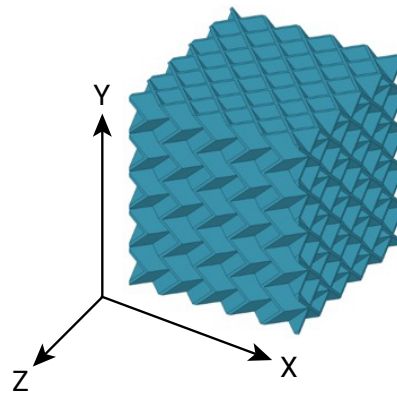


**Figure 5:** The [MO] unit cell and MetaCORE [MO] tessellation in a cuboidal envelope.

shear forces resulting in high shear strength. [MO] also has uniaxial channels creating compartments that can be left open to allow for mass or energy transport. Conversely, sealing the channels results in a structured closed-cell “foam” with the potential to provide thermal insulation.

A key milestone in MetaCORE’s development was mapping the relationship between the [MO] geometry and effective metamaterial properties to identify the highest performing products. When more is known about the application, the variables defining a particular embodiment of [MO] can be determined with multi-objective optimization techniques to maximize MetaCORE’s functional properties and performance. This mathematical parameterization can also be leveraged to customize the geometry to conform to arbitrary curved or compound-curved envelopes without sacrificing performance. These optimizations are ideal for bespoke 3D-printed parts but can always be transferred to a thermoforming mold if the application requires more scale.

### 2.2.1. Negative Poisson’s ratio

Most materials respond by bulging outward when squeezed. The ratio quantifying how much bulging occurs for a given amount of squeezing is called the Poisson’s ratio (Figure 6). Its value is typically a positive number greater than 0 but less than 1.

Because the Poisson’s ratio is a kinematic property, the equations for the [MO] unit cell can be used to calculate MetaCORE’s Poisson’s ratio. The shocking result is that MetaCORE [MO] is a negative Poisson’s ratio material independent of its base material. Negative Poisson’s ratio materials, sometimes called auxetic materials, are extremely uncommon. Nevertheless, they offer high-value opportunities for engineering applications. For example, auxetics

“gather” when impacted resulting in greater impact and fatigue resistance. They also naturally expand in the transverse direction to fill available space when pulled in the longitudinal direction.

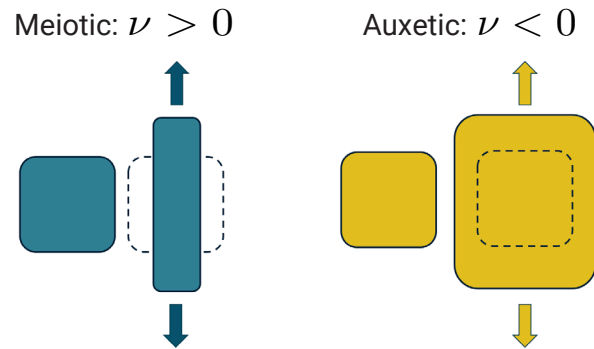


**Figure 6:** Most materials are meiotic and have a positive Poisson’s ratio,  $\nu$ . When pulled one way, they “neck” in the perpendicular direction. Negative Poisson’s ratio materials, sometimes called auxetics, have the opposite behavior. When pulled one way, they expand in the perpendicular direction. Auxetic behavior is uncommon but useful for engineering applications.

### 2.2.2. Stabilized geometry

Another useful aspect of MetaCORE is that its response to loading can be stabilized by fixing the boundary conditions. This phenomenon occurs mostly in MetaCORE sandwich panels where the panel’s compressive properties are substantially increased by bonding MetaCORE to two skins. The adhesive interaction prevents the kinematic deformation of MetaCORE’s geometry, leading to added stiffness and strength independent of base material.

## 2.3. MetaCORE base materials

Choosing the base material for MetaCORE is a down-selection process informed by the application (Figure 7). Thermoplastics offer a variety of choices including overall grade, neat vs. fiber-reinforced, and amorphous vs. semi-crystalline. As a confounding factor, some thermoplastics can be either amorphous or semi-crystalline depending on how they're treated. These polymer phases are distinguished by several key characteristics.

Proven thermoplastics for fabricating MetaCORE are listed in the infographic (Figure 8).

The operating environment is typically the first consideration when choosing the base material. Temperature fluctuations, moisture, corrosive agents, UV exposure, ionizing effects, and vibration are just some of the conditions engineered systems must operate in. When the likely range of conditions are known, they provide a basis for ruling options out. Additional information to keep in mind about base materials includes:

- Higher grades of thermoplastic are generally compatible with higher working temperatures and an increase in overall resilience to environmental stresses.
- Even though composite thermoplastics (thermoplastics with glass or carbon fiber reinforcement) have superior mechanical properties, they are more difficult to recycle or reuse.
- A variety of additives can be introduced to set color, promote adhesive properties, improve flammability ratings, etc.

- Some thermoplastics absorb moisture more readily than others. Depending on the application and operating environment this factor may immediately rule out certain base materials.
- Radio frequency response, electromagnetic shielding, and photonic properties of mechanical metamaterials are related to the base material's dielectric and susceptibility response functions. Electromagnetic metamaterials are a separate class of metamaterials with its own body of technical literature and engineering applications.

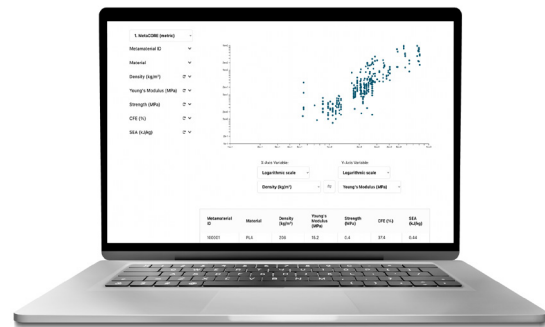


**Figure 7:** What are the properties of MetaCORE for a given base material? Multiscale Systems is constantly working with new materials to answer this question. While specific proven materials are provided in Figure 8, an online interactive catalog gives access to a robust set of up-to-date information.

<https://multiscalesystems.com/research/metamaterial-selector/>

## Proven Thermoplastics for Fabricating MetaCORE

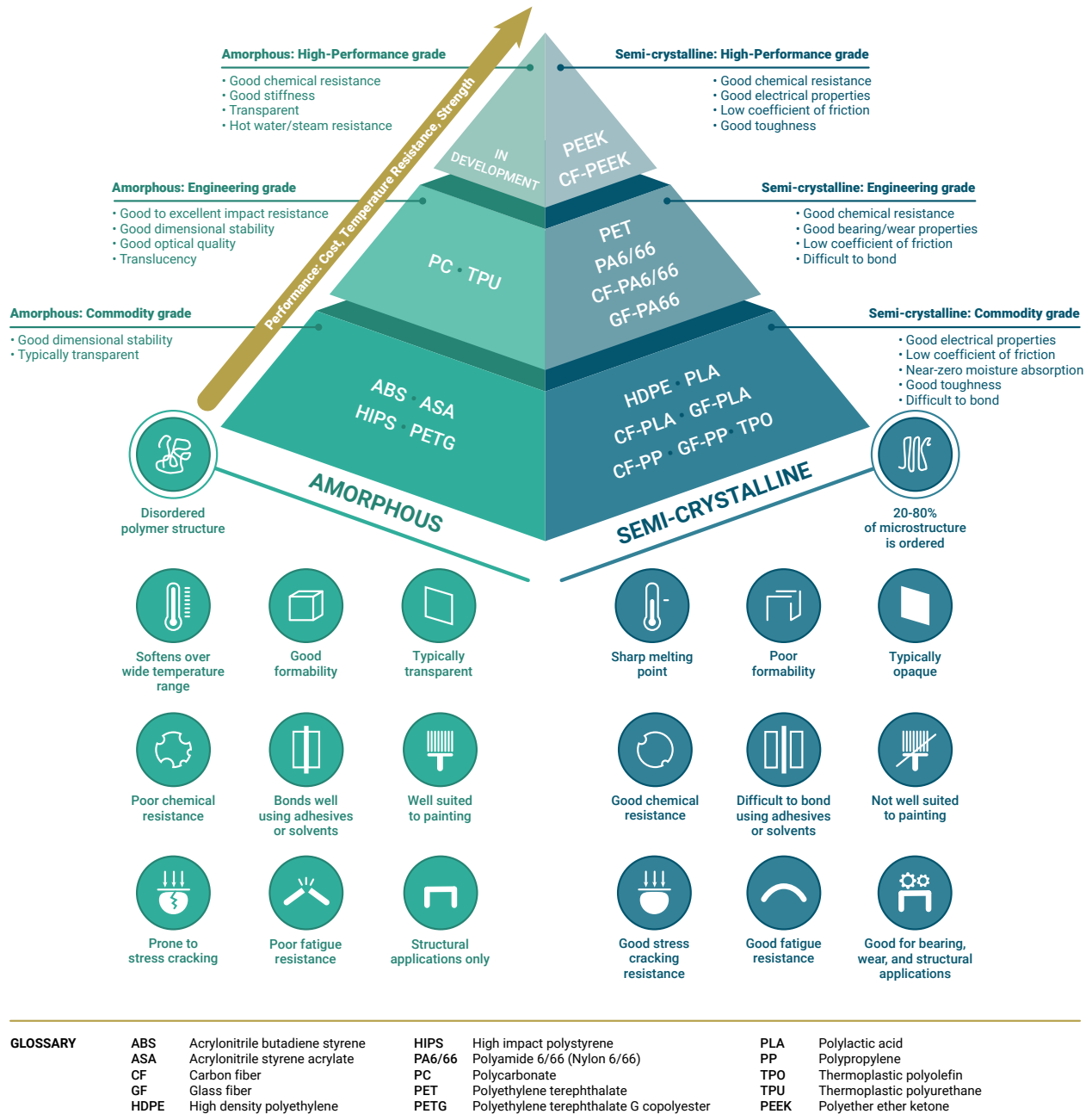


**Figure 8:** There are a wide variety of thermoplastics available as the base material for MetaCORE. This illustration provides insights on picking the right one for a given application.

## 2.4. MetaCORE mechanical data

### 2.4.1. Generic mechanical response

MetaCORE was designed for use as a lightweight core material. The compressive stress-strain response of MetaCORE (Figure 9) is particularly good for applications requiring impact energy absorption. This benefit derives from the plateau stress over a large portion of the compression stroke. This portion of the stress-strain response is an energy-absorbing process with nominal variations in force. Useful things to know about MetaCORE are:

- The ratio of crush strength divided by peak strength is called the crush force efficiency (CFE). Values for CFE are between 0 and 1. A CFE near 1 is desirable for crushable materials because a higher CFE correlates with reduced head and neck injuries.
- The area under the stress-strain curve is proportional to the energy absorbed. Dividing this quantity by MetaCORE's density gives the specific energy absorption (SEA). At strains around 70%, material compactification provides an additional energy absorbing mechanism as well as material hardening.
- MetaCORE is designed to promote isotropic mechanical response. This pro-isotropic characteristic makes MetaCORE more foam-like than honeycomb-like and is explored in greater detail in the appendix. Isotropic impact absorption is desirable since it mitigates uncertainty inherent in a crash scenario and increases the operational envelope for crash protection.

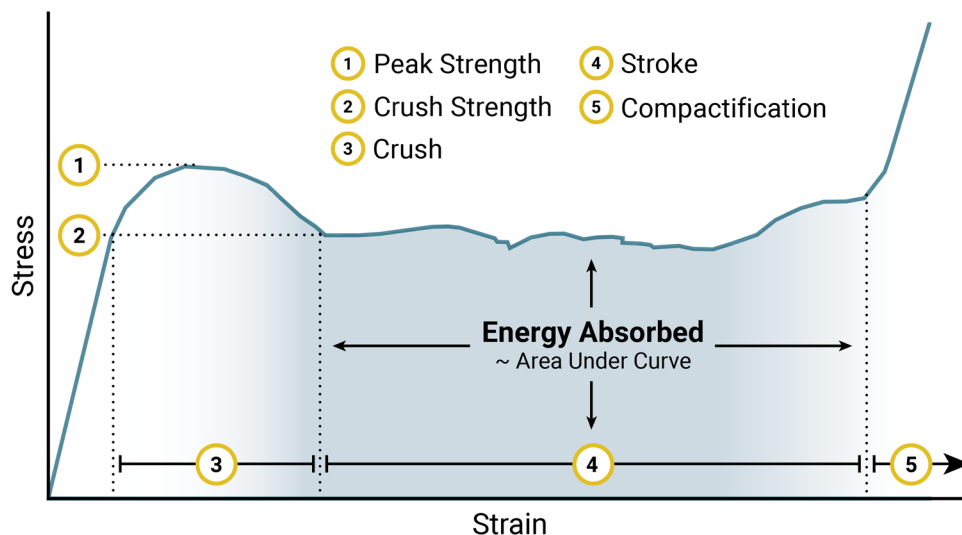


**Figure 9:** An example stress-strain response showing typical MetaCORE mechanical behavior. The shape arises from the geometry and the overall magnitude is related to the base material.

## 2.4.2. Defining density

There are three densities to consider when working with MetaCORE:

Base material density, $\rho_b$	Intrinsic to the molecular composition of the selected base material.
Metamaterial density, $\rho$	Computed as the specimen's mass divided by the volume of its overall envelope.
Effective density, $\rho^* = \rho/\rho_b$	A dimensionless number between 0 and 1 determined by dividing the metamaterial density, $\rho$ by the base material density, $\rho_b$ . This quantity is useful for expressing weight savings by converting the decimal to percentage. Many theoretical predictions of metamaterial properties depend on the effective density.

## 2.4.3. Key metrics of mechanical response

Empirical measurements presented in this document were acquired using the following standard methods.

Property	SI Unit	Method	Notes
Compressive (Young's) modulus, $E$	Pa	ASTM D695-15	Evaluated at 10 mm/min strain rate; typical values are $10^6$ Pa, making MPa a common unit.
Peak strength, $\sigma_p$ Crush strength, $\sigma_c$	Pa	ASTM D695-15	Evaluated at 10 mm/min strain rate.
Crush Force Efficiency, $CFE$	-	ASTM D7336-16	Evaluated at 10 mm/min strain rate.
Specific Energy Absorption, $SEA$	kJ/kg	ASTM D7336-16	Evaluated at 10 mm/min strain rate.
Shear modulus, $G$	Pa	-	Evaluated at 10 mm/min strain rate; Measured by mounting samples in resin plates and shearing load.

## 2.4.4. Material selection with Ashby plots

Part of the challenge when selecting a material for a given application is navigating dozens of different material properties. One way to visualize this information is to construct an Ashby plot, which is essentially a scatter plot comparing properties for different materials. They are especially useful tools for material selection and evaluating trade-offs.

For example, selecting a stiff lightweight material is aided by plotting the Young's modulus on one axis and the density on the other axis (Figure 10). The plot then identifies materials with a high stiffness-to-weight ratio. Ashby plots come in many varieties. Some examples are strength vs density, strength vs relative cost per unit volume, thermal expansion vs thermal conductivity, Young's

modulus vs embodied energy per unit volume. Essentially, any metrics of relevance to the material selection decision can be paired to make an Ashby plot.

Ashby plots often use logarithmic axes to comfortably visualize the vast orders of magnitude in difference material properties can span. A feature of log-log plots is that the slope of a straight line corresponds to the exponent in a scaling relation. For example, Young's modulus  $E$  for foams typically scales as  $\rho^2$ , whereas the Young's modulus for honeycomb loaded in-plane  $n$  scales as  $\rho^3$ . On a modulus vs density Ashby plot with logarithmic axes, foams of various densities will follow a straight line with slope 2, whereas honeycomb with various densities will follow a straight line with slope 3. Appendix C on cellular solids explores the origins of these scaling laws in more detail.

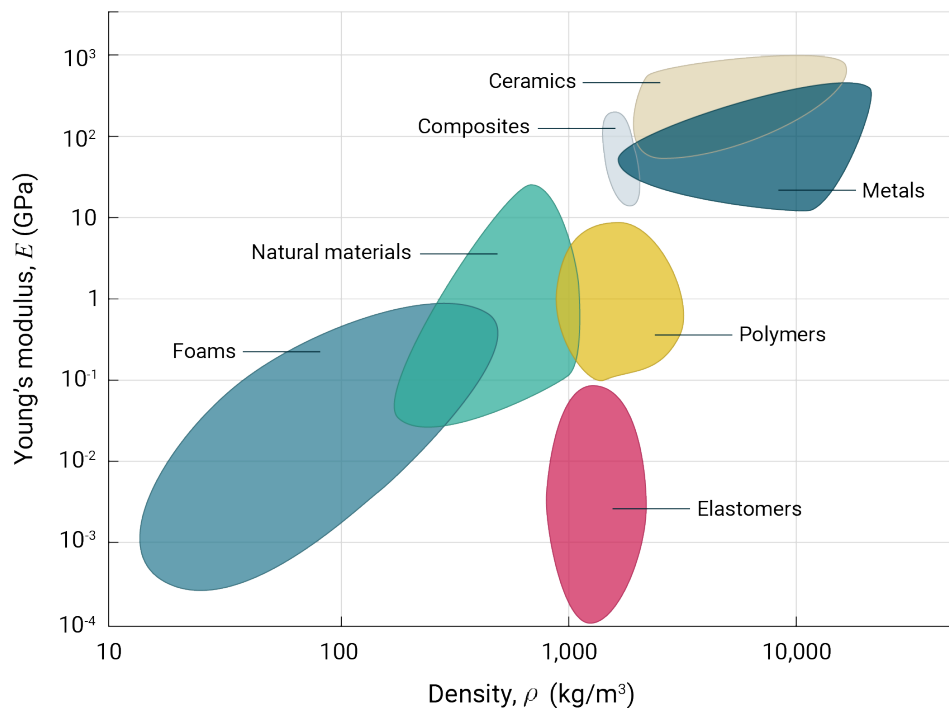


**Figure 10:** Typical example of an Ashby plot showing material properties for different types of materials. Organizing data this way aids in creative problem solving and ultimately leads to informed engineering decisions.

In a short three-year span, over 400 variations of MetaCORE were designed, fabricated, and destructively tested. This data is organized and available online in an [interactive data selector](#). With dynamic filters and real-time updating, this tool provides both scatter plot and tabular visualizations as a modern alternative to traditional data tables and the

limitations of pre-formatted static documents.

The following plots are example charts for MetaCORE:

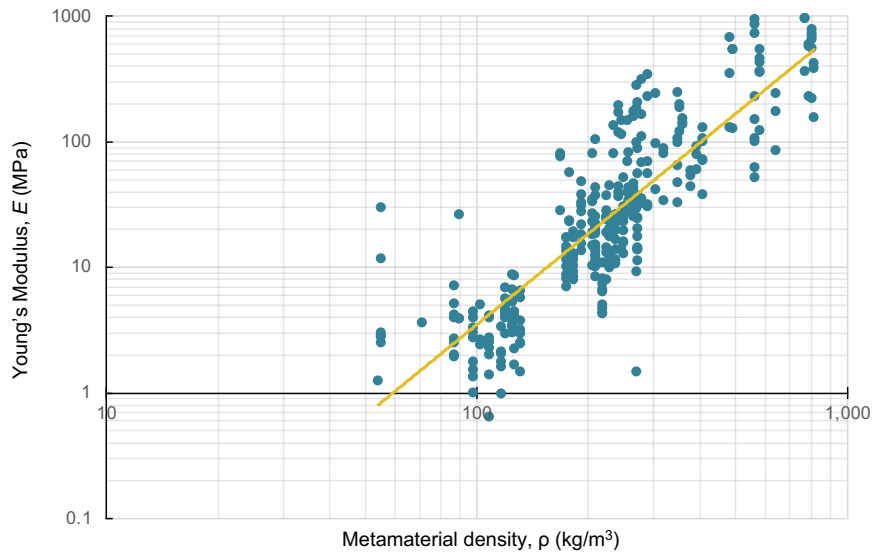


**Figure 11:** Compressive Young's modulus as a function of metamaterial density follows a power law with exponent  $2.46 \pm 0.07$ . Theoretical prediction for this exponent is 2.39, which agrees to within error. This remarkable success derives, in part, from the fact that the modulus of a material is a linear property. Constitutive nonlinearities in the base material and geometry therefore do not contribute to the scaling behavior, making it easier to predict.

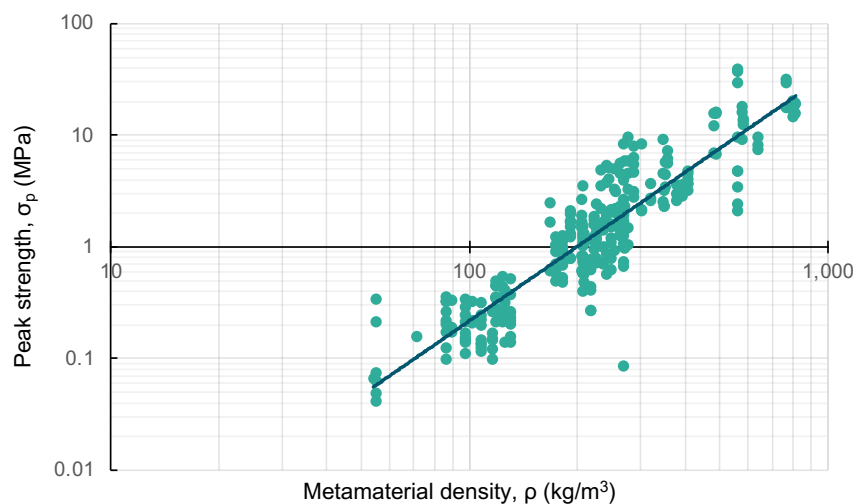


**Figure 12:** Peak strength is a highly non-linear property depending on the constitutive material, the geometry, and the fabrication methods. Empirical results give a density-dependent scaling with exponent around 2.2 to 2.3.

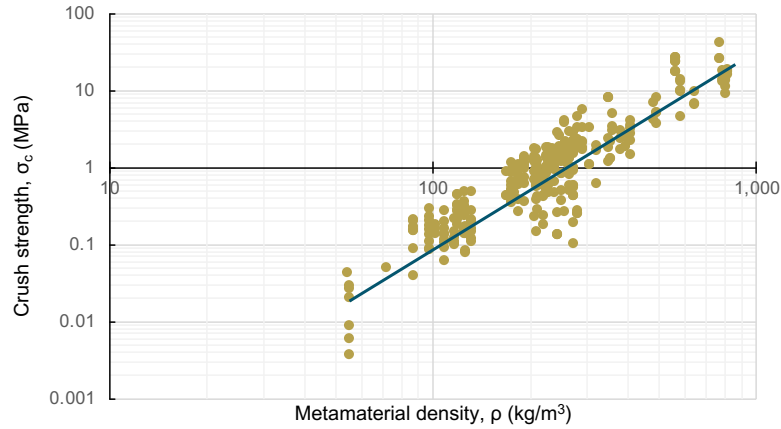


**Figure 13:** Crush strength is another highly non-linear property depending on the constitutive material, the geometry, and the fabrication methods. Empirical results give a density-dependent scaling with exponent around 2.1 to 2.4.

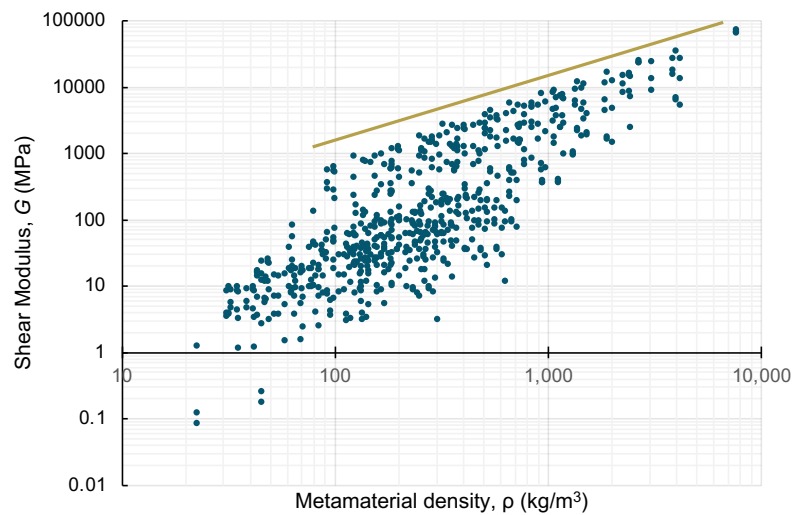


**Figure 14:** Computational results show the MetaCORE shear modulus and density scale with an exponent around 1.1 +/- 0.1.

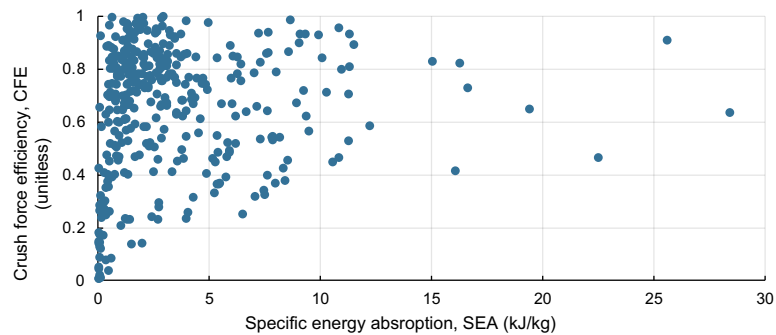


**Figure 15:** Two important metrics for evaluating energy absorbing properties are plotted here. The ideal energy absorber should maximize both CFE and SEA.

### 2.5.1. Thermal conductivity

Thermal conductivity quantifies the flow of energy through a material when two opposite ends are exposed to different temperatures. While MetaCORE's base thermoplastics have isotropic thermal conductivity, its geometry introduces directionally anisotropic effects.

The anisotropy can be engineered for a given application. Examples in the following table are not exhaustive, but indicate ranges for selected base materials and geometries.

Base material	Base material thermal conductivity, $K$ (W/m°C)	Range of thermal conductivity achievable in vacuum (as a % of base value)
Amorphous PET	0.17	0.55% to 97%
HDPE	0.48	0.19% to 34%
PA6 (Nylon-6)	0.24	0.39% to 68%

### 2.5.2. Effects of heating

When working with thermoplastics and thermoplastic composites, there are some key limits to keep in mind at elevated temperatures.

- The first temperature to pay attention to is the heat deflection temperature (HDT). At this temperature, a thermoplastic will deflect a given amount under a specified load. ASTM D648 determines the HDT using a three-point bending load of 0.455 MPa or 1.82 MPa and elevating the temperature by 2 °C/min until a 0.25 mm deflection has occurred. The mechanical properties of MetaCORE behave as one would expect when the HDT is approached. The base material softens and the geometry cannot overcome this reality.
- The second temperature to be aware of is the glass transition temperature,  $T_g$ . While

the HDT is a practical measurement,  $T_g$  is defined by the underlying polymer structure and molecular organization. It serves as an alternative measurement for when the polymer's normally rigid structure becomes soft and non-load bearing.

- The third temperature to be mindful of is the melt temperature,  $T_m$ . This is the temperature when the thermoplastic (or thermoplastic composite) flows like a liquid.

While operating briefly near the HDT will likely cause irreversible deformation to a loaded MetaCORE specimen, the result will be less catastrophic than an equivalent loading at  $T_g$  or  $T_m$ .

Annealing is a heat-treatment process for relaxing thermal stresses and increasing the operational temperature of some thermoplastics. The process involves

elevating a specimen's temperature and slowly cooling it down so the molecular structure can rearrange. Testing with both thermoplastic (Figure 16) and thermoplastic composite (Figure 17) samples shows Young's

modulus and peak strength remains largely unchanged by annealing. The stress-strain curve during the primary crushing stroke of annealed specimens are less smooth than an unannealed sample resulting in lower SEA.



**Figure 16:** Photographs of 3D printed MetaCORE [MO] made from PEEK. The darker amber are as-printed, whereas the lighter beige is the appearance after annealing. Notice the difference in number of discrete pieces in the samples that were crushed to failure. While annealing does not measurably affect the modulus or strength, the annealing causes the post-yield behavior to go from ductile-like to brittle-like.

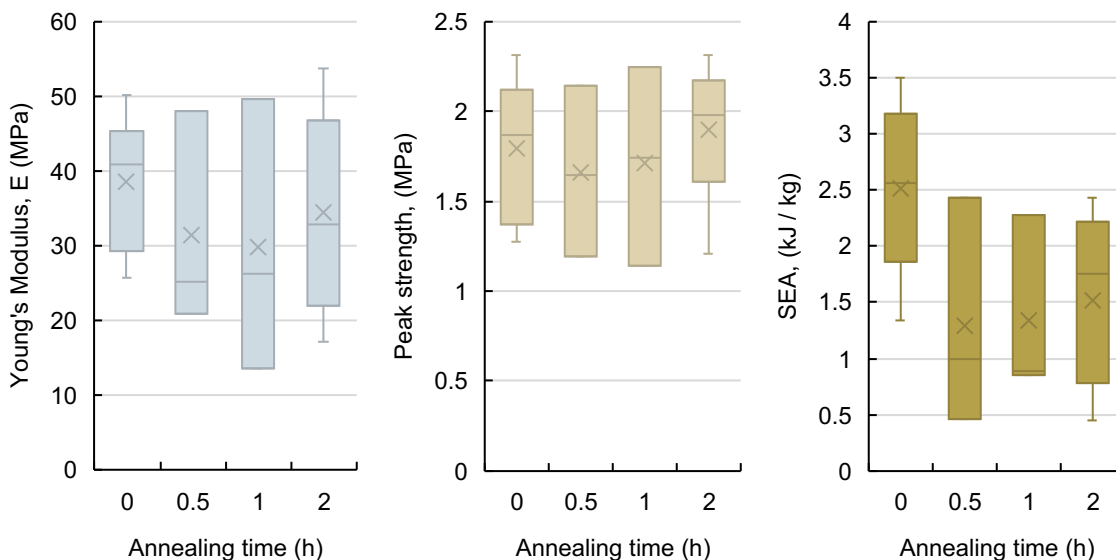


**Figure 17:** Annealing is a process for increasing the operational temperature of some thermoplastics. The effect on Young's modulus and peak strength are nominal, whereas the effect is more pronounced for the SEA. This data is for carbon fiber reinforced PLA, but the effect is observed in neat thermoplastics, too.

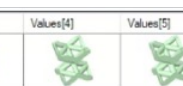
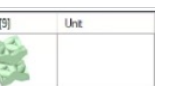
## 2.6. MetaCORE in computer models

Computer modeling, finite element analysis (FEA), and multi-physics simulations are an integral component of modern engineering practice. Increasingly detailed simulations require greater computational resources and creates a higher risk of failing to converge. Fortunately, explicitly reproducing the 3D geometry of MetaCORE is usually unnecessary when building large computer models.

Computational studies examining finite size effects show that 3D volumes of MetaCORE containing more than 4 x 4 x 4 unit cells are

effectively a continuous material. These simulation studies show that beyond a certain limit, the effective material properties are size-independent and explicit meshing becomes unnecessary.

Therefore, simple material cards can be created and assigned to components of a 3D FEA model. These material cards are routinely produced using Ansys Material Designer, resulting in simplified orthotropic material models (Figure 18). More details about the computational and theoretical details can be found in Appendix D.

Name	Values[0]	Values[1]	Values[2]	Values[3]	Values[4]	Values[5]	Values[6]	Values[7]	Values[8]	Values[9]	Unit
											
Parameters											
Volume Fraction	0.05	0.1	0.15	0.2	0.25	0.3	0.35	0.4	0.45	0.5	
Engineering Constants											
E1	5.2937E+08	2.1257E+09	4.6953E+09	8.1971E+09	1.2671E+10	1.8131E+10	2.4702E+10	3.2482E+10	4.1602E+10	5.2089E+10	Pa
E2	5.0688E+08	2.0461E+09	4.5409E+09	7.9617E+09	1.2347E+10	1.7728E+10	2.4228E+10	3.1939E+10	4.1002E+10	5.1438E+10	Pa
E3	3.1327E+08	8.0865E+08	1.5439E+09	2.6001E+09	4.074E+09	6.0009E+09	8.795E+09	1.2383E+10	1.7083E+10	2.3057E+10	Pa
G12	1.1194E+09	2.4864E+09	4.1151E+09	6.0414E+09	8.3033E+09	1.0918E+10	1.3913E+10	1.7301E+10	2.1059E+10	2.5167E+10	Pa
G23	5.2451E+08	1.227E+09	2.129E+09	3.2667E+09	4.6796E+09	6.4064E+09	8.5059E+09	1.1035E+10	1.4048E+10	1.7587E+10	Pa
G31	5.2832E+08	1.237E+09	2.1479E+09	3.2976E+09	4.7259E+09	6.4701E+09	8.5889E+09	1.1138E+10	1.4165E+10	1.7714E+10	Pa
nu12	0.80727	0.65241	0.54733	0.47301	0.41729	0.3738	0.33785	0.30796	0.28298	0.26347	
nu13	0.28017	0.43893	0.51239	0.53776	0.53814	0.52579	0.50806	0.48957	0.4721	0.456	
nu23	0.27306	0.42824	0.49999	0.52459	0.52548	0.51367	0.49705	0.47994	0.46394	0.44973	
Density											
rho	392.5	785	1177.5	1570	1962.5	2355	2747.5	3140	3532.5	3925	kg m <sup>-3</sup>
Thermal Conductivity											
K1	1.4759	3.1621	5.0267	7.0718	9.3105	11.749	14.41	17.308	20.436	23.777	W m <sup>-1</sup> C <sup>-1</sup>
K2	1.4524	3.1164	4.9606	6.9874	9.2092	11.633	14.285	17.177	20.304	23.649	W m <sup>-1</sup> C <sup>-1</sup>
K3	0.61893	1.3944	2.3165	3.3991	4.6636	6.1362	7.8588	9.8682	12.206	14.895	W m <sup>-1</sup> C <sup>-1</sup>
Specific Heat											
cp	434	434	434	434	434	434	434	434	434	434	J kg <sup>-1</sup> C <sup>-1</sup>
Generated Material											
Include	<input checked="" type="checkbox"/>										
Logs											
RVE log											
Solver logs											

**Figure 18:** These material cards homogenize complicated 3D geometry into effective material properties. These material properties can be assigned to an object in an FEA simulation, bypassing the need for complicated metamaterial meshes.

PART 3

# Practical applications

## 3.1. Composite sandwich panels

Composite sandwich structures are in every modern spaceship, airplane, and Formula 1 race car. They're also in cheap DIY furniture, disposable cardboard box padding, and low-budget building construction materials. When extremely high-performance vehicles and inexpensive commodities are using the same engineered structure, you start to wonder why.

The common thread tying these applications together is a requirement for lightweight, rigid structures. I-beams meet this description, but they're better suited for the skeleton of a sheet-and-post style structure. When simpler assembly is required, sandwich panels are an excellent alternative since their surfaces can function as the main load-bearing element.

### Why use a sandwich panel?

A sandwich panel is a class of composite materials fabricated by attaching two thin, stiff skins to a lightweight, thick core. A well-designed sandwich panel will provide the required stiffness and strength at minimal weight and cost. Some simplifying assumptions are necessary, but it's a good rule of thumb to estimate the flexural rigidity of a composite sandwich panel as proportional to:

$$(Young's\ modulus\ of\ the\ skin) \times (thickness\ of\ the\ skin) \times (thickness\ of\ the\ core)^2$$

In contrast, the weight is proportional to:

$$(density\ of\ skin) \times (thickness\ of\ two\ skins) + (density\ of\ core) \times (thickness\ of\ core)$$

	Stiffness	Weight	Stiffness-to-weight ratio
	1	2	0.5
	4	2.2	1.8
	12	2.5	4.8

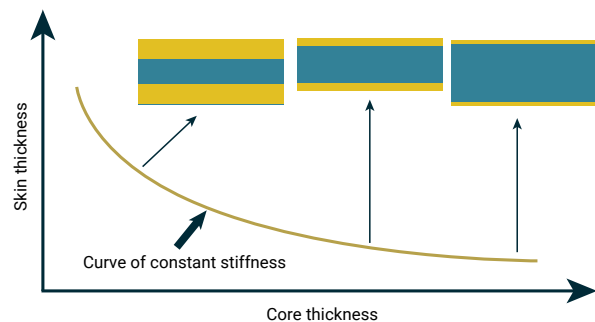


**Figure 19:** A sandwich panel increases its stiffness-to-weight ratio by separating high stiffness skins with a low weight core. The benefit is to retain bending stiffness of the overall panel while keeping its weight low (top). Since this is a composite (the skins and core are different materials), there are many ways to construct a panel with the same stiffness (bottom).

Roughly, these equations mean a sandwich panel can be made substantially stiffer without adding a lot of weight. The scaling of the stiffness-to-weight ratio is the key property that makes sandwich panels useful for so many diverse applications (Figure 19).

### Making a better sandwich panel with MetaCORE

There are a lot of things that can happen when a sandwich panel is pushed to the point of failure. Sometimes the skin will delaminate and wrinkle. Other times the core will crack

along a shear plane. Of course, everything will depend on the materials the panel is fabricated from. Since non-linear material behavior near the point of failure is tricky to model, predicting the strength of a sandwich panel is quite difficult.

One of the few methods for making analytical progress is to build a failure mode map. To show why MetaCORE makes a superior sandwich panel, we'll compare a traditional open-cell foam (PUR, XPS, EPS, etc.) sandwich panel to the geometry of MetaCORE. At the microscale, open-cell foams look like tiny

truss networks. As a result, their stiffness is driven by a "bending-dominated" mechanical response resulting in a Young's modulus proportional to the effective density squared. Instead of acting like a truss network, MetaCORE's cells are better characterized by intersecting polygons. The stiffness for these structures is driven by a "stretching-dominated" mechanical response resulting in a Young's modulus proportional to the effective density (Appendix C). Similar arguments can be made for the strength and the results can be summarized as:

	Open-cell foam (PUR, XPS, EPS, etc.)	MetaCORE (intersecting polygon structure)
Effective Young's modulus of core, $E_c$	$E_c \sim E \left(\frac{\rho_c}{\rho}\right)^2$	$E_c \sim E \left(\frac{\rho_c}{\rho}\right)^{2.4}$
Effective yield strength of core, $\sigma_c$	$\sigma_c \sim \sigma \left(\frac{\rho_c}{\rho}\right)^{3/2}$	$\sigma_c \sim \sigma \left(\frac{\rho_c}{\rho}\right)^2$
Effective shear strength of core, $\tau_c$	$\tau_c \sim \tau \left(\frac{\rho_c}{\rho}\right)^{3/2}$	$\tau_c \sim \tau \left(\frac{\rho_c}{\rho}\right)$

Here,  $E$  is the base material's Young's modulus,  $\rho$  is the density of the base material, and  $\rho_c$  is the density of core material (either foam or MetaCORE).

To build a failure mode map, we'll consider three possible ways a composite panel can

fail in 3-point bending: yielding of the skin, wrinkling of the skin, and shearing of the core. These scenarios assume the skin and core stay perfectly bonded at the point of failure. Calculating the failure loads and summarizing the results in a table gives:

	Open-cell foam (PUR, XPS, EPS, etc. - <i>bending dominated</i> )	MetaCORE (intersecting polygon structure)
Load for yielding of the skin	$\sim 4bc\sigma_s \left(\frac{t}{L}\right)$	$\sim 4bc\sigma_s \left(\frac{t}{L}\right)$
Load for wrinkling of the skin	$\sim 2.28bcE_s^{1/3}E^{2/3} \left(\frac{t}{L}\right) \left(\frac{\rho_c}{\rho}\right)^{4/3}$	$\sim 2.28bcE_s^{1/3}E_z^{2/3} \left(\frac{t}{L}\right) \left(\frac{\rho_c}{\rho}\right)^{8/5}$
Load for shearing of the core	$\sim 2bc\sigma \left(\frac{\rho_c}{\rho}\right)^{3/2}$	$\sim 2bc\sigma \left(\frac{\rho_c}{\rho}\right)$

The variables  $b$ ,  $c$ ,  $t$ , and  $L$  are dimensions of the panel (Figure 20). The modulus  $E_c$  is the Young's modulus of MetaCORE in the panel's normal direction, the modulus  $E_s$  is the Young's modulus of the skin, and the strength  $\sigma_s$  is the yield strength of the skin

### Fundamentally shifting the performance trade-off curve with MetaCORE

The failure loads do more than just estimate the maximum force a sandwich panel can withstand. These equations can be used to draw a map for how panels of various sizes and cores of various densities will perform (Figure 20). The boundaries of the map are determined by setting the various failure modes equal to each other and solving for how  $\rho_c/\rho$  depends on  $t/L$ .

Comparing two sandwich panel designs allows an at-a-glance understanding of the benefits of MetaCORE (Figure 20). The first design is a steel-skinned HDPE foam core common in semi-trailer construction. The second design is an equivalent sandwich panel with HDPE MetaCORE. Notice the smaller region where core shear is the primary culprit for failure. This change is attributable to MetaCORE's large shear strength. The larger design space for failure by skin yielding is preferable, since the skins tend to be the strongest element in the panel. Hence, core shear, which is a structurally catastrophic failure mode, has been overtaken by face wrinkling, which is an aesthetic – not structural – failure.

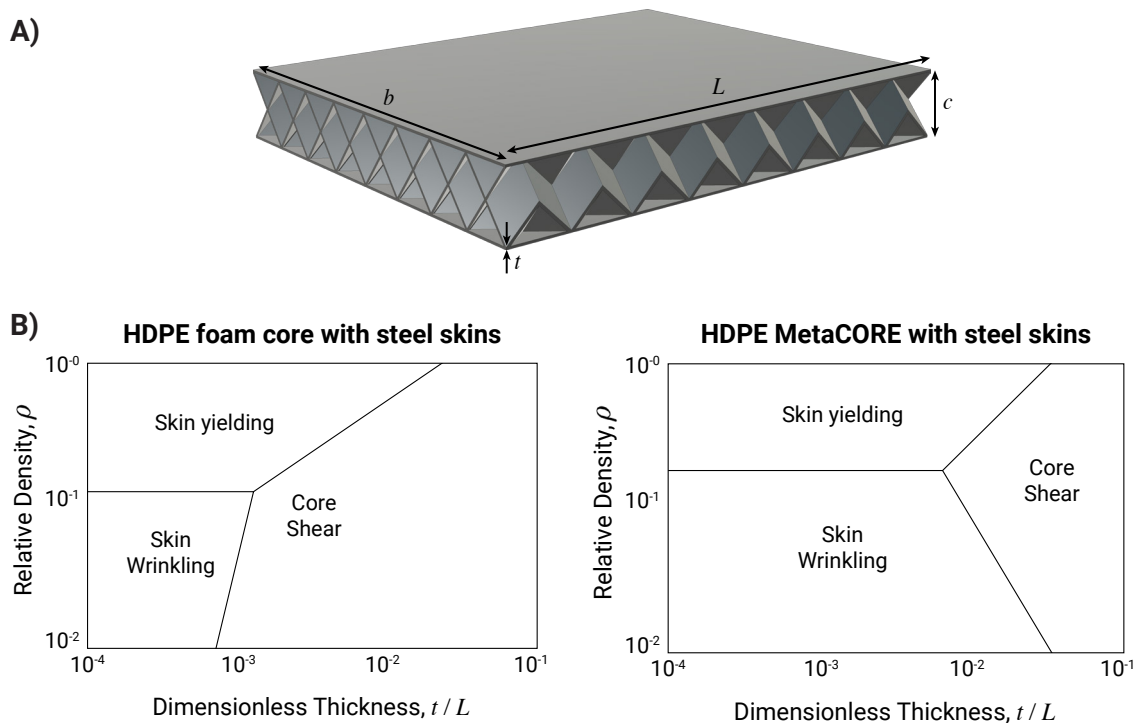


**Figure 20:** Making sandwich panels. (A) Image of a MetaCORE sandwich panel labeling various key dimensions. (B) Failure modes calculated for steel skinned HDPE foam core sandwich panels compared to MetaCORE sandwich panels with the same skins. The weakest part of the panel is generally the core, and thus core shear is the largest contributor of failure. The enhanced mechanical properties of MetaCORE lead to a subdominant core shear failure mode, and a better overall panel design.

## 3.2. Lightweighting semi-trailers

---

Most of the products we interact with on a day-to-day basis were hauled in the back of a semi-trailer. Whether as raw materials, components for integration, or a finished part, over-road hauling is common practice throughout the supply chain due to low costs and substantial flexibility. With the significance of this industry in mind, lightweighting in the transportation sector is critically important for at least two major reasons.

The first reason is that American highways are regulated for a maximum weight capacity. For example, class 8 semi-trailers are not allowed to weigh more than 80,000 pounds at capacity without special permit. Therefore, every pound reduced from the weight of the semi-trailer is another pound available for cargo.

The second reason is that lighter vehicles are more energy efficient. Whether the engine is combustion, electric, or a hybrid of both, reducing the weight of the semi-trailer results in fewer pounds of dead weight. With decarbonization as a front-and-center goal for both public and private sectors, energy efficient commercial transportation is an appealing way forward.

### A tale of two sandwich panels

Modern 53 ft semi-trailer design uses composite sandwich panels consisting of steel skins and HDPE foam. The HDPE foam is 70% to 80% solid thermoplastic, and a target for weight savings with a better core material. The panels are typically installed in 4 ft by 9 ft sections and riveted together to form the trailer's sidewalls. At  $\sim 2$  lb/ft<sup>2</sup> and  $\sim 1,100$  ft<sup>2</sup> per trailer, these panels make up about 10% of the unloaded trailer's weight.

Designing a next-generation sandwich panel involves extensive testing of legacy panels to evaluate their physical attributes and to verify mechanical properties are consistent with established composite sandwich panel theory. Fortunately, the standard composite sandwich panels widely used in semi-trailer design hold few surprises, making it a straight-forward exercise in composite engineering to design a better panel with MetaCORE.

For the ArmorONE™ product launch, HDPE MetaCORE [MO] was integrated with high-strength steel skins for a strong-but-light product (Figure 21). In the most advanced prototypes, nearly 1,200 lb of weight savings on a standard 53' trailer could be achieved (Figure 22). This remarkable weight savings was made possible by the unique scaling laws governing MetaCORE's mechanical properties and how the geometry distributes shear stresses between the panel's two skins.

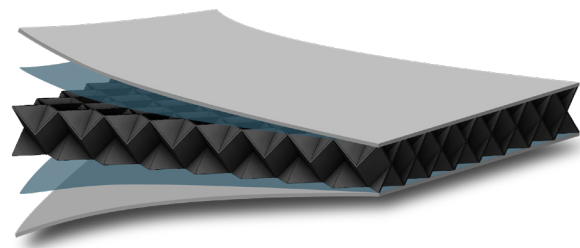


**Figure 21:** ArmorONE panel with MetaCORE core.

### How do you use your weight savings?

Saving 1,200 lb off a semi-trailer leads to meaningful benefits for fleet owner/operators. This freed-up weight can be allocated to new cargo, turned into fuel savings, or simply used to offset added weight from quality-of-life amenities installed in the cab. Though decisions on what to do with weight savings

are made on a case-by-case basis, they rely on the existence of lightweight materials ready to be integrated into semi-trailer design.

Contact representatives at Armory Technologies ([armorytechnologies.com](http://armorytechnologies.com)) to learn more about this MetaCORE-enhanced product and how it can benefit your application.

	Legacy panel	ArmorONE™		
Core	HDPE foam	MC-1000	MC-2000	MC-3000
Panel thickness (in)	0.3	0.35	0.34	0.32
Skin thickness (in)	0.016	0.044	0.036	0.013
Density (lb/ft <sup>2</sup> )	2.37	0.97	1.71	1.37
Weight per panel (lb)	86	35	62	50
Weight savings per panel	0%	59%	28%	42%
Strength	Legacy technology	Comparable to legacy	Stronger than legacy	Strength of steel, weight of aluminum

**Figure 22:** This data table for ArmorONE products gives examples of MetaCORE-enhanced sandwich panels engineered to compete with existing products on the open market.

## 3.3. Unmanned aerial vehicles

---

Projections for the next decade highlight the imminent challenge for equitable access to medicine and medical supplies. U.S. Census Bureau data shows 97% of the country's land mass is rural and home to one in five Americans. Video conferencing and high-speed internet opens the door to telemedicine as a partial solution. When diagnostics, medicines, or other physical components are necessary for a healthy resolution, an all-virtual experience becomes inadequate.

Similar challenges accessing healthcare are faced abroad, especially in developing countries where hospitals and clinics are few and far between. Fortunately, the solutions developed in some of the poorest areas of the world give insights for how to solve the problem for rural America.

Unmanned Aerial Vehicle (UAV) delivery services are already improving lives with lifesaving medicines, vaccines, and blood transfusions in Rwanda and Botswana. Similar UAV technology is the ideal complement to telemedicine that addresses rural America's challenge to equitable medical access. Because medical payloads are often sensitive and fragile, ensuring their safe delivery is a top technical priority for the future of medical UAV delivery services.

### **Challenges for rapid medical UAV delivery in the U.S.**

Whether resupplying a rural clinic with viral test kits or providing emergency insulin to a disaster relief shelter, the challenge is clear. A one-size-fits all approach for rapid medical UAV delivery is not realistic given the vast differences in the built and natural environment. Lightweight solutions for protecting sensitive cargo are needed

whether to prevent damage in a failed delivery or to mitigate impact for parachuted payloads.

Foam core and honeycomb are common lightweight energy absorbing materials with potential use in this application. However, there are several trade-offs to consider. What volume and weight of impact mitigating material is necessary? Will the payload be protected if it lands at an odd angle? Are there cost and supply chain barriers that must be addressed?

### **Comparing MetaCORE, foam, and honeycomb for UAV payload impact protection**

Since the only way to make an omelet is to crack some eggs, we performed a series of destructive drop tests to compare foam, honeycomb, and MetaCORE for the UAV delivery application.

To overcome the variability and uncertainty in how medical payloads are being prepared for delivery, we simplified the setup by casting 44 identical polyurethane shells to use as UAV bodies. The volume of each shell was  $980 \text{ cm}^3$  ( $\approx 60 \text{ in}^3$ ), and it was loaded with a 3-axis accelerometer protected from impact by either foam, honeycomb, or MetaCORE (Figure 23). In each case, the accelerometer was encased by  $240 \text{ cm}^3$  ( $\approx 14 \text{ in}^3$ ) of the impact absorbing material. Once loaded and sealed shut, the model UAV body was mounted in a drop tower and allowed to crash onto a test platen. The crash resulted in up to 75 J of energy being directed into the UAV body, which is equivalent to a 5 kg ( $\approx 11 \text{ lb}$ ) plate dropped from a height of 1.5 m ( $\approx 5 \text{ ft}$ ).

Performance of the different impact

absorbing materials was evaluated by two key metrics. The first is the percentage of kinetic energy absorbed on impact, and the second is the peak acceleration.

The summary graphs show an average over multiple tests for each impact absorbing material (see graphs below). Overall, foam core and honeycomb perform similarly, absorbing about 94% of the impact energy but delivered high peak accelerations of up to 500 g's of force. In contrast, MetaCORE absorbs 87% of the impact energy, but reduced impact g-force by 33%. In passenger vehicles, high g-forces are associated with head and neck injuries, crushed bones, and, in extreme cases, death. MetaCORE's ability to drastically reduce g-force impact while still absorbing vast majority of energy increases the chances of payload survivability.

These performance metrics suggest medical supplies packaged in MetaCORE and delivered by UAVs are likely to have fewer failures than other commonly used alternatives. As a lightweight and low-cost impact absorbing material, MetaCORE is ready to be integrated with sensitive payloads and support more equitable access to lifesaving medical care.

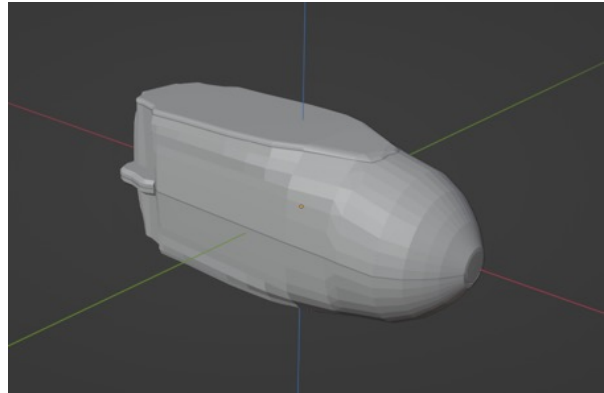
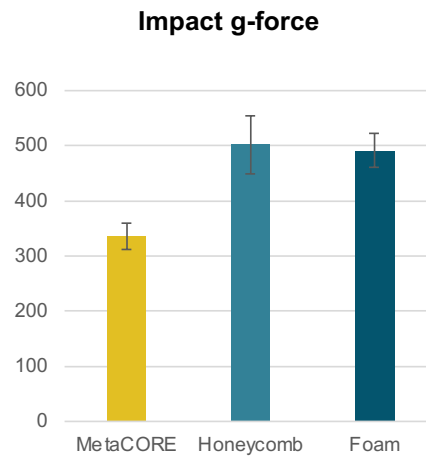
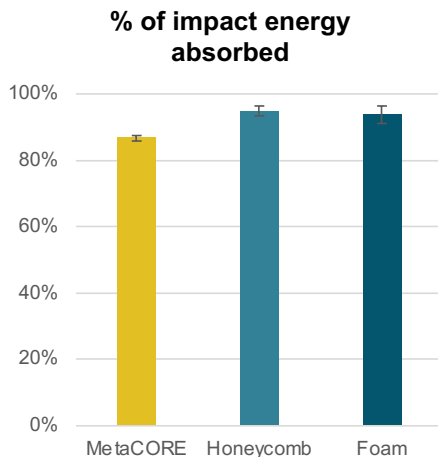


**Figure 23:** Given the fractured and nascent market for UAV medical delivery, we designed a generic UAV shell to act as a surrogate for existing systems. A render of the shell is shown in the top image, and 3 cast replicates are shown in the photograph below. These three replicates are housing HDPE MetaCORE [MO] (black material), foam (white material), and honeycomb (amber material). The 3-axis accelerometer is in the UAV loaded with MetaCORE and ready to be sealed for drop testing.



## 3.4. Battery Boxes

Individual states are phasing out sales of new gas-powered vehicles to meet their net zero carbon emission targets. Increased efficiency and decreased costs of batteries manufactured for the transportation sector drives optimism that these goals can be met. However, whether for planes, trains, or automobiles, batteries require special care to protect people in the event of a collision. Even the slightest crack in a battery cell can lead to catastrophic thermal runaway and chemical fire. Preventing damage to the batteries is therefore top priority for engineering safety in all modes of future transportation.

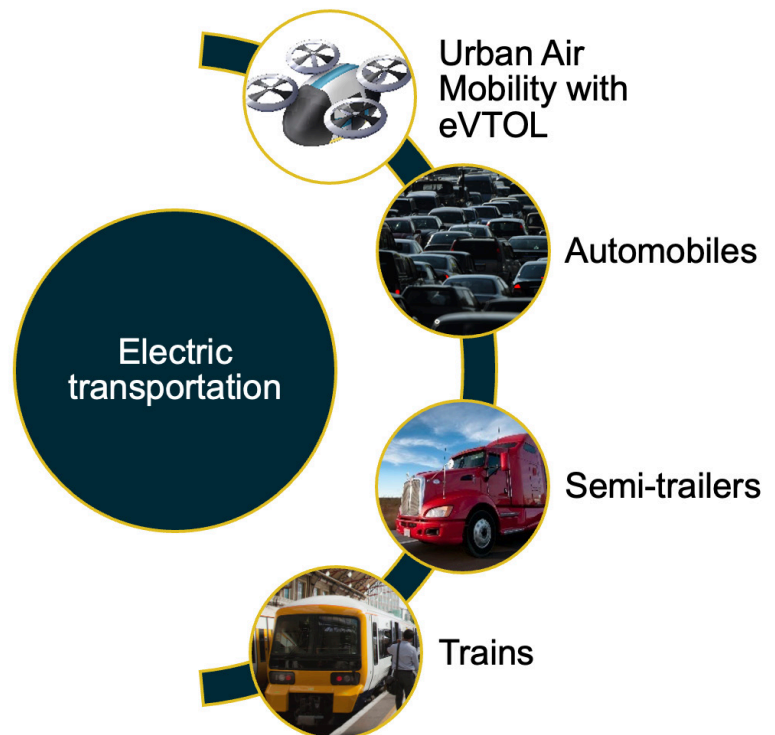
From an engineering perspective, the technical requirement is to create a complete battery system that is simultaneously lightweight, compact, and low-cost, while still being safe and efficient. Part of this balancing act is that added components for safety contribute to overhead weight and undesired thermal insulation. Active cooling components help by maintaining a safe operating temperature, but they also add weight and create a parasitic power drain during normal operation.

### Today's battery box modules

Lithium-ion batteries commonly used in today's electric vehicles are integrated into battery box modules to address size, weight, power, cost, and safety trade-offs. These modular boxes help mitigate impact forces in the event of a collision and provide an integrated cooling solution. Aluminum is an attractive material for fabricating battery boxes for its low cost, light weight, ability to bear load, and high thermal conductivity. Nevertheless, its impact absorption abilities are less desirable.

### A MetaCORE-enhanced battery box module

MetaCORE is a lightweight material designed to optimize energy absorption. It can be used to fabricate a better battery box by bonding with glass fiber reinforced skins. These skins provide comparable puncture strength to aluminum and a smooth exterior surface. Without MetaCORE, a box made from just the skins is non-load bearing and non-impact absorbing.



Impact testing the full thermoplastic composite structure offers a unique opportunity to demonstrate MetaCORE's benefits over a simple aluminum battery box design. Rather than filling the box with active battery cells and risking an uncontrolled fire, ceramic payloads are a useful surrogate to evaluate the relative differences between HDPE MetaCORE, PETG MetaCORE, and

aluminum designs.

Boxes filled with the ceramic surrogate were subjected to repeated testing with up to 3.6 kN of load ( $\approx$  830 pounds force) dropped from a 1.3 m ( $\approx$ 4 ft) height. After 5 drops, the payloads were removed from the boxes and inspected for damage. Survival rates are much higher with the MetaCORE thermoplastic composites. Analysis of slow-motion videos show the thermoplastic boxes “bounce” the payload whereas aluminum distorts and intrudes into the payload cavity. In addition, PETG being a somewhat more brittle thermoplastic than HDPE dissipates energy by fracturing.

### Added value with MetaCORE

Lightweight battery boxes are multi-piece assemblies with dedicated components for battery thermal management, electronics, and structural systems. These subsystems each have separate, but necessary functions for safe operation. Electric vehicles can

become more efficient if battery boxes are made smaller and lighter, but no singular feature of current battery enclosure design can be eliminated without introducing safety concerns.

Rather than eliminating components, part consolidation with MetaCORE combines multiple battery module components into one.

The MetaCORE geometry achieving the enhanced impact protection includes continuous 6 mm to 10 mm channels that run laterally through the walls. These channels can be utilized to integrate a thermal management system directly into the crash protection element of the box’s walls. By using existing elements in the energy absorber as a cooling channel, MetaCORE removes the need for separate parts dedicated to singular tasks while still embodying necessary safety features. The multifunctionality of MetaCORE in battery box modules eliminates extraneous material, lowers overall weight and volume, and simplifies construction.

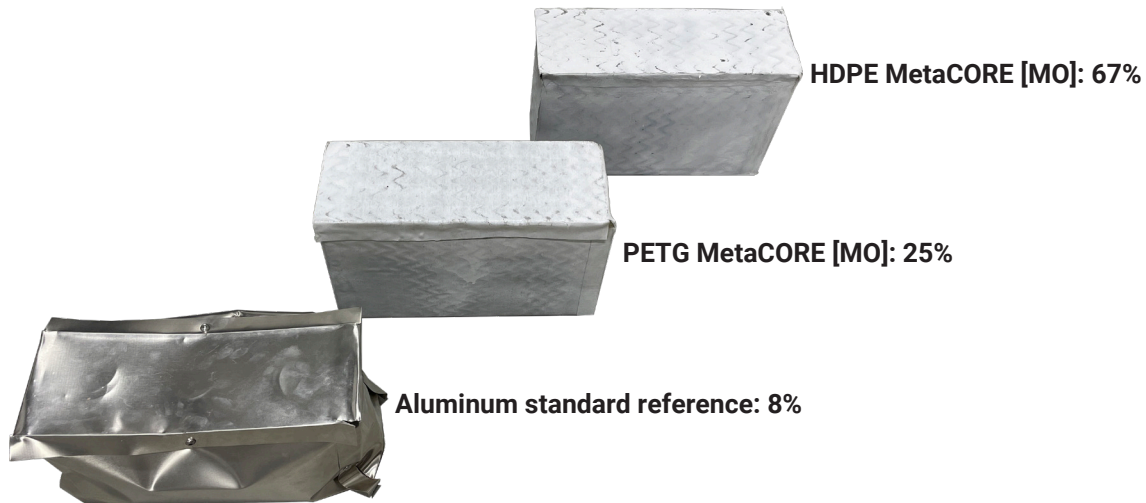


**Figure 24:** Modular battery boxes after destructive testing and their corresponding ceramic payload survival rates.

## 3.5. Aerial delivery and energy absorbing material

---

The US Army is the largest global logistics organization. Whether it's food, water, equipment, or personnel, mission success requires getting people and supplies to some of the most inaccessible corners of the world under extremely challenging circumstances. One especially useful approach for getting things where they need to go is aerial delivery. Essentially, cargo is flown over the delivery site and deployed out the back of a plane with a self-releasing parachute.

Given the range of materials required to support an agile force, aerial delivery platforms including Joint Precision Aerial Delivery Systems (JPADS), High Altitude Low Opening (HALO), and airdrop from Unmanned Aerial Systems (UAS) are available to respond to specific needs. Even though these aerial delivery systems have different operational envelopes, they all fundamentally face the same technical challenge: hard impacts break stuff. Moreover, increased demand for multi-domain operations combined with growing adversarial anti-air threats put aerial delivery solutions under pressure to continuously innovate and achieve high delivery success rates of larger cargo with increased precision from greater distances.

### Technical considerations for successful aerial delivery

Parachutes, airbags, and Energy Absorbing Devices (EADs) are various technical solutions to achieve softer landings and ensure mission-capable delivery of supplies. The science of impact mitigation has an extensive history and various metrics for crash protection are already established. These metrics help to optimize and evaluate the effectiveness of EADs while remaining neutral to the crash-protection technology.

Characteristics of high-performing EADs include:

1. Irreversible energy conversion from kinetic energy to inelastic energy through brittle fracture, plasticity, viscous losses, etc.;
2. Low bare compressive strength (or "peak stress") to minimize the deceleration at impact;
3. Constant crush strength (or "crush stress") to balance high energy absorption with low acceleration;
4. A long stroke distance to maximize the work done by the EAD; and
5. Repeatable deformation characteristics across a wide range of loading conditions and orientations.

From these five desirable EAD characteristics, effective solution should optimize for specific energy absorption (SEA) and crush force efficiency (CFE). These two quasi-static metrics of energy absorption and crush efficiency are useful since data showing impacts at speeds <20 m/s generally activate quasi-static failure response.

### Current Solutions for Aerial Delivery

When comparing impact mitigating solutions, a standard System, Weight, Power, and Cost (SWaP-C) analysis, combined with SEA and CFE provide a robust picture. One of the capabilities under active improvement for JPADS, HALO, and UAS systems is focused on increasing the horizontal travel distance between the aerial release and the landing site. Larger horizontal travels allow greater reach for the delivery system, which both

decreases flight crew risk and increases likelihood of overcoming adversaries. Therefore, the directional dependence of all key technical metrics is also important since horizontal glides are associated with greater shear forces and more uncertainty in the landing conditions.

### Cardboard honeycomb vs MetaCORE

Honeycomb materials are widely used in aerospace, transportation, and construction industries and are available from numerous manufacturers in a variety of specifications. As their name implies, these structured materials consist of hexagonally shaped open-air cells that are frequently sandwiched between two panels. While lightweight, there are several drawbacks to honeycomb as an EAD material despite its wide prevalence. For example:

- Honeycomb has unidirectional functionality and off-axis loading causes the material to collapse.
  - Honeycomb has a high peak stress, which means it transmits significant accelerations and risks payload damage due to its low CFE. Pre-crushed honeycomb is manufactured specifically to mitigate this problem but has limited availability and reduced load bearing capacity.
  - The costs of aerospace-grade honeycomb are quite high due to the materials, resins, and testing standards involved. Cardboard honeycomb for aerial delivery is less expensive to purchase, but there are significant shipping and storage costs due to the large volume of single-use material typically required. The operational expense of cardboard honeycomb is comparable to the cost of shipping or storing “boxes of air” due to its overall low mass density.
- Because honeycomb is a well-established technology, key IP is already owned by large financially entrenched organizations doing little to innovate
  - Honeycomb is an anticlastic material and does not conform well to shapes with positive Gaussian curvature such as an aerodynamic body or a curved, signature-reducing electromagnetic absorber.
  - Honeycomb is often damaged, crumpled, or torn when integrated into a product.

Since honeycomb cardboard is commonly used for aerial delivery, FEA simulations with LS-DYNA help identify how the anisotropic properties of this material are going to be increasingly problematic for the future of US Army aerial delivery operations (Figure 25). Analogous simulations with MetaCORE provide a glimpse into how the metamaterial's structure promoting isotropic impact absorption provides benefits for the future of aerial delivery (Figure 26).

These data show distinct differences between the anisotropic properties of honeycomb and the pro-isotropic properties of MetaCORE [MO] under identical impact scenarios. The table below (Figure 27) highlights key performance metrics that summarize the findings and demonstrates capabilities outside the  $\pm 15^\circ$  operational cone of honeycomb (Figure 28).

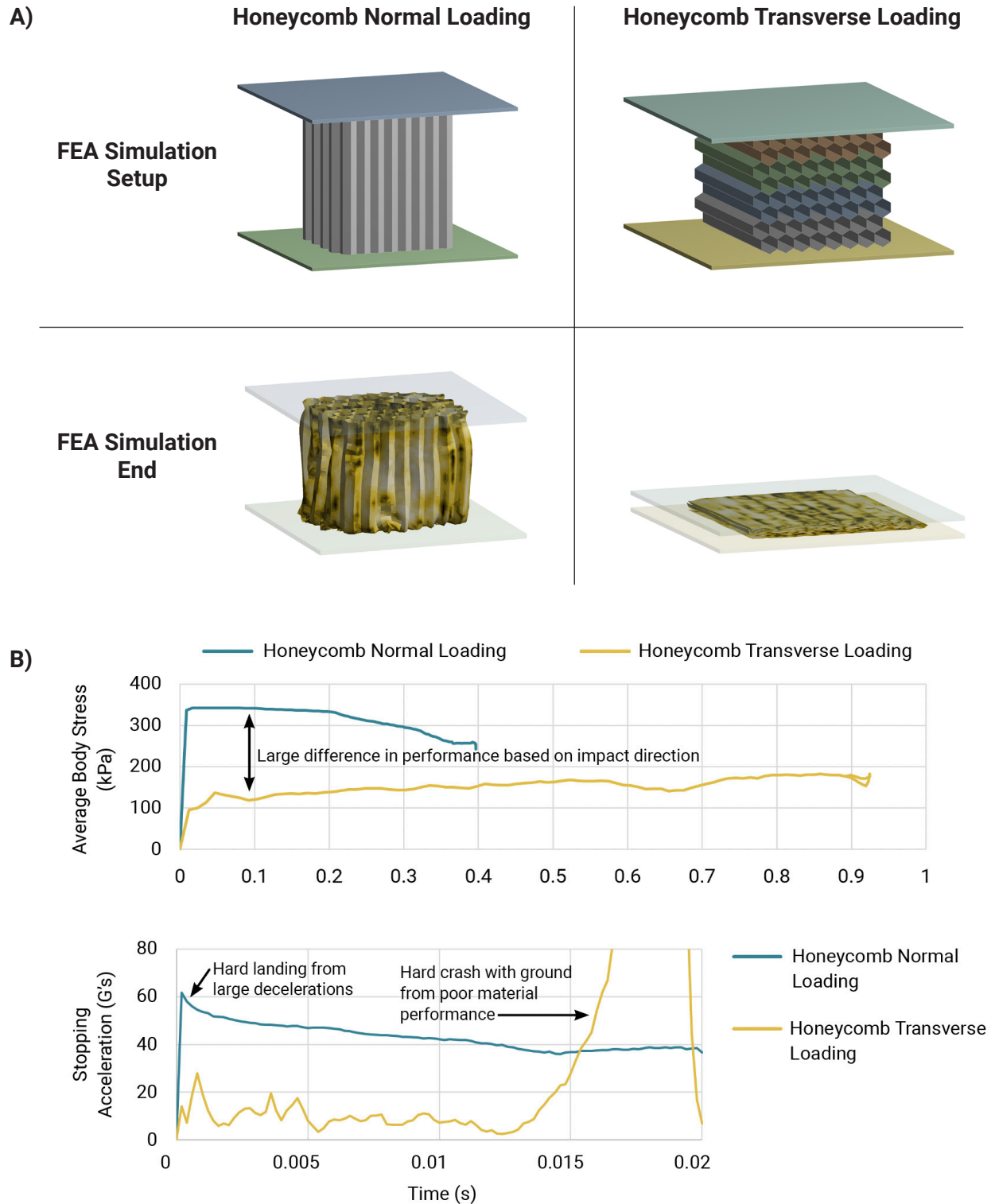


**Figure 25:** FEA simulations of honeycomb show **(A)** the response to crushing loads, and **(B)** the vastly different mechanical responses that can occur depending on the loading orientation.

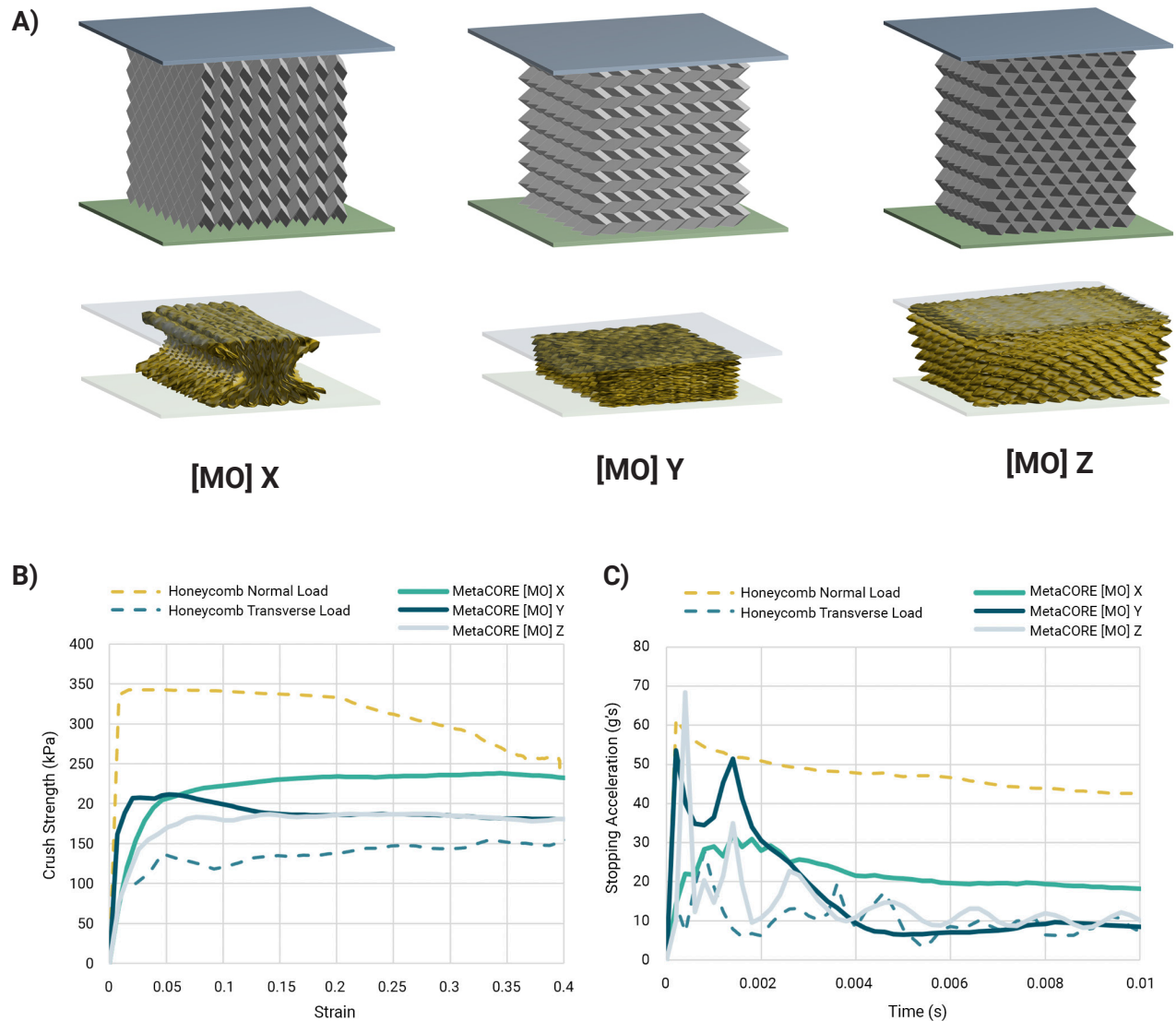


**Figure 26:** (A) MetaCORE is a class of cellular materials that dissipates energy as they are crushed. Gray 3D renders of MetaCORE [MO] show all three orientations of its nominal structure, while colorful renders below show the fully compressed state from FEA simulations. (B) Comparative FEA simulation data from LS-DYNA show the stress versus strain for honeycomb (dashed lines) and MetaCORE [MO] (solid lines) when the impact comes from various directions. Notice how honeycomb has a large performance difference depending on whether the impact is normal or transverse to the honeycomb flute. In contrast, MetaCORE [MO] has a nearly isotropic performance. Also note the shape of the MetaCORE stress-strain curve, which has been optimized for a near-ideal CFE and maximum SEA. (C) The same simulation data as panel (B) but looking at the stopping decelerations (expressed as g-force) immediately after the collision event, which occurs at time = 0 s. Honeycomb has large differences in performance depending on orientation, whereas MetaCORE [MO] is far more consistent regardless of orientation.

Loading Orientation	SEA (J/kg)		CFE		Specific Modulus (MPa)		Crush Strength (kPa)		% of Initial Energy Retained by Payload	
	[HC]	[MO]	[HC]	[MO]	[HC]	[MO]	[HC]	[MO]	[HC]	[MO]
Normal / X	1,070	940	0.8	0.92	25	7.8	270	220	0%	30%
Transverse / Y	460	740	0.0	0.87	5.2	7	150	160	68%	54%
- / Z	-	800	-	0.86	-	16	-	180	-	52%

**Figure 27:** Summary of comparative simulations quantifying the functional properties of cardboard honeycomb and cardboard MetaCORE [MO] subjected to loading from various conditions. Data highlights the pro-isotropic properties of MetaCORE [MO] suggesting its potential to increase the operational envelope of future aerial delivery missions. [HC] = Honeycomb; [MO] = MetaCORE [MO].

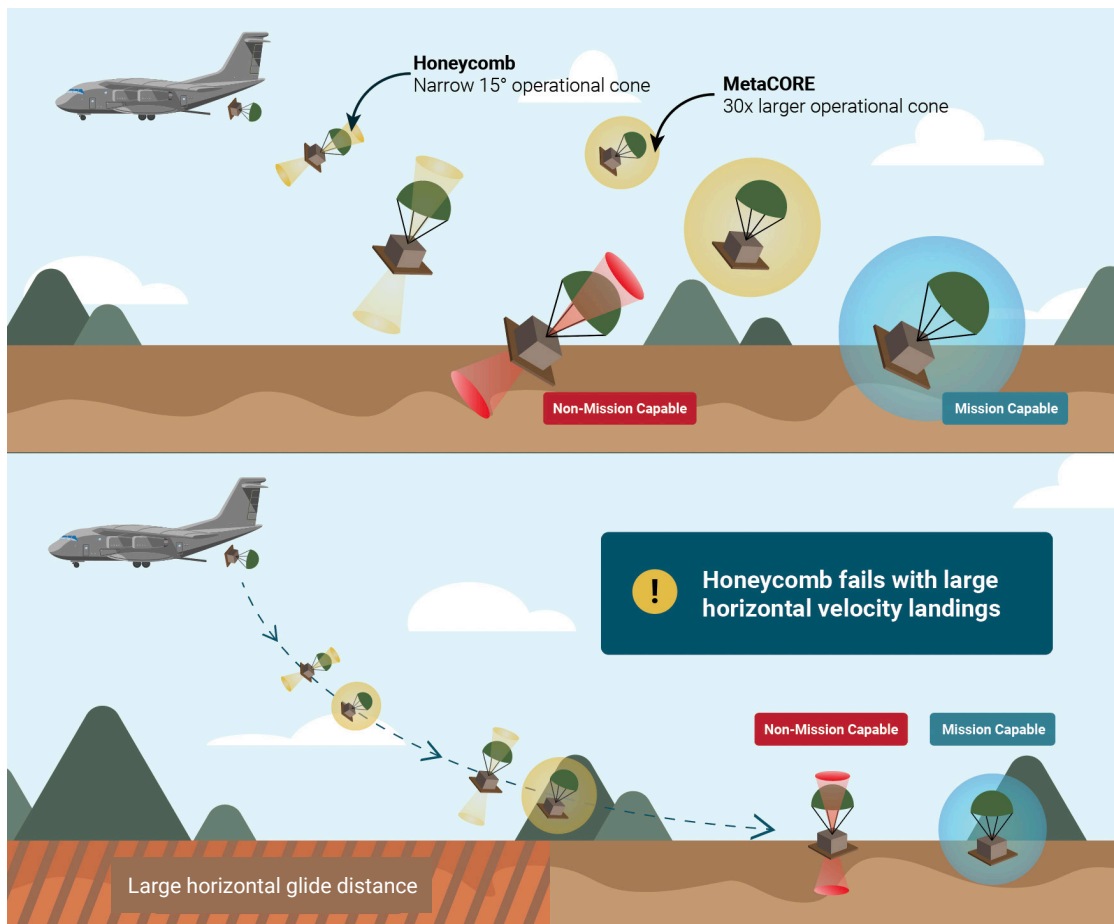


**Figure 28:** Current airdrops require near-vertical landings to ensure 100% mission capable cargo delivery. Tomorrow's airdrops need to achieve much larger horizontal glide distances, which induce shearing forces beyond what today's solution can support. Because its energy absorbing properties are omni-directional, MetaCORE increases today's operational envelope and enables tomorrow's missions.

PART 4

# **Guide for working with MetaCORE**

## 4.1. Quick reference fabrication tips

---

Thermoformed MetaCORE is well suited for applications requiring scale. For these applications, MetaCORE is most easily produced by thermoforming 2D sheets with the doubly corrugated geometry of the [MO] unit cell's XY face (Figure 5).

While cost-effective to produce, fabricators are responsible for integrating sheets of MetaCORE into finished parts (Figure 29).

This guide gives recommended best practices for working with MetaCORE. The data was collected primarily from HDPE sheet stock with thickness ranging from 0.030 in to 0.080 in. The recommendations are collated in a short list in this section for easy reference and generally apply to other resins or sheet thicknesses. Detailed explanations and quantitative data are supplied for advanced users to have a better understanding of why the recommendations are being made.

### Flat surfaces:

1. Maximize consistency between parts by using the same section of each sheet for identical parts.
2. Get the best performance by minimizing distortions of the geometry during fabrication.
3. The top and bottom surfaces of a sheet are interchangeable for flat parts.
4. Maximize adhesion between sheets and substrates to maximize the benefits of stabilized cores.

### Corners:

5. Corners are more resilient when they're made by compressing the sheet into a mold with the top surface in contact with the mold.
6. For 90° corners, use the sheet's x-axis to increase in-plane stiffness on load-bearing corners.
7. There's no wrong way to orient the sheet when it comes to the resilience of corners to general handling.
8. Increase resilience of right-angle corners to general handling by using two bends instead of one.
9. To get the best performance from multiply corners, use thin skins to prevent layers of fabric from nesting together.

### Singly-curved surfaces:

10. The top and bottom surfaces of the sheet are interchangeable when wrapping around a curved surface, but some wrappings are easier to form than others.
11. MetaCORE's negative Poisson's ratio means cylinders deform in surprising ways under compression, making it easier to fit into tight spaces.
12. Maximize adhesion between the sheet and substrate to maximize benefit of composite tubes
13. The benefits of composite optimization require that layups and orientations match the design specification.
14. Use test methods relevant for the end use application to verify composite layup performance.

### Compound-curved surfaces:

15. MetaCORE's negative Poisson's ratio makes fabricating parts with compound curvature easier than other materials.
16. Since there are a variety of proven methods for fabricating domes and structures with similar compound curvature, select the approach most suitable for the application's requirements.
17. Since there are fabrication-related differences in mechanical performance of domes, engineering and fabrication teams should work closely to define the right method for the application.
18. Make sure the unit cell size is larger than the inverse curvature of the surface to keep mechanical properties predictable.

### 4.1.1. Handling precautions

When working with MetaCORE thermoplastic materials it is advisable to wear heat-resistant gloves throughout the entire operation. This helps to keep the core and skins clean and affords protection for the operator's hands.

Glass fiber dust is an irritant. Avoid breathing the dust generated by cutting operations, and do not rub the eyes with hands which may be contaminated with the dust.

The usual precautions should be observed while working with synthetic resins.

The information contained herein is believed to be the best available at the time of printing but is given without acceptance of liability, whether expressed or implied, for loss or damage attributable to reliance thereon. Users should make their own assessment of the technology's suitability for their own conditions of use and, before making any commitment with regard to the information given, should check that it has not been superseded.



**Figure 29:** This photograph of MetaCORE is made with HDPE resin and tooling based on the XY face of the [MO] unit cell. This surface is a doubly corrugated tessellation of "mountains" (coming out of the page) and "valleys" (going into the page). The mathematical geometry is up-down symmetric, meaning that the mountains and valleys are indistinguishable when flipped. In manufactured parts, thermoforming breaks the symmetry giving an up-to 50% difference between the thickened mountains and thinned valleys. Moreover, the center of a thermoformed part can be overall 10% thinner than the edges. These real-world effects of manufacturing are at the heart of the information in this section.

## 4.2. Flat surfaces

### Relevant engineering examples

---

- Sandwich panels
- Cladding
- Boxes or containers
- Energy absorbing devices
- Battery modules

### Engineer's constraints and considerations

---

- Envelope (i.e., plate thickness)
- System weight
- Modulus
- Strength
- Desired energy absorption
- SEA
- CFE
- Operational environment

### Fabrication tips

---

- |              |   |        |
|--------------|---|--------|
| <b>Tip 1</b> | Maximize consistency between parts by using the same section of each sheet for identical parts. | Pg. 38 |
| <b>Tip 2</b> | Get the best performance by minimizing distortions of the geometry during fabrication.          | Pg. 39 |
| <b>Tip 3</b> | The top and bottom surfaces of a sheet are interchangeable for flat parts.                      | Pg. 40 |
| <b>Tip 4</b> | Maximize adhesion between sheets and substrates to maximize the benefits of stabilized cores.   | Pg. 41 |

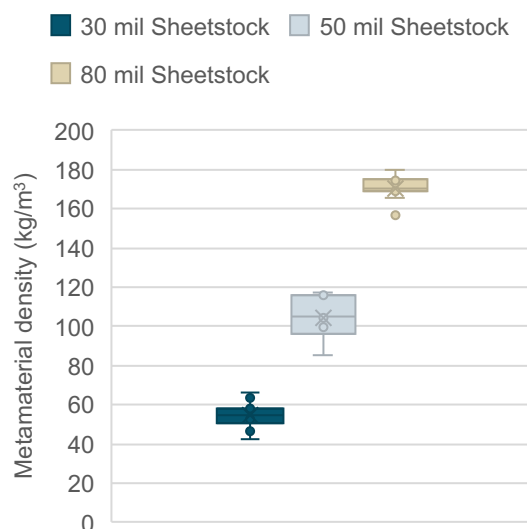
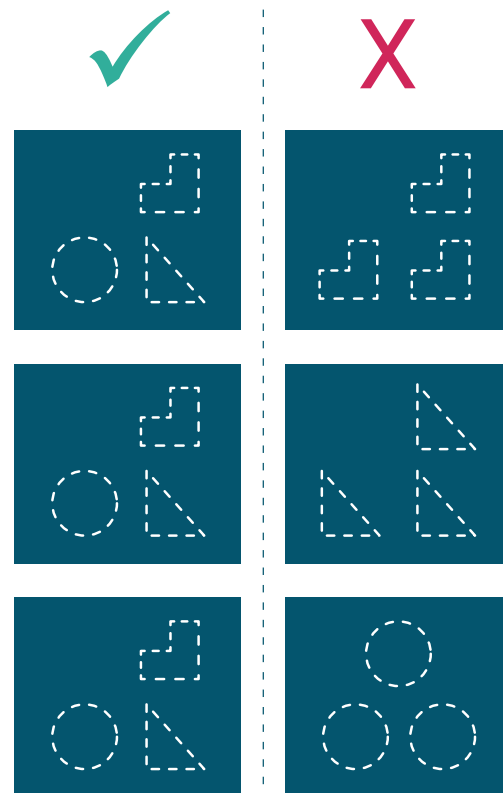
## Tip 1 | Maximize consistency between parts by using the same section of each sheet for identical parts

### How to navigate the expected variability from manufacturing

Sheets of MetaCORE are made at scale by heating thermoplastics and molding them on tooling with metamaterial geometries. As the unformed sheet is heated, it begins to sag under its own weight and thin due to viscous flow. The result can be as much as a 10% difference when comparing the thickness of the center of the sheet to the edge. When the thermoplastic contacts tooling, further wall variations arise as the thermoplastic is drawn over mountains and into valleys, resulting in as much as 50% variation in thickness within a single unit cell.

For example, an unformed 80 mil sheet was heated and drawn onto [MO] tooling. The middle of the sheet formed geometry with 30 to 60 mil thickness. The edge of the sheet formed geometry with 35 to 65 mil thickness.

Spatial gradients in formed part thickness result in variations in metamaterial density, and as a direct consequence, mechanical properties. Data shown here are for samples excised from different areas of a formed sheet. To maximize consistency across multiple parts, make sure to use the same section of a sheet for identical parts.



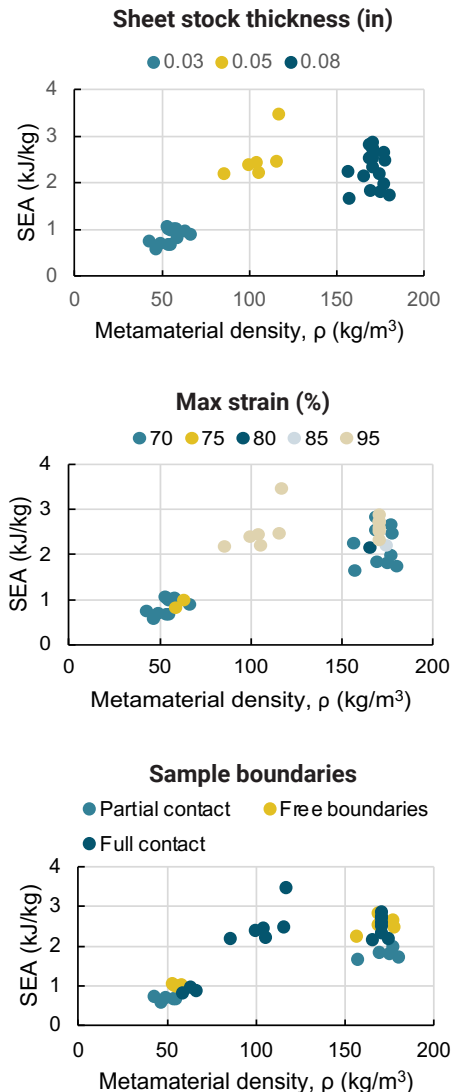
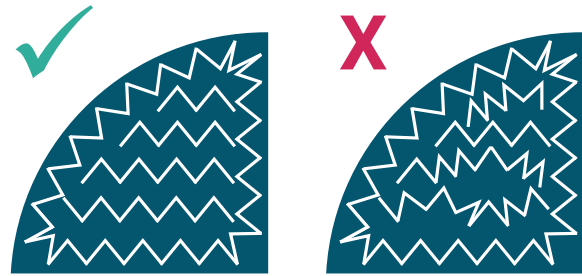
## Tip 2 | Get the best performance by minimizing distortions of the geometry during fabrication

### Density variations predict performance variations

The strongest correlate of mechanical performance is the metamaterial density,  $\rho$ . Unintended distortion to the geometry during fabrication can create variations in density, which reduces predictability of mechanical properties. Since predictable performance is required for any material used in engineering applications, these distortions are generally undesirable.

Sources of variation that leave the density unaffected are less correlated with mechanical performance and therefore more tolerable. As evidence, consider how sensitive performance metrics are on different sources of variation. For demonstration purposes, the SEA is useful because it depends on intrinsic material properties (density), loading characteristics (maximum compressive strain), and system integration (boundary conditions).

The SEA measurements form tight clusters when color-coded by density but show no meaningful correlation when color-coded by maximum compressive strain or boundary conditions. One way of understanding this data is to recall that the SEA scales as the crush strength divided by density, which means  $SEA \sim \rho^{1.1}$  to  $\rho^{1.4}$ . The scaling of SEA with the maximum strain or boundary conditions is more complicated to analyze, but these effects are evidently not pronounced enough to account for performance variability.

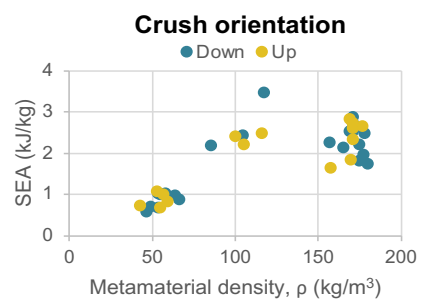
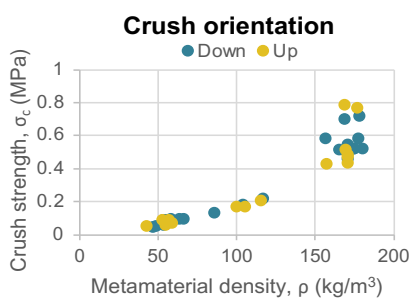
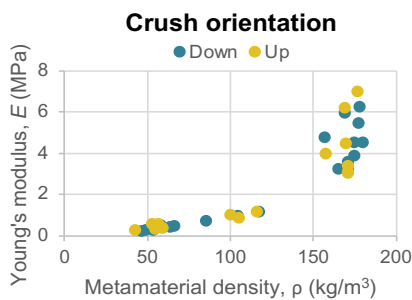
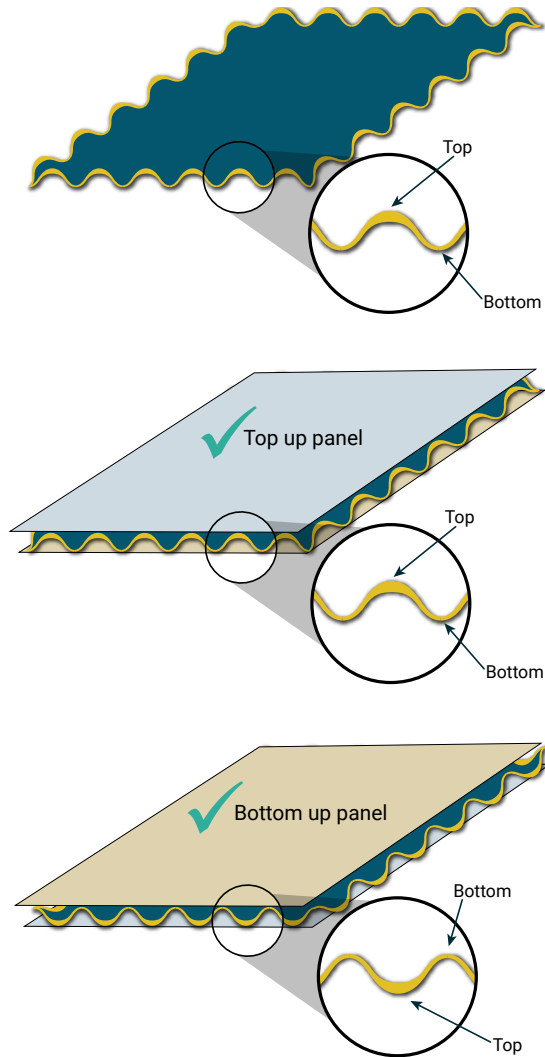


## Tip 3 | The top and bottom surfaces of a sheet are interchangeable for flat parts

### Mechanical properties normal to the XY surface are symmetric despite deep draw thermoforming's asymmetry

MetaCORE [MO] tooling is a 2D tessellation of the basic unit cell's XY face (Figures 5 and 29). This unit cell geometry is up-down symmetric. The manufactured part, however, is not since the heated thermoplastic resin makes contact with "mountains" before "valleys" when it is being drawn into the mold. This feature of large format vacuum thermoforming can result in valleys that are up to 50% thinner than mountains depending on the manufacturing process details.

How does this up-down asymmetry affect performance metrics? For normal compression of planar surfaces, it doesn't! The Young's modulus, crush strength, and SEA are all uncorrelated with whether the sample is "right side up" or "upside down" as would be expected when the compressive axis is parallel to the sheet's normal axis. Direct measurements support the intuitive result.

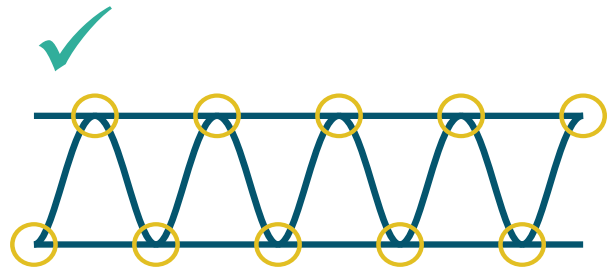


## Tip 4 | Maximize adhesion between sheets and substrates to maximize the benefits of stabilized cores

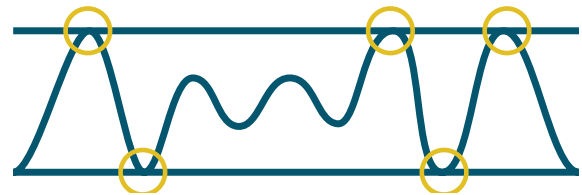
### Stabilizing cores increases crush stress

Bonding sheets of MetaCORE to high tensile strength substrates increases the compressive stiffness and strength of MetaCORE. Common substrates include sheet metal and fiber reinforced skins. Bonding thermoplastic to metals is challenging, but possible with the right adhesive and process. Bonding thermoplastic to thermoplastic is much easier and can be as simple as applying heat and pressure to melt the area of contact into one another.

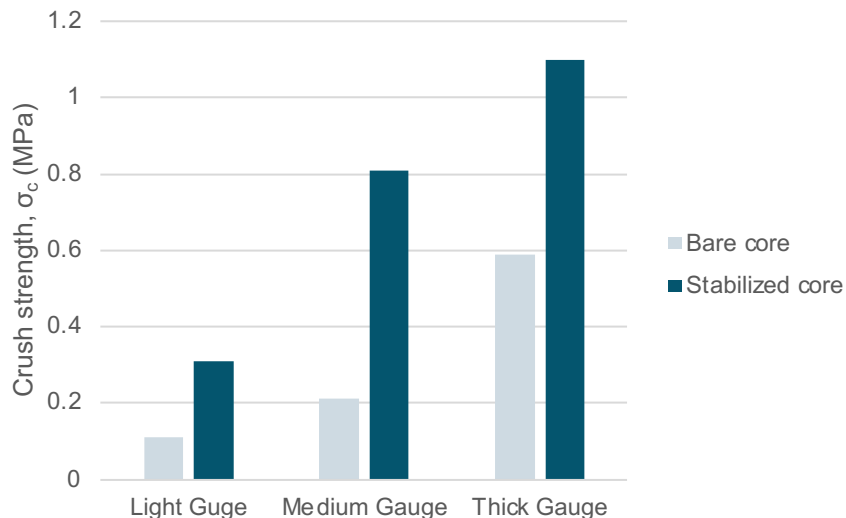
In a series of tests, HDPE MetaCORE [MO] was hot melted onto a glass-fiber reinforced PE substrate. The matched thermoplastics create a high-quality adhesive bond between the sheet of MetaCORE and substrate layer resulting in a 2x to 4x jump in crush strength. Sub-optimal adhesion reduces this effect and limits the benefits of stabilization.



**Good adhesion = more benefits of stabilization**



**Poor adhesion = fewer benefits of stabilization**



## 4.3. Corners

### Relevant engineering examples

---

- Boxes
- Containers
- Joinery
- I-beams
- Complex structures

### Engineer's constraints and considerations

---

- Angle of corner
- Material thickness
- Energy absorption
- SEA
- CFE
- Orientation of sheet principal axes and edge

### Fabrication tips

---

- Tip 5** Corners are more resilient when they're made by compressing the sheet into a mold with the top surface in contact with the mold. Pg. 43
- Tip 6** For 90° corners, use the sheet's x-axis to increase in-plane stiffness on load-bearing corners. Pg. 44
- Tip 7** There's no wrong way to orient the sheet when it comes to the resilience of corners to general handling. Pg. 45
- Tip 8** Increase resilience of right-angle corners to general handling by using two bends instead of one. Pg. 46
- Tip 9** To get the best performance from multi-ply corners, use thin skins to prevent layers of fabric from nesting together. Pg. 47

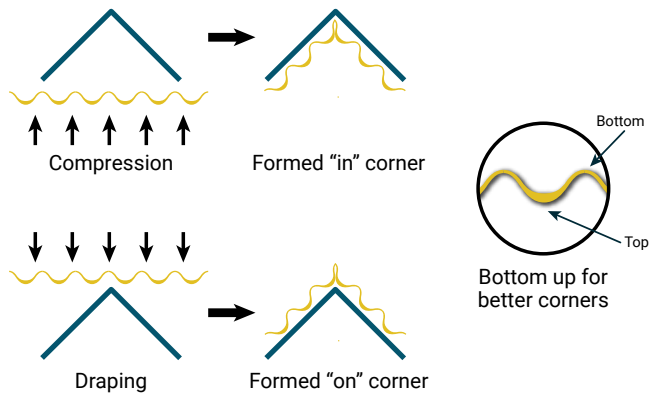
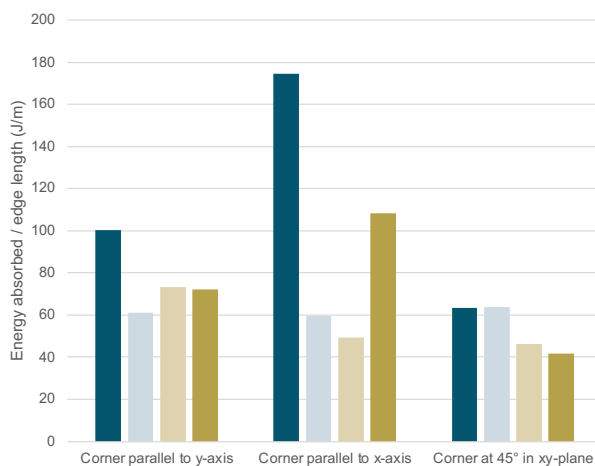
## Tip 5 | Corners are more resilient when they're made by compressing the sheet into a mold with the top surface in contact with the mold

### “Valley-side in” makes for better corners

Thermoplastic MetaCORE is produced by heating sheet stock and forming it on a mold tool with appropriate pressure. One of the benefits of working with thermoplastic parts is that they can be re-heated and re-formed to mold MetaCORE into an integrated part. An example of molding MetaCORE is fabricating a lightweight impact-absorbing box. In this example, molding 90° edges and corners is an essential step.

There are a variety of general and application-specific considerations to address when fabricating a corner. For example, should the [MO] sheet be draped over a 90° mold, or pressed into a 90° mold? Should the top of the [MO] sheet be in contact with the mold or the bottom?

As a rule of thumb, superior mechanical performance is achieved by (1) compressing [MO] “into” the mold corner rather than



draping “around” a mold corner, and (2) ensuring the bottom surface of the [MO] sheet is in contact with the mold tooling. In this configuration, performance benefits are generally better than the other three alternatives.

The recommended fabrication approach results in the thinner “valley-side” of the core on the exterior of the molded angle while the thicker surface is gathered on the interior of the molded angle. Effectively, the thinner side of the sheet stretches, and the thicker side comes into self-contact at the bend point, which reinforces the corner. Measurements applying compressive load on the corner show a greater amount of energy absorbed per length in the recommended fabrication configuration.

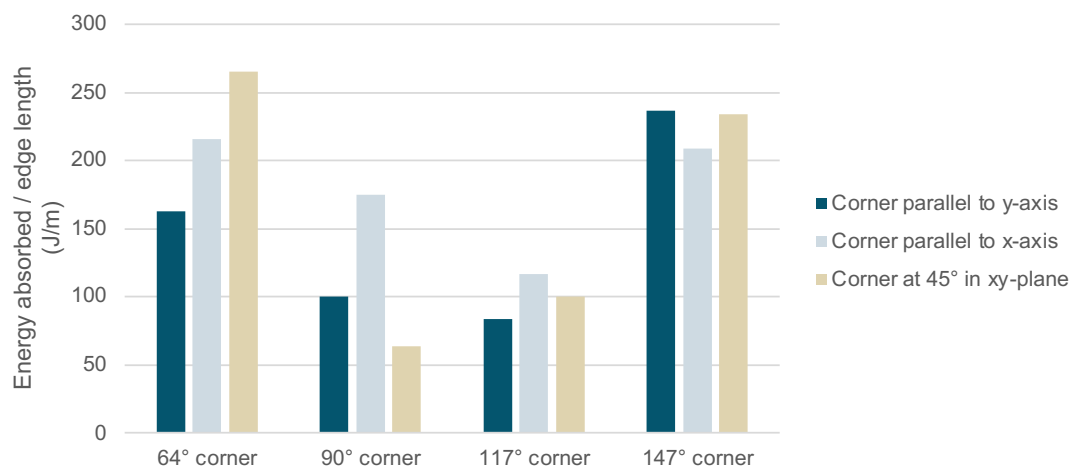
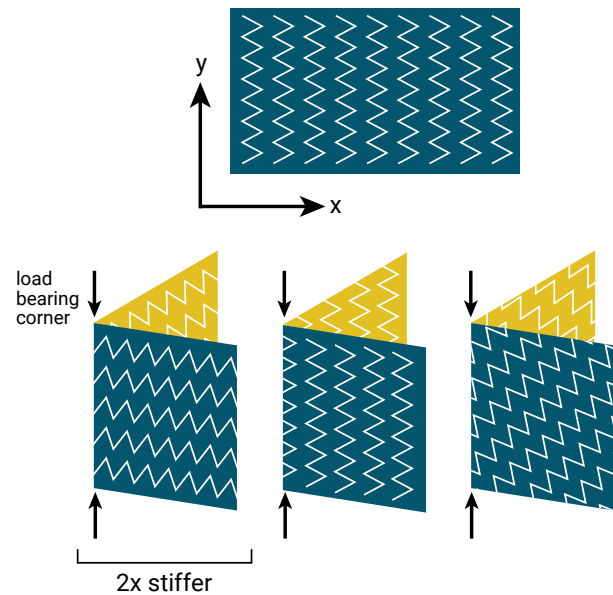
- Compression into mold - Thin surface on angle exterior
- Compression into mold - Thin surface on angle interior
- Draping over mold - Thin surface on angle exterior
- Draping over mold - Thin surface on angle interior

**Tip 6** For 90° corners, use the sheet's x-axis to increase in-plane stiffness on load bearing corners

**Use rotations to make better load bearing corners**

MetaCORE [MO] sheets can be molded to make corners of various angles. This corner can be parallel to the x-axis, y-axis, or at any angle between the two. Forming [MO] into a corner deforms the geometry and measurements of in-plane stiffness show how the mechanics of the corner depend on these variables. Since 90° corners are most common, it's important to note the relative increase in stiffness these corners have when they're molded parallel to the x-axis.

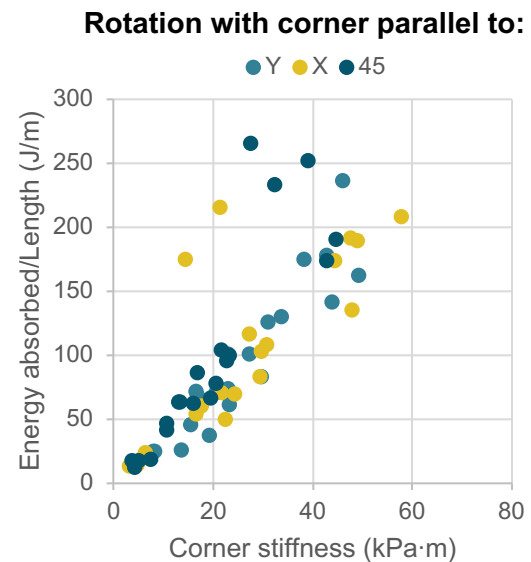
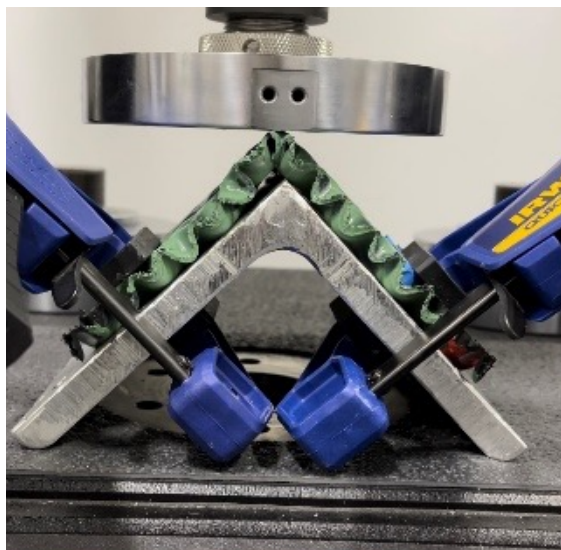
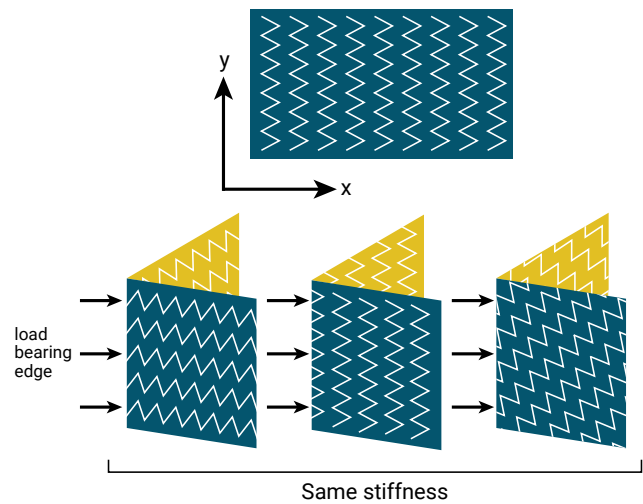
However, the optimal orientation varies with respect to the angle of the corner and designers are advised to test fabricated samples on a case-by-case basis to determine the orientation for their application.



**Tip 7** | There's no wrong way to orient the sheet when it comes to the resilience of corners to general handling

**Normal loading is rotationally independent**

While molded corners have an optimal answer when orienting [MO] sheets for in-plane loads, normal-loads characteristic of general handling conditions are less sensitive to orientation. Acquiring compressive measurements of corners at various rotations show no correlation between the sheet orientation and the corner orientation. This means the [MO] sheet's in-plane orientation imposes no constraints with respect to this loading criteria.



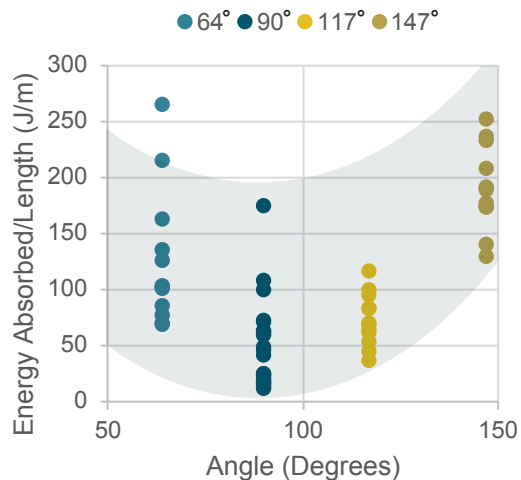
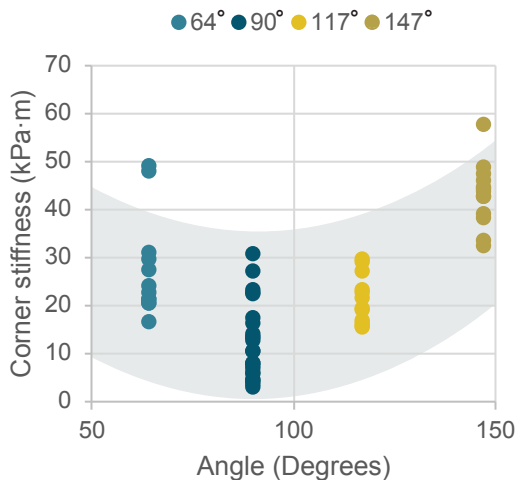
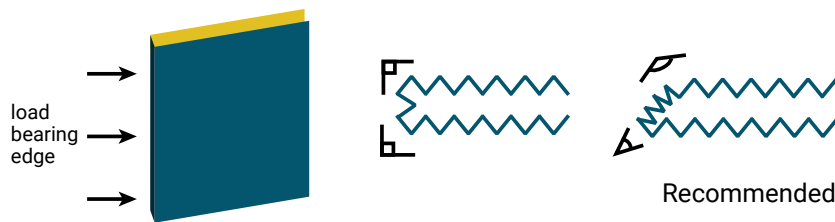
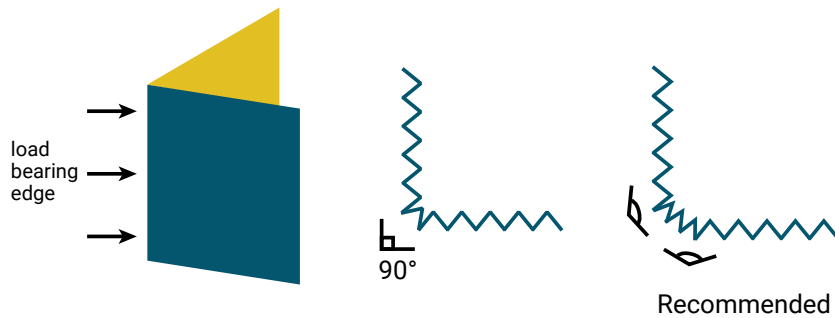
## Tip 8 | Increase resilience of right-angle corners to general handling by using two bends instead of one

### Response to normal loads depends on the angle of the molded corner

While sharp 90° corners are likely to be used in most cases, the mechanics of corners are generally superior at more obtuse and acute angles. Creating 90° corner by 2 or more obtuse angles effectively rounds-out

the corner and results in better mechanical performance.

Likewise, instead of using two 90° corners to create a multi-ply layup, more resilient corners can be made by pairing an obtuse and acute angle to achieve similar effect.

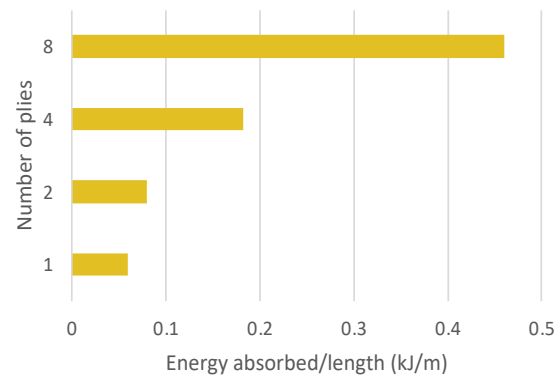
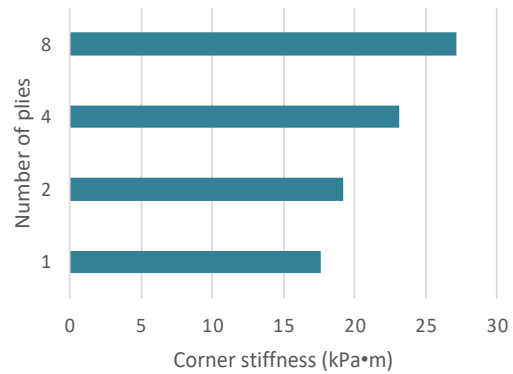
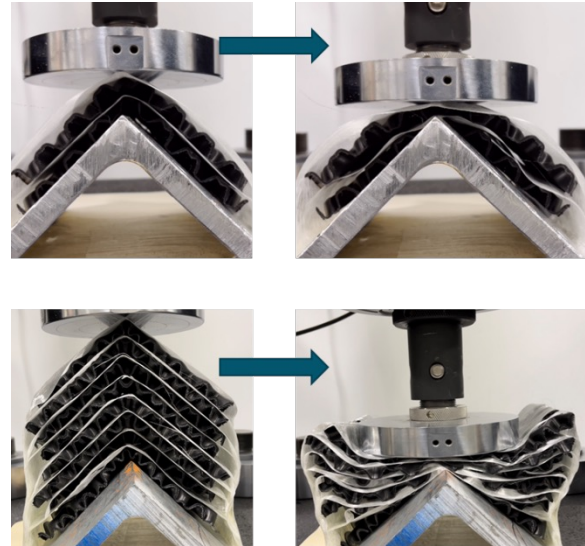


**Tip 9** | To get the best performance from multi-ply corners, use thin skins to prevent layers of sheets from nesting together

**Multi-ply corner mechanics are proportional to ply count**

Testing was performed with 1, 2, 4, and 8 ply structures in which the layers of MetaCORE [MO] were bent and stacked. Initially, several of the sheets nested into one another resulting in a densified corner with undesirable properties. Thin sheets of continuous glass-fiber reinforced thermoplastic sheets were inserted between the [MO] layers to prevent them from shifting and nesting together.

Mechanical tests were used to evaluate these composite multi-ply corners. Across the tests the normal stiffness slightly increased with the number of plies. Energy absorption, on the other hand, scales quadratically with the number of plies. This behavior can be understood by more closely examining the testing conditions. The contact area with the compression platen increases throughout the loading cycle. At peak compression, the contact area is proportional to the length of the edge and number of plies. Moreover, the stroke distance is also proportional to the number of plies so that the energy absorbed scales quadratically with the number of layers of MetaCORE in the corner. Hence, this nonlinear scaling of energy absorption with ply count is to be expected.



## 4.3. Singly-curved surfaces

### Relevant engineering examples

---

- Crush tubes
- Airfoils
- Fuselage
- Jet engines
- Rocket bodies
- Tubular connectors
- Struts

### Engineer's constraints and considerations

---

- Radius of curvature
- Operational environment
- Modulus
- Strength
- Desired energy absorption
- SEA
- CFE

### Fabrication tips

---

- Tip 10** The top and bottom surfaces of the sheet are interchangeable when wrapping around a curved surface, but some wrappings are easier to form than others. Pg. 49
- Tip 11** MetaCORE's negative Poisson's ratio means cylinders deform in surprising ways under compression, making it easier to fit into tight spaces. Pg. 50
- Tip 12** Maximize adhesion between the sheet and substrate to maximize benefit of composite crush tubes. Pg. 51
- Tip 13** The benefits of composite optimization require that layups and orientations match the design specification. Pg. 52
- Tip 14** Use test methods relevant for the end use application to verify composite layup performance. Pg. 54

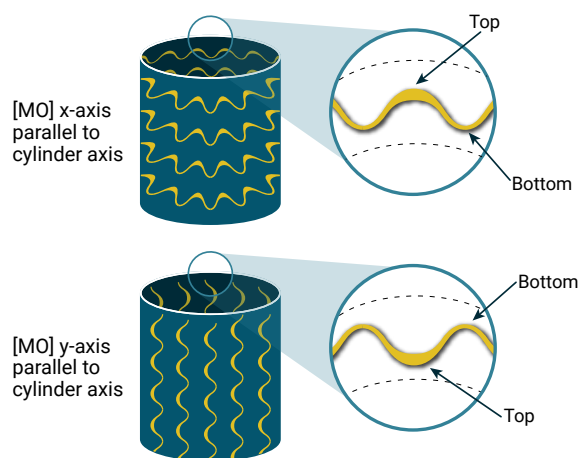
**Tip 10** | The top and bottom surfaces of the sheet are interchangeable when wrapping around a curved surface, but some wrappings are easier to form than others

### Forming cylinders with MetaCORE's discrete unit cells

Cylinders represent one of the simplest forms of mean curvature and an important mechanical design component. The symmetry of MetaCORE's geometry offers two simple and distinct ways of creating an interlocking, continuous cylinder. Flat sheets of thermoformed MetaCORE can be heated and formed around a mold of the desired inner radius with either the x- or y-axis parallel to the axis of the cylinder. At the joining of the material, a seam can be made by overlapping and interlocking unit cells and securing with sufficient heat and pressure.

The up-down sheet asymmetry has a small effect on curvature, and cylinders with the x-axis parallel to the cylinder axis are most easily formed with the thick mountain side of the thermoformed sheet on the exterior of the cylinder. Cylinders with the y-axis parallel to the cylinder axis are most easily formed with the thin valley side on the exterior of the cylinder. Though this difference exists, it is entirely feasible to form cylinders in the opposing direction.

Helical wrappings are also possible with the helix pitch coming in discrete steps of unit cells. Mechanics of these structures are more complicated and should be explored on an application-specific basis.



**Orientation X Cylinders:** X-axis parallel to the axis of the cylinder and thicker mountain side of the thermoformed sheet on the exterior.

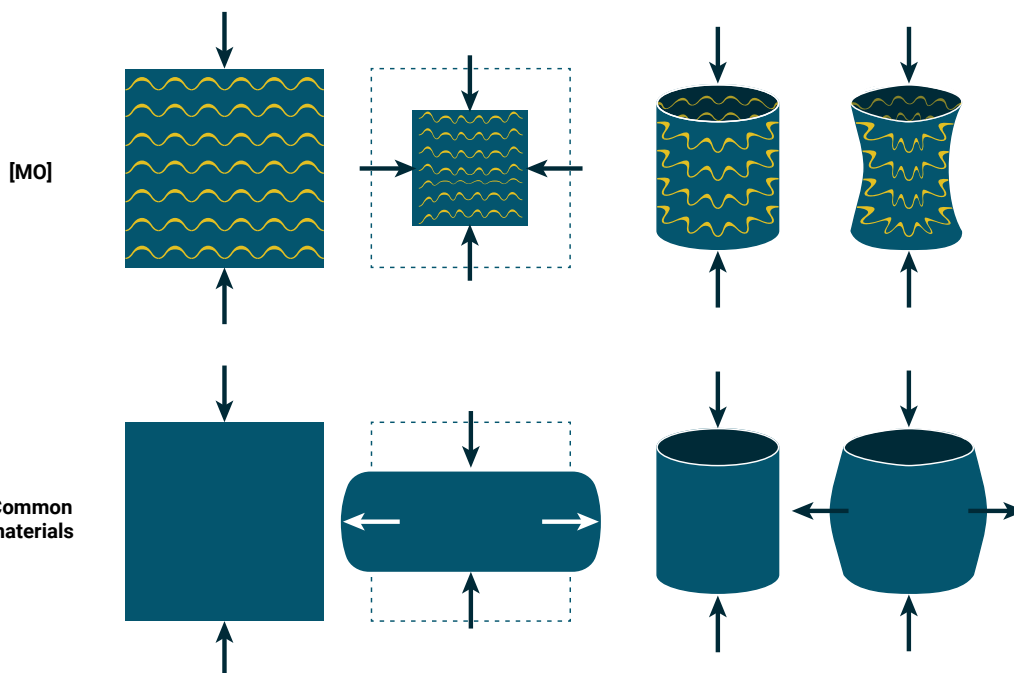
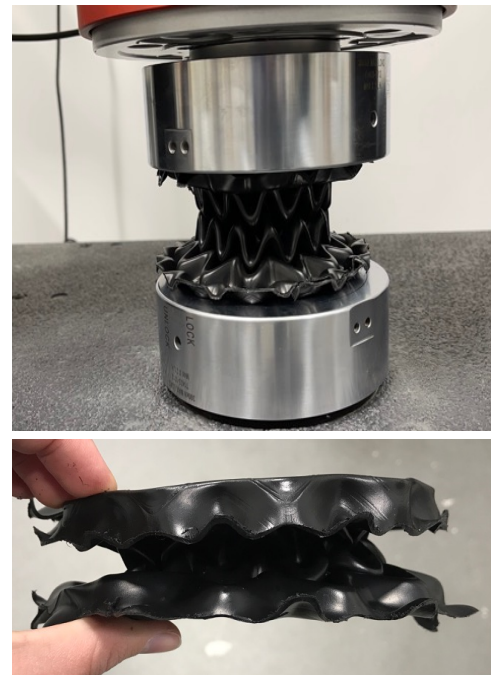


**Orientation Y Cylinders:** Y-axis parallel to the axis of the cylinder and thinner valley side of the thermoformed sheet on the exterior.

## Tip 11 | MetaCORE's negative Poisson's ratio mean cylinders deform in surprising ways under compression, making it easier to fit into tight spaces

### MetaCORE can promote self-stabilization of crushed cylinders

With the x-axis of MetaCORE [MO] parallel to the axis of the cylinder, the tube exhibits a self-stabilization effect. This phenomenon is driven by the material's negative Poisson's ratio. The negative Poisson's ratio causes the crush tube to neck at both ends, effectively securing the tube to off-axis or irregular loading without the need for external supports. Self-stabilization increases the amount of material participating in compression, which is a useful effect for engineering crush tubes.



## Tip 12 | Maximize adhesion between the sheet and substrate to maximize benefit of composite crush tubes

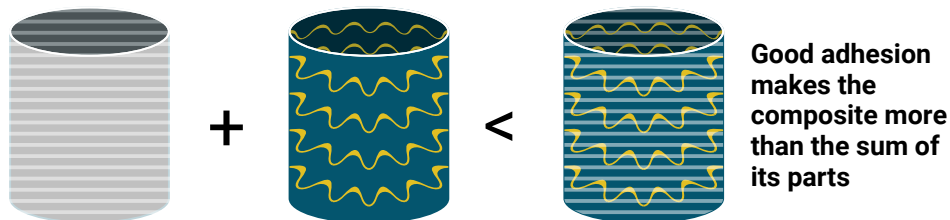
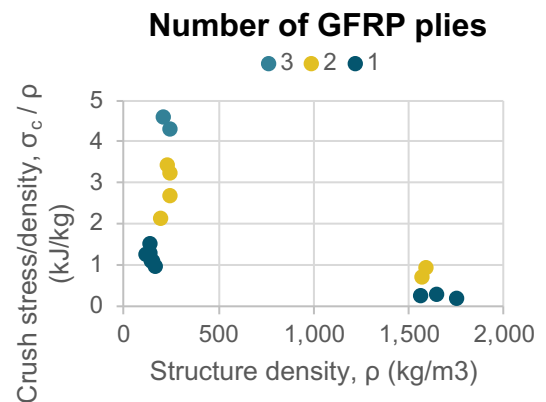
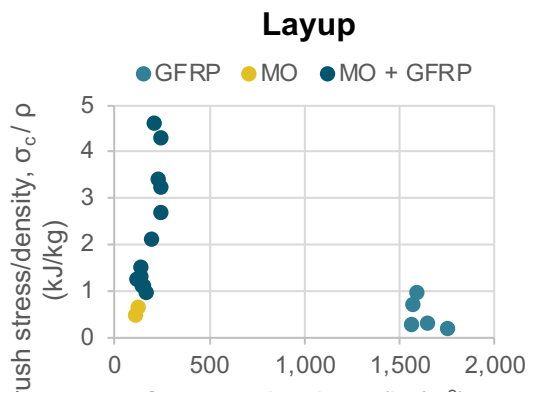
### Composites are “stronger together”

Crush tubes are useful for absorbing impact energy in a variety of applications. Composite crush tubes using fiber-reinforced skins typically engineer the cylinder geometry to promote a specific failure mode that maximizes the amount of fiber tension and breakage as the energy dissipative mechanism.

Composite crush tubes fabricated with MetaCORE [MO] and glass fiber reinforced thermoplastic (GFRP) plies were destructively tested to measure their performance. In general, the composite crush tube was stronger than either component and substantially less dense than the skins alone. Moreover, the crush tube strength is readily increased by increasing the number of GFRP plies with up to 350% increase in strength over a bare GFRP skin.

For maximum energy absorption, the core and skin must be bonded properly. Bonding like-resin cores and skins is simple with heat and pressure. Using heat shrink tape and an inner mold has proved to be an effective way of

getting evenly applied pressure on the entire cylinder. The convenience of this approach is one of the many advantages thermoplastics offer over thermosets.



## Tip 13 | The benefits of composite optimization require that layups and orientations match the design specifications

**While the number of layup orientations grows combinatorically with number of plies, capturing performance benefits for no added weight penalty makes it worth carefully studying design choices**

Optimizing composite layups is its own field of expertise with value-added engineering. Fabricating composite structures with MetaCORE requires similar care and skill.

Making crush tubes with glass fiber reinforced thermoplastic (GFRP) sheets and MetaCORE [MO] offers a useful demonstration of the possibilities when metamaterial composite optimizations are leveraged to full effect. Consider the various possible layups where fiber and [MO] orientations are rotated relative to the cylinder's central axis. At 0° GFRP orientation, the fibers wrapped axially around the tube, at 90° they run parallel to the tube axis, and at 45° they wrap helically around the tube.

Destructive testing shows a variety of interesting results.

Simple GFRP tubes are thin-walled structures, but their density is more than ~10x high than [MO]. Despite this difference, these materials have similar performance

as measured by crush stress / density. When GFRP and [MO] are combined, there is a nominal increase in density, but a dramatic increase in mechanical performance.

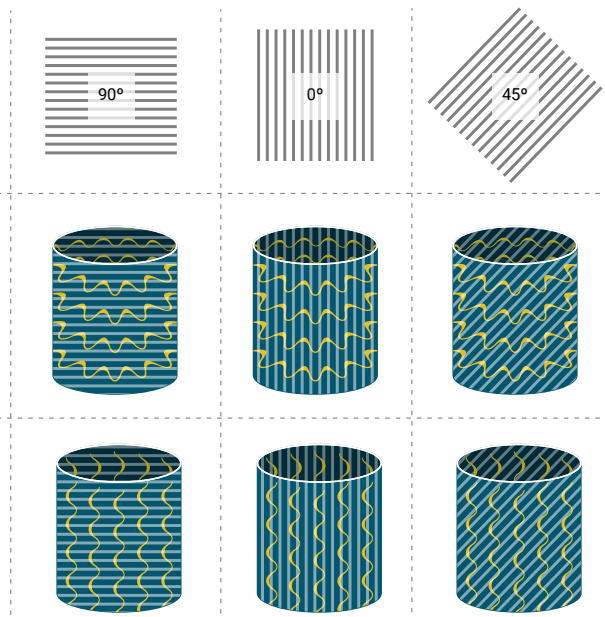
The 2-ply +/-45° orientation increase the crush strength for no change in weight or cost relative to the 2-ply 0°/90°. This increase in performance is because the +/-45° GFRP winding crushes in a more axisymmetric fashion (top photo) than the 2-ply 0°/90° fiber wrapping (bottom photo).

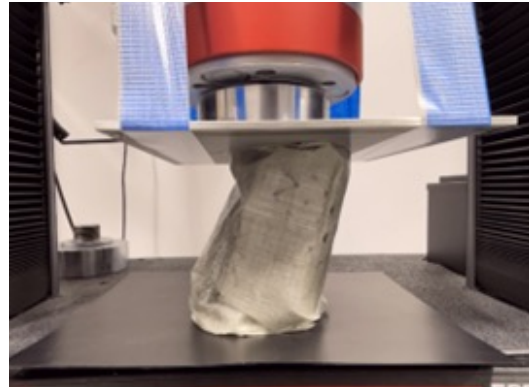
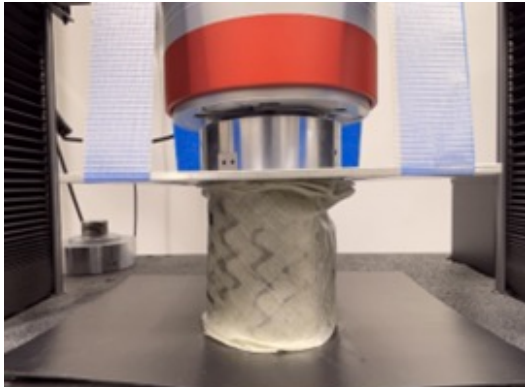
This example illustrates the more general proposition that reinforcing composite tubes with MetaCORE increases the energy absorption for relatively little weight penalty, and these improvements can be further optimized by refining the layup orientations.

**6 layups with non-equivalent mechanics**

X parallel to cylinder axis

Y parallel to cylinder axis





	Density (kg/m <sup>3</sup> )			Crush Stress/Density (kJ/kg)		
	No [MO]	[MO] x-axis    cylinder axis	[MO] y-axis    cylinder axis	No [MO]	[MO] x-axis    cylinder axis	[MO] y-axis    cylinder axis
<b>GFRP</b>						
<b>1-ply</b>						
0°	1,749			0.19		
45°	1,562			0.26		
90°	1,645			0.31		
<b>2-ply</b>						
0/90°	1,590			0.95		
+/- 45°	1,565			0.72		
<b>[MO]</b>						
<b>0-ply</b>						
N/A		107	124	0.48		0.63
<b>[MO] + GFRP</b>						
<b>1-ply</b>						
0°		135	149	1.31		1.10
45°		137	167	1.52		0.97
90°		119	147	1.26		1.12
<b>2-ply</b>						
0/90°		240	192	2.68		2.13
+/- 45°		230	244	3.42		3.25
<b>3-ply</b>						
+/-/+ 45°		241	208	4.31		4.60

## Tip 14 | Use test methods relevant for the end use application to verify composite layup performance

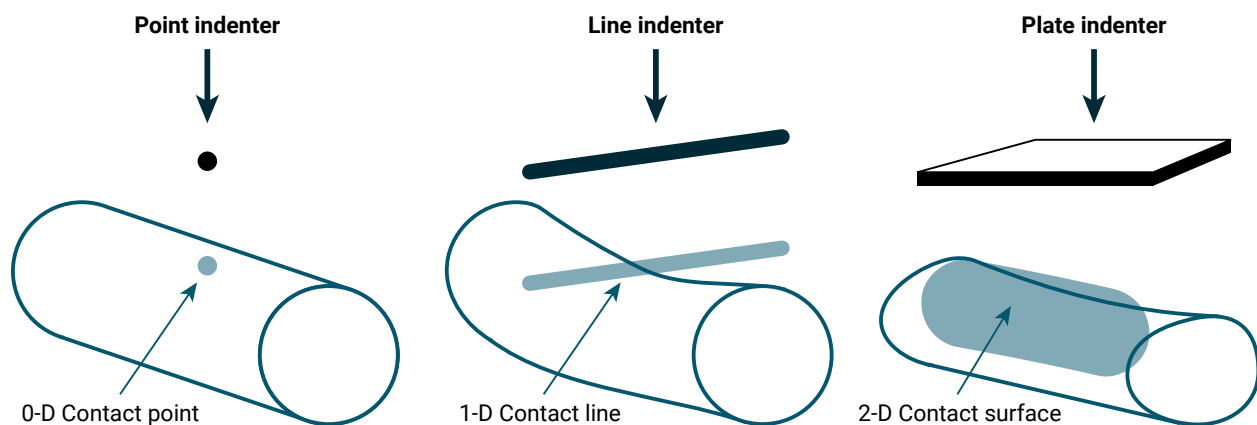
### There are many ways to apply load to a curved surface

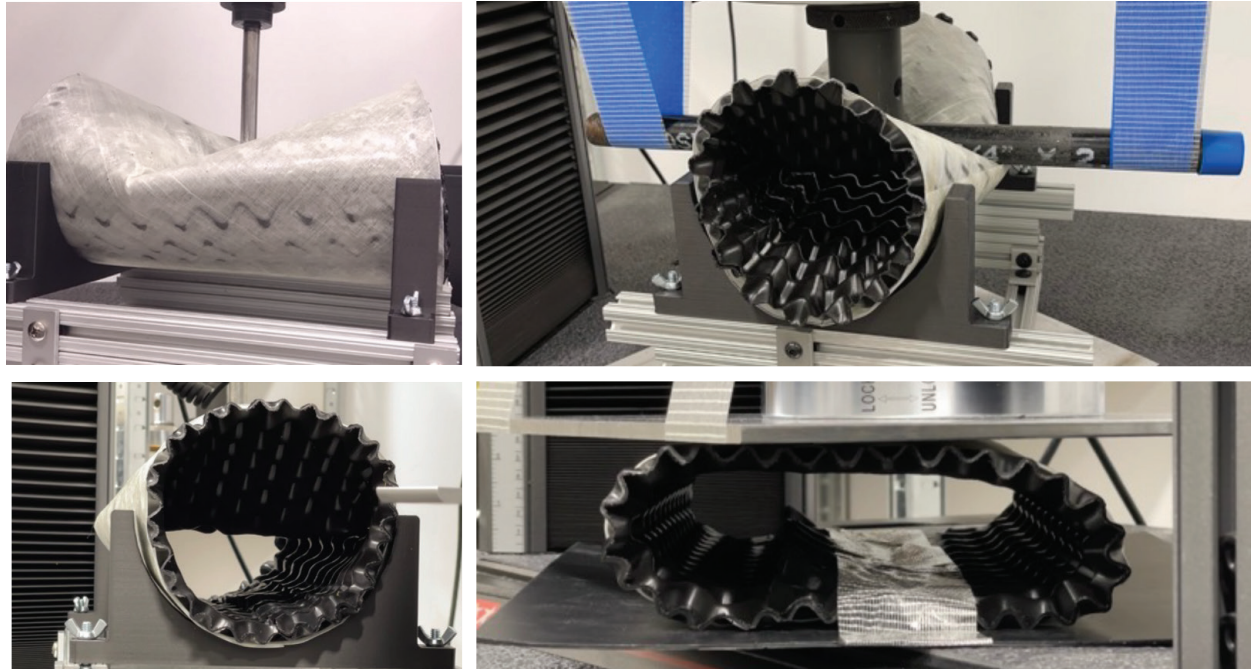
Standard test methods define consistent lab measurement practices. Real-world conditions, however, offer far less control and can lead to important differences compared to lab results. For example, crush tubes are typically engineered for axial loading. Off-axis loading occurring during a real-world collision is undesirable but provides a glimpse into the importance of ensuring first article approval includes all considerations relevant to the application.

Varying the contact method for radially oriented loads is already enough to generate an abundance of data for how a crush tube responds to different forms of undesired

off-axis collisions. Three distinct possibilities are: zero dimensional (0-D) point indenters, one dimensional (1-D) line indenters, and two dimensional (2-D) plate indenters. As before, GFRP, [MO] and [MO] + GFRP composite structures were fabricated with various orientations of the [MO] core relative to the crush tube's axis.

Destructive tests show that otherwise identical structures can give very different results when the indenter is varied. An infinite variety of testing conditions can be concocted to further test fabricated structures. Ideally, relevant methods should be articulated by designers so that composite fabricators have clear performance benchmarks to evaluate their work.





	Density (kg/m <sup>3</sup> )	Energy absorbed / mass (kJ/kg)		
		[MO] x-axis    cylinder axis	[MO] y-axis    cylinder axis	No [MO]
<b>GFRP (1-py)</b>				
0-D (Point Indenter)	1,740			0.089
1-D (Rod Indenter)	1,767			0.208
2-D (Plate Indenter)	1,703			0.039
<b>MO</b>				
0-D (Point Indenter)	122	0.081	0.078	
1-D (Rod Indenter)	118	0.097	0.071	
2-D (Plate Indenter)	121	0.133	0.238	
<b>MO + GFRP (1-ply)</b>				
0-D (Point Indenter)	234	0.255	0.177	
1-D (Rod Indenter)	271	0.351	0.344	
2-D (Plate Indenter)	232	0.195	0.070	

## 4.4. Compound-curved surfaces

### Relevant engineering examples

---

- Nose cones
- Aerodynamic bodies
- Hydrodynamic bodies

### Engineer's constraints and considerations

---

- Primary and secondary radii of curvature;
- Operational environment
- Modulus
- Strength
- Desired energy absorption

### Fabrication tips

---

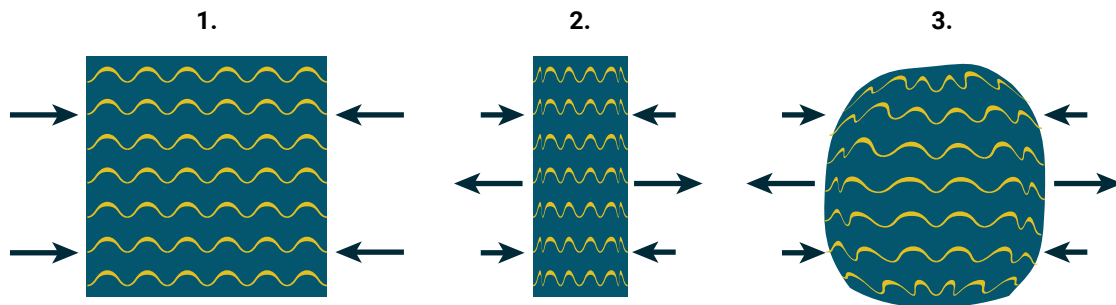
- |   |        |
|---|--------|
| <b>Tip 15</b> MetaCORE's negative Poisson's ratio makes fabricating parts with compound curvature easier than other materials.  | Pg. 57 |
| <b>Tip 16</b> Since there are a variety of proven methods for fabricating domes and structures with similar compound curvature, select the approach most suitable for the application's requirements.   | Pg. 58 |
| <b>Tip 17</b> Since there are fabrication-related differences in mechanical performance of domes, engineering and fabrication teams should work closely to define the right method for the application. | Pg. 59 |
| <b>Tip 18</b> Make sure the unit cell size is larger than the inverse curvature of the surface to keep mechanical properties predictable.   | Pg. 61 |

## Tip 15 | MetaCORE's negative Poisson's ratio makes fabricating parts with compound curvature easier than other materials

**Negative Poisson's ratio is an uncommon material property that can leveraged to make higher performance parts.**

The geometry of MetaCORE [MO] has a negative Poisson's ratio (see Section 2.2.1). This makes integration of MO into envelopes of positive Gaussian curvature easier than conventional core materials with positive Poisson's ratio.

1. Start by compressing the top and bottom of a sheet along the y-axis. Pin the four corners in place.
2. Next, pull the gathered material apart along the mid-line.
3. The negative Poisson's ratio property of the material will drive biaxial expansion in the middle of the sheet and induce a positive Gaussian curvature.



**Tip 16** | Since there are a variety of proven methods for fabricating domes and structures with similar compound curvature, select the approach most suitable for the application's requirements

### There's more than one way to form a dome

There are several ways to form surfaces with positive Gaussian curvature. In addition to leveraging MetaCORE's negative Poisson's ratio, four additional methods are proven. These methods are: darts, *papier mâché*, can-cuts, and direct forming. Each of these methods takes advantage of the unique properties of thermoplastics and their ability to be manipulated post-processing.

The darts method is akin to methods used in sewing. Triangles of materials are cut out of 4 corners. The remaining sheet is gathered and seamed together at each corner using heat and pressure.

The *papier mâché* method uses multiple strips of material which all overlap and interlock in the center. The strips are then folded up and seamed.

The can method seams together a circular flat sheet and a long strip that has been seamed together into a cylinder. This is different from the darts method because it involves multiple pieces, and different from *papier mâché* because the formed surface is single ply.

The direct forming method heats a flat sheet to the resin's working temperature then presses it into a mold of the desired shape to cool and set. This is the only method that does not require seams.



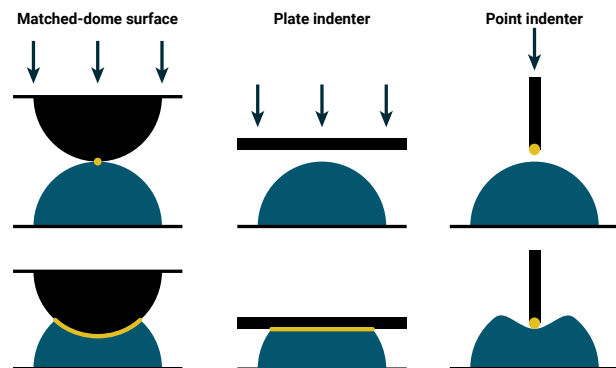
**Tip 17** | Since there are fabrication-related differences in mechanical performance of domes, engineering and fabrication teams should work closely to define the right method for the application

### Forming methods affect mechanical performance

Having options for how to fabricate a part with a complex envelope is useful since it provides Technicians application-specific flexibility. Destructive testing shows different methods for producing compound curvature yields different mechanical performance as measured by energy absorbed per unit mass. Understanding the relative merits of these approaches is therefore critical for producing high quality results with MetaCORE.

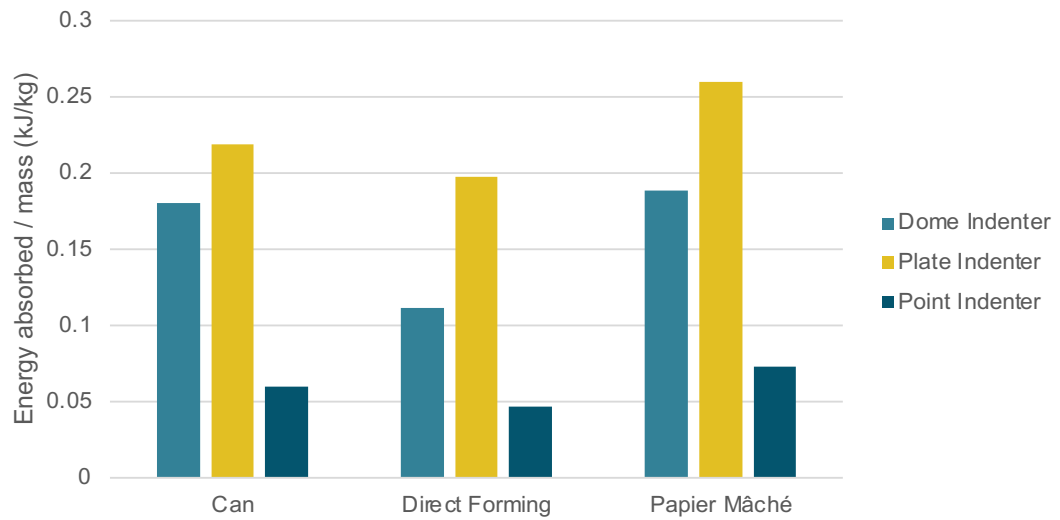
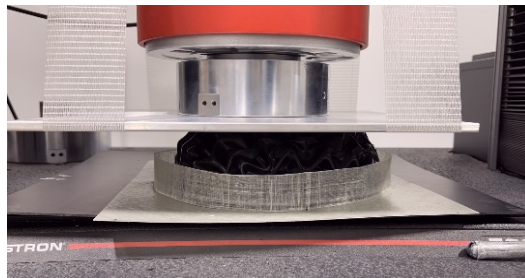
There is an abundance of standard and non-standard methods for evaluating mechanical performance in destructive tests. MetaCORE hemispheres were fabricated and indented using loads with various radii of curvature.

- **Curvature of dome = Curvature of indenter.** A matched-dome surface maintains an indentation with constant radius of contact.
- **Curvature of dome > Curvature of indenter.** A plate indenter is a surface with zero radius of curvature.
- **Curvature of dome < Curvature of indenter.** A point indenter is effectively a load with infinite radius of curvature.



The boundary conditions were held constant for each test by fixing the edges of the dome with a fiberglass cylinder of the same radius. This variety of indenter contact geometries leads to insights on the broadest possible range of real-world loading conditions.

The main finding is that fluctuations in mechanical properties were about 15% to 25% for different fabrication methods, and around 55% to 65% for different indenter geometries. This means there is about 3x to 4x more variability arising from the type of loading than from the fabrication method. Engineering and fabrication teams should use these insights and work closely to evaluate options at both design and testing phases before finalizing parts for production.



## Tip 18 | Make sure the unit cell size is larger than the inverse curvature of the surface to keep mechanical properties predictable

### Energy absorption is independent of dome diameter

Put enough atoms together and their effective behavior is that of a “material.” Put enough [MO] unit cells together and their effective behavior is that of a “metamaterial.” In the same way a few million atoms work collectively to define a material’s modulus and strength, few dozen unit cells work together to define the metamaterial’s modulus and strength.

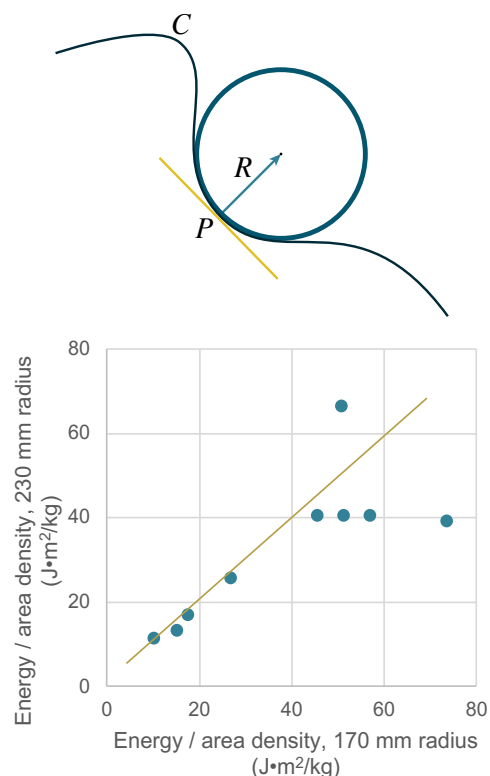
When fabricating metamaterial parts with curvature, it’s important to pay attention to the magnitude of the radius of curvature. Intuitively, a circle with radius  $R$  fit to a curved surface  $C$  at point  $P$  defines the local radius of curvature. For 2D surfaces, the same intuition works, but with ellipses aligned to the principal axes instead of plane circles. If the radius  $R$  is much larger than the [MO] unit cell size, then MetaCORE looks like a continuous material. If the radius  $R$  is similar to or smaller than the [MO] unit cell size, then finite size effects become important and notion of a metamaterial as a material becomes murky (see discussions of finite size in Section 2.6).

For heuristic purposes, design and fabricate parts with a radius of curvature larger than 4 or 5 unit cells for the most reliable results.

For sizes larger than the heuristic, it’s easy to show mechanical properties are predictable and consistent. Eighteen domes were fabricated; 9 had a radius of 170 mm, and 9 had a radius of 230 mm. Both sets of domes were fabricated using the can, direct forming,

and *papier mâché* methods (3 methods x 3 replicates x 2 radii = 18 parts). They were then destructively tested using the point, plate, and matched indenter tests. The energy absorbed by compression (J) was normalized by the area density ( $\text{kg}/\text{m}^2$ ) to calculate a metric independent of part size.

Comparing measurements with the same fabrication and indenter methods but different radii give a direct evaluation of the effect of curvature. Plotting measurements from different radii on each axis shows, aside from outliers, the results fit reasonably well to a line of slope 1. Hence, for sufficiently large radii of curvature, MetaCORE [MO] has size-independent properties just like conventional materials.



PART 5

# Appendices

## Appendix A: A primer on thermoforming

---

### A.1. Thermoforming concepts

Manufacturing MetaCORE with thermoforming involves heating a polymer sheet to the working temperature and forming it with MetaCORE mold tooling. In some applications, the tooling is one-part and utilizes vacuum to draw the heated polymer into the mold. For more demanding applications, two-part molds are utilized using a matched die forming method. Either way, thermoforming is highly cost effective for large production quantities or large part sizes. Thermoforming is also amenable to a wide variety of thermoplastic resin systems including neat and fiber-reinforced formulations.

A limitation of thermoforming is that large draw-depth tooling creates inherent variations in the structure's geometry that deviate from the intended design. As a result, polymer flow simulations and empirical prototyping should always be undertaken to evaluate performance when creating new tooling.

### A.2. Vacuum thermoforming

Vacuum thermoforming (Figure A1) is one of the most common methods to form material, and requires a polymer sheet, heaters, and a single mold tool equipped with appropriate vacuum and cooling channels.



**Figure A1:** In vacuum thermoforming a heated polymer sheet is placed on a mold which then applies a vacuum, pulling the sheet into full contact with the mold surface. After a predetermined amount of time the mold is released and the finished part is ready for trimming.

---

### A.3. Matched-die thermoforming

Matched die thermoforming (Figure A2) is a more capital-intensive method for thermoforming sheets because it requires

two molds instead of one, as well as a compression molding system capable of handling the added tooling. Heating, cooling, and sheet feeding requirements are otherwise the same as vacuum thermoforming.

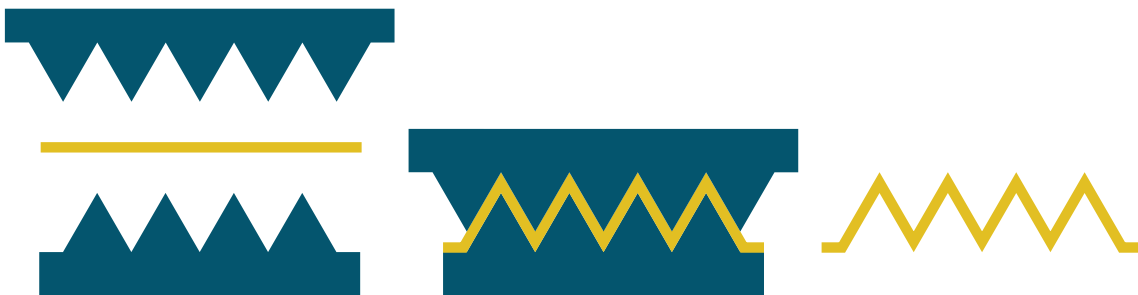


**Figure A2:** In matched die forming two molds "sandwich" a heat polymer sheet to form the final part. Advantages over vacuum thermoforming include uniformity of wall thickness, but often more machinery and tooling is required.

---

## A.4. Thickness variation from vacuum thermoforming

There are at least three important sources of thickness variation to identify and understand when working with thermoformed parts:

1. Variation between the initial unformed sheet's gauge and the final formed part's wall thickness
2. Long length-scale thickness variations spanning the part
3. Short length-scale thickness variation in the formed walls due to the vertical draw

For the first type of variation, a simple heuristic prediction can be made by using the Areal Draw Ratio (ADR) of the part to determine how the final thickness differs from the initial gauge. The ADR computes the surface area of the mold face and compares it to the area of the unformed blank. The resulting ratio is the factor by which one can anticipate global thinning of the formed part. A specific example is given in the next subsection.

For the second type of variation, independently controlled heating and cooling

zones on the thermoforming equipment can be configured to offset this effect.

For the third type of variation, it's important to understand the nature of vacuum thermoforming leads to wall thickness variations that are ultimately unavoidable. As the heated material touches the cooler mold, it immediately begins to lose malleability, and thus regions of the part that contact the mold first tend to have a larger thickness. This thickness variation can be predicted, but it is more difficult since it is dependent on several environmental variables.

With [MO] tooling, the cross-sectional thickness variations typically look like the following sketch with thicker "mountains" on "top" of the sheet, and thinner "valleys" on the "bottom" (Figure A3). These differences can become important in a handful of specific applications (see Section 4).

Importantly, the second and third type of wall thickness variations listed above are negligible in matched-die thermoforming when compared to vacuum thermoforming. As such, parts made with two-part tooling have more consistent thickness and are generally better for manufacturing high-performance parts.

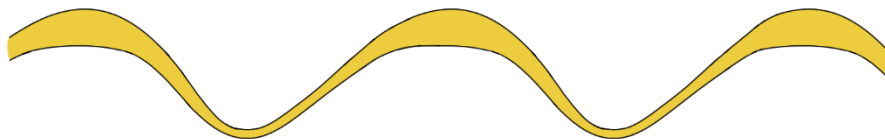


**Figure A3:** Schematic cross section based on MetaCORE [MO] of how wall thickness can vary in a thermoformed part. Areas higher up on the mold cool off sooner, and thus have a tendency to be thicker than parts lower in the mold.

## A.5. ADR for thermoformed MetaCORE

Both the size and geometric complexity of a part will affect the overall thickness variations and quality of the metamaterial being formed. Since metamaterials are based on well-defined mathematical parameters,

estimates for wall thickness variation can be made based on the geometry of the part. Figure A4 below shows the ADR of MetaCORE sheets for different sizes and shapes. The ADR should ideally be as low as possible to mitigate wall thickness variation from sag, as well as the local variations associated with steep walls.

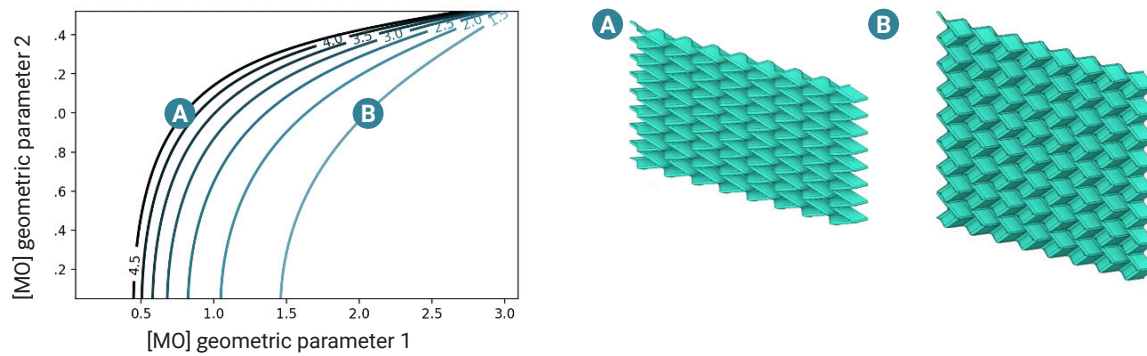


**Figure A4:** Left: a contour plot of ADR for a MetaCORE [MO] sheet. Different angles produce wildly different draw ratios. Right: rendering of the shapes from the contour plot with ADR of 4.5 and 1.5, respectively. (A) Has a steeper incline to the pattern, and as a result more surface area to form compared to (B). This change in draw ratio will lead to larger thickness changes in the final part.

## Appendix B: A primer on 3D printing

---

### B.1. Introduction

Additive manufacturing is a generic term describing any manufacturing processes wherein material is added to create the working part. 3D printing is a type of additive manufacturing technology that itself encompasses a wide variety of systems, technologies, and material choices. Two important uses of 3D printing are:

- Cost-effective rapid prototyping
- Small batch production with low-cost customization

Most of the 3D printers in operation today function by heating and extruding thermoplastic filament onto a build-plate. On one hand, there's no additional tooling costs when changing part designs. On

the other hand, parts are produced layer-by-layer at a relatively slow rate. Like with other manufacturing methods, these thermoplastics can be either neat or fiber reinforced. In fact, MetaCORE was largely prototyped and developed using 3D printing technology (Figure B1).

High-performance materials and industrial 3D printing systems are useful when small batch volumes of production-ready parts are involved. For example, carbon fiber reinforced resins, high-temperature corrosion-resistant polymers, and metal alloys are commercially available options (Figure B2). 3D printing with these materials makes mass customization of parts affordable, and supply chain logistics can be radically simplified by maintaining an ample supply of feedstock and a digital library of functional parts.

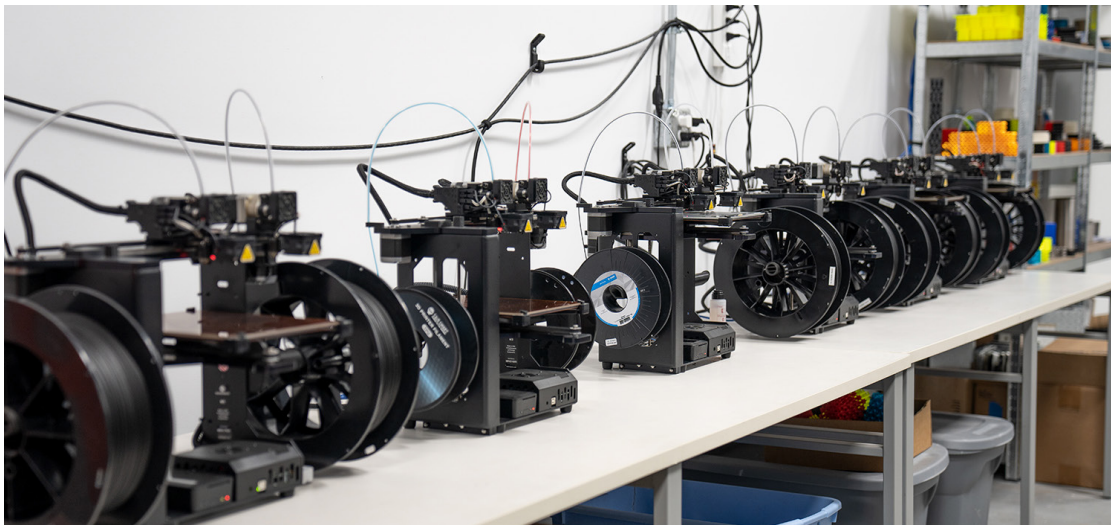


*Figure B1: Photograph of a 3D printer “farm” or “cluster” fabricating low-cost prototypes for design optimization. Each printer is producing a part with slightly different geometry. Each part will be mechanically tested to validate the relationship between geometry and performance.*

Considerable resources are necessary to fully understand the implications of 3D printing for mechanical metamaterials. Two of the important lessons learned from these ongoing efforts address:

- How to maintain part-to-part quality and consistency
- How to address orthotropy from the layer-by-layer fabrication process

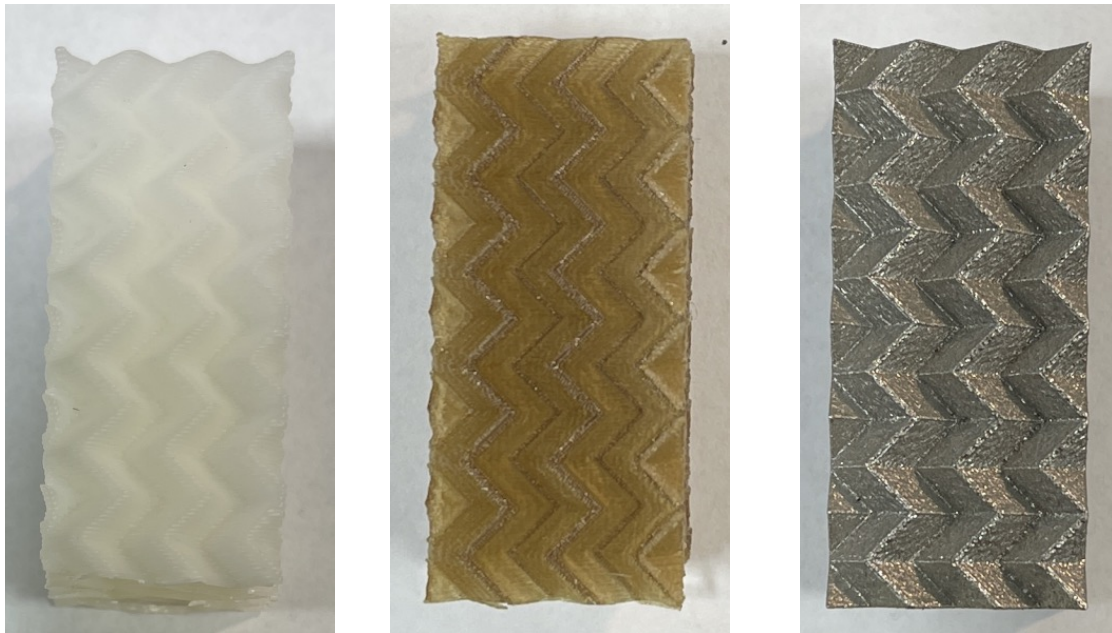


**Figure B2:** From left-to-right, 3D printed MetaCORE test coupons fabricated using low-cost commodity ABS, high-performance PEEK, and 316L stainless steel.

## B.2. Anisotropy in 3D printing

There are many different methods of 3D printing, with each approach's details determining the mechanical response of the final part. 3D printing by stereolithography

(SLA) and powder bed fusion (PBF) result in parts that are essentially isotropic, but fused filament fabrication (FFF) methods create parts that are orthotropic.

### B.3. Implications for metamaterials

FFF printed parts acquire intrinsic orthotropy from the printing method (see Appendix C). In addition, MetaCORE is also inherently orthotropic due to the geometry of the unit cell. The material orientation for an FFF printed MetaCORE part therefore has two sources of material anisotropy, one from the build orientation and one from the geometry of the cells. These sources need to be considered and potentially calibrated when performing experiments (Figure B3).

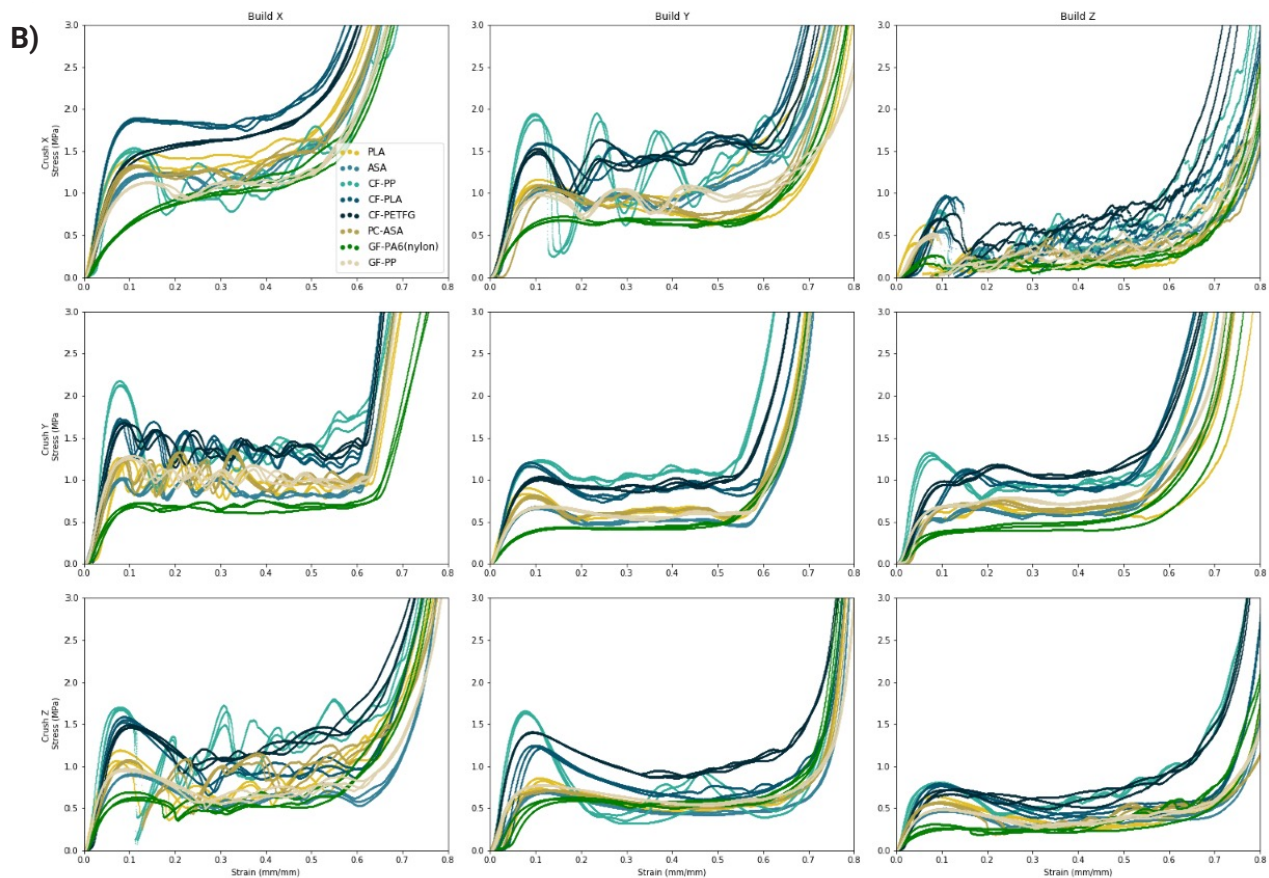
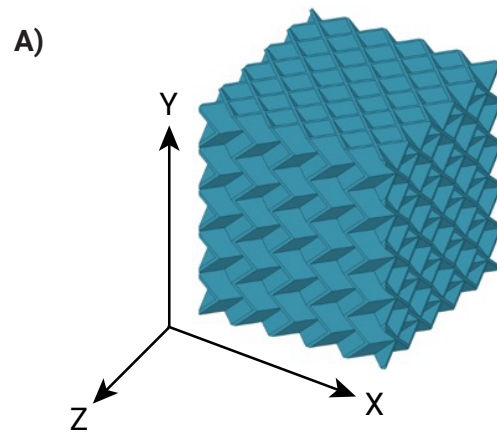


**Figure B3:** (A) MetaCORE [MO] has three principle axes labeled here. It can be 3D printed using FFF in all three directions. (B) This matrix of plots show stress-strain measurements for all pairs of possibilities of the printing direction ( $x,y,z$ ) and the compressive load direction ( $x,y,z$ ). Different colored lines correspond to different 3D printed materials. An important result is that all orientations have the same generic energy absorbing stress-strain response, but the strength and stiffness can vary depending on which pairs of printing and crushing directions are examined.

## Appendix C: Cellular solids

### C.1. Introduction

Cellular solids occur in both natural and engineered materials, from cork and bone to 3D printed architected materials like honeycomb and MetaCORE. The mechanics of a cellular solid depend in large part on the geometry and topology of interconnected struts or plates and is a relatively complicated area of continuum solid mechanics to fully understand. This appendix discusses the fundamentals of cellular solids and makes quantitative comparisons between honeycomb, foam, and MetaCORE.

### C.2. Symmetry and mechanics: A primer on anisotropic materials

Composite materials are often stronger in one direction than another since they are made from a combination of fiber reinforcement and a polymer matrix. The arrangement of the fiber reinforcement determines the ultimate mechanical behavior of the material. In the case of cellular solids like honeycomb and MetaCORE, the geometry itself affects the material characteristics. The overall directional dependence of a composite material is determined by its symmetry, and we discuss some of the more common arrangements below.

### C.3. Stiffness and compliance of a material

For a solid material, there are three compressive/tensile directions and three shear directions that determine how stiff or soft that material is when loaded along those

axes. Usually, these stiffnesses are gathered in a matrix to quantitatively determine the mechanical characteristics

$$\begin{pmatrix} \epsilon_{xx} \\ \epsilon_{yy} \\ \epsilon_{zz} \\ \epsilon_{xy} \\ \epsilon_{xz} \\ \epsilon_{yz} \end{pmatrix} = S \begin{pmatrix} \sigma_{xx} \\ \sigma_{yy} \\ \sigma_{zz} \\ \sigma_{xy} \\ \sigma_{xz} \\ \sigma_{yz} \end{pmatrix}$$

Here the matrix  $S$  is called the compliance matrix of the material and contains all the material characteristics required to relate the stress and strain in linear response.

### C.4. Isotropic materials

Conventional materials are usually isotropic, and they include most metals, ceramics, and plastics. The material has the same mechanical response in all directions. The compliance matrix is

$$S = \frac{1}{E} \begin{pmatrix} 1 & -\nu & -\nu & 0 & 0 & 0 \\ -\nu & 1 & -\nu & 0 & 0 & 0 \\ -\nu & -\nu & 1 & 0 & 0 & 0 \\ 0 & 0 & 0 & 1+\nu & 0 & 0 \\ 0 & 0 & 0 & 0 & 1+\nu & 0 \\ 0 & 0 & 0 & 0 & 0 & 1+\nu \end{pmatrix}$$

There are two elastic constants: the Young's modulus  $E$  and Poisson's ratio  $\nu$ .

### C.5. Transverse isotropic materials

Examples of transverse isotropic materials include unidirectional fiber-reinforced

materials and regular honeycomb. These types of materials have a slightly more complicated compliance matrix

$$S = \begin{pmatrix} \frac{1}{E_1} & -\frac{\nu_{21}}{E_1} & -\frac{\nu_{31}}{E_3} & 0 & 0 & 0 \\ -\frac{\nu_{12}}{E_1} & \frac{1}{E_1} & -\frac{\nu_{31}}{E_3} & 0 & 0 & 0 \\ -\frac{\nu_{13}}{E_1} & -\frac{\nu_{13}}{E_1} & \frac{1}{E_3} & 0 & 0 & 0 \\ 0 & 0 & 0 & \frac{2(1+\nu_{12})}{E_1} & 0 & 0 \\ 0 & 0 & 0 & 0 & \frac{1}{G_{13}} & 0 \\ 0 & 0 & 0 & 0 & 0 & \frac{1}{G_{13}} \end{pmatrix}$$

For these materials, there are five elastic constants: two Young's moduli  $E_1, E_2$ , a shear modulus  $G_{13}$ , and two Poisson's ratios  $\nu_{12}, \nu_{13}$ .

### C.6. Orthotropic materials

Examples of orthotropic materials include multi-ply composite lay-ups, and grid structures such as irregular honeycomb, orthogrids, and MetaCORE. The compliance matrix for an orthotropic material is

$$S = \begin{pmatrix} \frac{1}{E_1} & -\frac{\nu_{21}}{E_2} & -\frac{\nu_{31}}{E_3} & 0 & 0 & 0 \\ -\frac{\nu_{12}}{E_1} & \frac{1}{E_2} & -\frac{\nu_{32}}{E_3} & 0 & 0 & 0 \\ -\frac{\nu_{13}}{E_1} & -\frac{\nu_{23}}{E_2} & \frac{1}{E_3} & 0 & 0 & 0 \\ 0 & 0 & 0 & \frac{1}{G_{12}} & 0 & 0 \\ 0 & 0 & 0 & 0 & \frac{1}{G_{13}} & 0 \\ 0 & 0 & 0 & 0 & 0 & \frac{1}{G_{23}} \end{pmatrix}$$

There are nine independent elastic constants: three Young's moduli, three shear moduli, and three Poisson's ratios. Since the compliance matrix is symmetric, there is a reciprocal relationship between the Poisson's ratios and Young's moduli, which is why there are only three independent Poisson's ratios instead of the what looks like six:  $\nu_{ij}E_j = \nu_{ji}E_i$

### C.7. Orthotropic example: Honeycomb

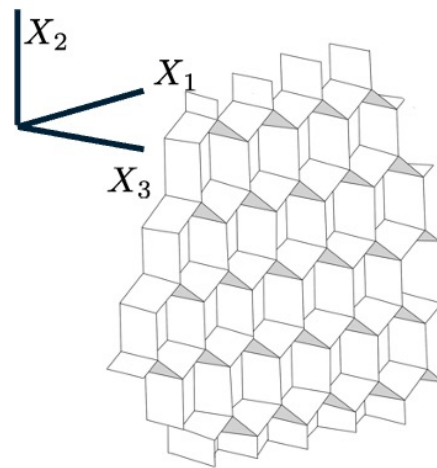


Figure C1: Schematic of honeycomb geometry.

Honeycomb structures (Figure C1) are often used as lightweight core materials in a variety of applications, from recreational equipment to load-bearing walls in aerospace vehicles. The repeated unit cell of the honeycomb puts it squarely in the cellular solid landscape, and this tessellated geometry simplifies some calculations for determining effective material properties.

The symmetry of the honeycomb means that it is an orthotropic solid, and thus requires nine independent elastic constants to fully specify its mechanical response. We will see below that honeycomb is highly anisotropic, with drastically different density scaling laws for its material properties.

### C.7.1. Geometric parameters

Honeycomb can be manufactured from a variety of different materials, including metals and thermoplastics, but the effective properties of the structure are largely determined by the geometry (Figure C2 schematically illustrates key variables). From these geometric parameters we can use the material properties of the solid (denoted by  $\rho_s, E_s$ , for the solid density, Young's modulus, etc.) to determine the effective material properties of the cellular honeycomb solid. For example, the effective density of the honeycomb is denoted by  $\rho^*$ , and we may determine this purely from geometry. For thin honeycombs, where the thickness  $t \ll l, h$ , the relative density scales as the solid density multiplied by the ratio of the thickness to the length. Specifically, we have that the relative density is equal to

$$\bar{\rho} = \frac{\rho^*}{\rho_s} = \left(\frac{t}{l}\right) \frac{h/l + 2}{2 \cos \theta (h/l + \sin \theta)}$$

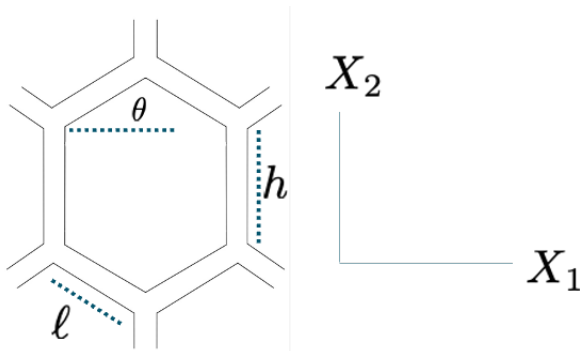


**Figure C2:** In-plane schematic of honeycomb.

It is important to distinguish the solid density, the effective density, and the relative density. For example, if we had an aluminum honeycomb with  $h = l = 10\text{mm}$ ,  $t = 1\text{mm}$ , and  $\theta = 60^\circ$ , the solid density

$\rho_s = 2,700 \text{ kg/m}^3$ , the value for bulk aluminum (which is independent of the geometry). In contrast, the effective density of this honeycomb is  $\rho^* = 312 \text{ kg/m}^3$  and the relative density is 11.5%.

### C.7.2. In-plane elastic properties

For in-plane loading we appeal to the symmetry of the unit cell to determine the force response of the structure. We apply a uniaxial stress, either in the  $X_1$  direction or the  $X_2$  direction. Each strut on the honeycomb is assumed to deform like a cantilever beam subjected to a load  $P$ , where  $P = \sigma_1 (h + l \sin \theta)H$  is calculated from the definition of stress ( $H$  is the length of the cell wall in the  $X_3$  direction). At the end points of each beam there is a torque  $M$ , such that  $M = Pl \sin \theta / 2$ . Standard beam theory calculations give that each beam deflects by an amount  $\delta = (Pl^3 \sin \theta) / (12E_s I)$ , where  $I$  is the moment of inertia of the cell wall ( $I = Ht^3 / 12$ ). The deflection can be used to determine the strain

$$\epsilon_1 = \frac{\delta \sin \theta}{l \cos \theta} = \frac{\sigma_1 (h + l \sin \theta)H}{12E_s I \cos \theta}$$

From this expression we may deduce the effective Young's modulus in the  $X_1$  direction

$$\frac{E_1^*}{E_s} = \left(\frac{t}{l}\right)^3 \frac{l \cos \theta}{(h + l \sin \theta)(\sin^2 \theta)}$$

Similar calculations can be used to deduce the Young's modulus in the  $X_2$  direction

$$\frac{E_2^*}{E_s} = \left(\frac{t}{l}\right)^3 \frac{(h + l \sin \theta)}{(l \cos^3 \theta)}$$

Calculating the in-plane Poisson's ratios come directly from the definition

$$\nu_{12}^* = -\frac{\epsilon_1}{\epsilon_2} = \frac{l(\cos \theta)^2}{(h + l \sin \theta) \sin \theta}$$

Similar calculations yield the in-plane shear modulus

$$G_{12}^* = \left(\frac{t}{l}\right)^3 \frac{h/l + \sin \theta}{(h/l)^2 (1 + 2 h/l) \cos \theta}$$

This accounts for four of the required nine elastic constants.

### C.7.3. Out-of-plane elastic properties

The out-of-plane Young's modulus is given simply by

$$\frac{E_3^*}{E_s} = \frac{\rho^*}{\rho_s}$$

The Poisson's ratios are also straightforward, with  $\nu_{31}^* = \nu_{32}^* = \nu_s$  and  $\nu_{13}^* = \nu_{23}^* = 0$ .

The shear moduli are more complex since the stress distribution in a sheared honeycomb is non-uniform. Nevertheless, upper and lower bounds may be set on these moduli, and we find that

$$\frac{G_{13}^*}{G_s} = \left(\frac{t}{l}\right) \frac{\cos \theta}{h/l + \sin \theta}$$

$$\frac{G_{23}^*}{G_s} = \left(\frac{t}{l}\right) \frac{h/l + \sin \theta}{(1 + 2 h/l) \cos \theta}$$

## C.8. Isotropic example: Foam

While many solid materials can be foamed, the most common foams we encounter are polymeric. Compared with honeycomb, foams are isotropic, so they can be described with two independent elastic constants instead of the nine required for an orthotropic solid.

### C.8.1. Linear elasticity of open cell foams

The simplest model of an open cell foam is a cubic array of struts with length  $l$  and square cross-sectional area of  $t^2$  (Figure C3). The mass of solid material in a unit volume is then  $m \sim t^2$ . Since the volume scales as the length cubed, the effective density of an open cell foam is  $\rho^* \sim (t/l)^2 \rho_s$ . The exact topology of the connecting struts needs to be known to find the proportionality constant missing from this expression. However, for scaling analysis, it is an order-one constant.

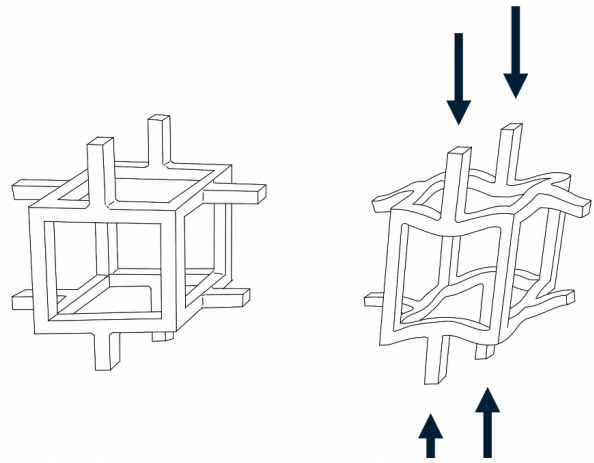


**Figure C3:** Foam schematic. Open celled foams can be represented as a series of beams that connect together in a skeleton. Under loading the skeleton deforms primarily by bending of these beams.

The Young's and shear moduli of the open cell foam both scale as the relative density squared,  $E^*/E_s \sim (\rho^*/\rho_s)^2$ . We can calculate this expression using a similar approach to one used in the analysis of honeycomb's elastic properties. If a force  $F$  is applied (Figure C3) we can use standard beam theory to determine how the strut will deflect. The deflection  $\delta$  is given by

$$\delta = \frac{Fl^3}{E_s I}$$

Where  $E_s$  is the Young's modulus of the solid, and the moment of inertia  $I$  for a beam is proportional to  $t^4$ . The compressive stress is  $\sigma = F/l^2$ , and the strain is  $\epsilon \sim \delta/l$ . Using the definition of the modulus we find that

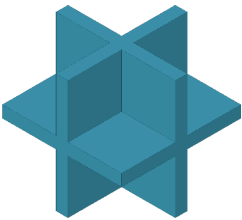
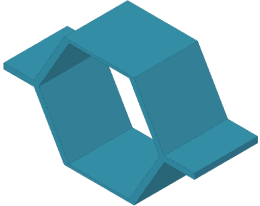
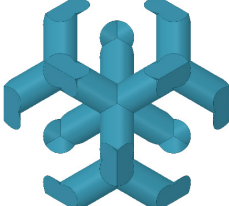
$$E^* = \frac{\sigma}{\epsilon} = \frac{F/l^2}{\delta/l} \sim \frac{E_s t^4}{l^4} \sim E_s (\rho^*/\rho_s)^2$$

### C.9. Honeycomb vs. Foam vs. MetaCORE

Honeycomb and foam mechanical properties have been extensively studied, and they have well-characterized relationships between stiffness, strength, and density. MetaCORE is more difficult to analyze, but it can be described well by distinguishing between several different types of cellular solids. The result of this analysis are characteristic scaling laws that relate the thermomechanical properties of the cellular material with the relative density, and other relevant geometric parameters. These scaling laws can then be compared to foam and honeycomb in an effort to understand their relative merits.

In general, cellular solids can be broadly categorized as being truss-like or plate-like,

with connectivity that is "bending-dominated" or "stretching-dominated". In the above examples, honeycomb is a plate-like cellular solid, and its in-plane properties are bending-dominated, while its out of plane properties are stretching-dominated. Open cell foams are lattice-like and bending dominated everywhere. Examples of cellular topologies that correspond to these categories are shown in the table below, and the expected scaling laws for various properties in the following tables.

Examples	Plate-like	Truss-like
Stretching-dominated	Cubic plate lattice 	Octet truss lattice 
	Honeycomb 	Diamond truss lattice 

Effective Young's Modulus	Plate-like	Truss-like
Stretching-dominated	$E \sim (\rho/\rho_s)$	$E \sim (\rho/\rho_s)$
Bending-dominated	$E \sim (\rho/\rho_s)^3$	$E \sim (\rho/\rho_s)^2$

Effective compressive strength	Plate-like	Truss-like
Stretching-dominated	$\sigma \sim (\rho/\rho_s)$	$\sigma \sim (\rho/\rho_s)$
Bending-dominated	$\sigma \sim (\rho/\rho_s)^2$	$\sigma \sim (\rho/\rho_s)^{3/2}$

The scaling laws for MetaCORE are a hybrid between what is expected for honeycomb and foam. Since MetaCORE is designed with *origami* principles, there are loading conditions under which it may deform freely, and thus behave like a bending-dominated plate-like structure (similar to honeycomb’s in-plane behavior). However, under general loading the complex geometry promotes a behavior that is in between stretching and bending. Moreover, MetaCORE under shear generically behaves as a stretching

dominated plate-like solid, achieving optimal scaling under shear load.

A summary table is provided below for comparisons between typical materials in their bulk form and values of mechanical properties in cellular solid form.

Property		Material				
		Metals	Rigid Foam	Al Honeycomb (perp, par)		MetaCORE
<b>Young’s modulus, <math>E</math></b>		-	$\sim \rho^2$	$\sim \rho_{\perp}^1$	$\sim \rho_{\parallel}^3$	$\sim \rho^{2.4}$
Typical range	MPSI	7 – 36	0.07 – 0.7	0.7 – 1.4	0.003 – 0.007	0.07 – 0.7
	GPa	50 – 250	0.05 – 0.5	5.0 – 10	0.02 – 0.05	0.05 – 0.5
<b>Shear modulus, <math>G</math></b>		-	$\sim \rho^2$	$\sim \rho_{\perp}^1$	$\sim \rho_{\parallel}^3$	$\sim \rho^1$
Typical range	MPSI	3 – 14	0.004 – 0.04	0.24 – 0.4	0.001 – 0.003	0.07 – 0.7
	GPa	20 – 100	0.03 – 0.3	1.7 – 3	0.007 – 0.02	0.05 – 0.5
<b>Uniaxial strength, <math>\sigma_c</math></b>		-	$\sim \rho^{3/2}$	$\sim \rho_{\perp}^{5/3}$	$\sim \rho_{\parallel}^2$	$\sim \rho^2$
Typical range	MPSI	14 – 100	0.07 – 1.4	2 – 6	0.1 – 0.5	0.07 – 1.4
	GPa	100 – 700	0.5 – 10	15 – 50	0.7 – 3.5	0.5 – 10
<b>Shear strength, <math>\sigma_s</math></b>		-	$\sim \rho^{3/2}$	$\sim \rho_{\perp}^1$	$\sim \rho_{\parallel}^3$	$\sim \rho^1$
Typical range	MPSI	8 – 60	0.04 – 0.4	1.5 – 3.0	0.08 – 0.15	0.07 – 1.4
	GPa	60 – 450	0.3 – 3.0	10 - 20	0.6 – 1.0	0.5 – 10
<b>Poisson Ratio, <math>\nu</math></b>		-	-	-	-	-
Typical values (unitless)		0.25 – 0.33	0.1 – 0.5	0	0.5 – 1	-6.0 – 9.0

## C.10. MetaCORE [EB]

The bulk of this design guide focuses on MetaCORE [MO], but there are several other geometries of interest derived from *origami* mathematics. One of those geometries is MetaCORE [EB].

[EB] exhibits high stiffness along one axis and promotes energy absorption across all three orientations. It has continuously connected channels across two axes to allow for thermal or fluid engineering as well as quality-of-life convenience for non-destructively integrating wiring or other cables.

[EB] is defined by the dihedral angle  $\theta$  and the sector angle  $\alpha$  (Figure C4). The representative volume element that makes up an actual solid is further defined with two lengths  $L_1$ ,  $L_2$ , and a thickness  $t$ . For very thin walls the orthorhombic dimensions in terms of two angles and two lengths are given by:

$$X = 2L_1 \sqrt{1 - \left(\frac{\cos \alpha}{\cos \theta}\right)^2}$$

$$Y = 2L_2 \sin \theta$$

$$Z = L_1 \cos \theta + L_2 \frac{\cos \alpha}{\cos \theta}$$

[EB] shows the same generic scaling law behavior as [MO].

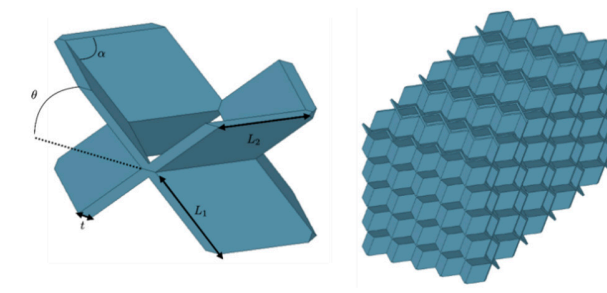


**Figure C4:** The [EB] unit cell and MetaCORE [EB] tessellation in a cuboidal envelope.

## C.11. MetaCORE [WB]

[WB] is a high-performing embodiment of MetaCORE best suited for additive manufacturing applications. Like other MetaCORE geometries, [WB] has continuously connected channels across two axes to allow for thermal or fluid engineering as well as quality-of-life convenience for non-destructively integrating wiring or other cables. Unlike the other MetaCORE geometries, [WB] is not defined by a system of parametric equations but simply by a length, width, and height (Figure C4). The representative volume element that makes up an actual solid is further defined with a thickness  $t$ .

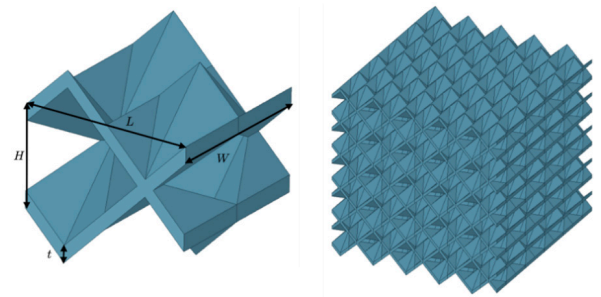


**Figure C5:** The [WB] unit cell and MetaCORE [WB] tessellation in a cuboidal envelope.

## Appendix D: MetaCORE in simulations

### D.1. Introduction

The theoretical underpinnings of MetaCORE are necessary for engineering new geometries, but they're largely unnecessary for many day-to-day applications. The primary method for computational analysis is performed using a homogenization technique in finite element analysis (FEA). This technique uses a Representative Volume Element (RVE) to perform FEA on a characteristic structure in order to distill the complex mechanics to an effective material. This appendix discusses some of the details behind the effects associated with analyzing RVEs, as well as the analytical details required to examine composite structures that are subjected to biaxial loading.

### D.2. RVEs using Computer Assisted Design (CAD)

The simple equations described in Section 2.2. of the design guide define the overall configuration of MetaCORE with zero wall thickness. This is considered the “*origami limit*” since *origami* is typically folded with paper that has effectively no thickness relative to the geometry's characteristic length scale.

To computationally model MetaCORE RVEs using CAD, the finite thickness of the part needs to be considered. One of the consequences of finite thickness is that a tolerance must be defined for overlap between the walls. This overlap tolerance modifies the volume and density of the cellular material. Using straightforward

trigonometry, we calculate the mass of the RVE to be

$$M_{RVE} = 4\rho_s L_1 W h \left(1 - \frac{13 \delta_x}{8 L}\right)$$

The effective density of the RVE is then given by

$$\rho_{RVE} = \frac{M_{RVE}}{(L - \delta_x)W(2H - \delta_z)}$$

Here the overlap tolerances  $\delta_x, \delta_y$  are defined in terms of the overall RVE dimensions. As shown in the (Figure D1), the density is given by solid lines and the calculated RVE density from finite element analysis is given as dots. Agreement is good. This is an approximation that may not hold for all thicknesses, but for  $t \ll L_1, L_2$  we expect that it will be fairly accurate. Note that the density of the [MO] configuration is non-monotonic in the angles  $\theta$  and  $\alpha$ . Determining the minimal density for a particular wall thickness, angles, and lattice size can be done using these formulae.

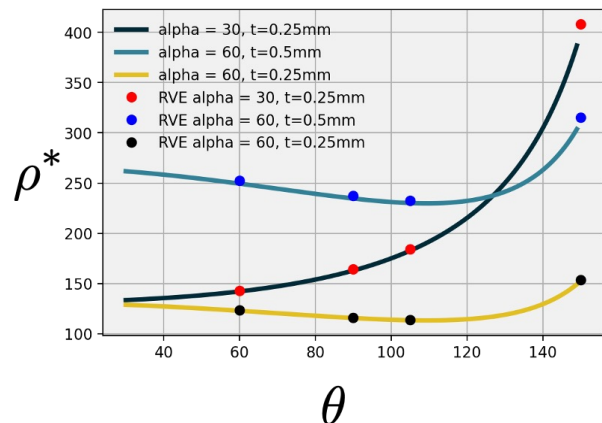


**Figure D1:** Effective density of [MO] RVE for various values of the geometric parameters. Solid lines are predictions from the equation for  $\rho_{RVE}$ , points are from simulations. There is near perfect agreement over a wide range of parameters.

### D.3. Material cards using RVEs

The homogenization procedure is used to calculate effective material properties for particular geometries. This method works

for both truss and plate-like geometries. An example for a lattice geometry for [EB] is shown in Figure D2.

Name	Values[0]	Values[1]	Values[2]	Values[3]	Values[4]	Values[5]	Values[6]	Values[7]	Values[8]	Values[9]	Unit
Image											
<b>Parameters</b>											
Volume Fraction	0.05	0.1	0.15	0.2	0.25	0.3	0.35	0.4	0.45	0.5	
<b>Engineering Constants</b>											
E1	5.2937E+08	2.1257E+09	4.6953E+09	8.1971E+09	1.2671E+10	1.8131E+10	2.4702E+10	3.2482E+10	4.1602E+10	5.2089E+10	Pa
E2	5.0688E+08	2.0461E+09	4.5409E+09	7.9617E+09	1.2347E+10	1.7728E+10	2.4228E+10	3.1939E+10	4.1002E+10	5.1438E+10	Pa
E3	3.1327E+08	8.0865E+08	1.5439E+09	2.6001E+09	4.074E+09	6.0809E+09	8.795E+09	1.2383E+10	1.7083E+10	2.3097E+10	Pa
G12	1.1194E+09	2.4864E+09	4.1151E+09	6.0414E+09	8.3033E+09	1.0918E+10	1.3913E+10	1.7301E+10	2.1059E+10	2.5167E+10	Pa
G23	5.2451E+08	1.227E+09	2.129E+09	3.2667E+09	4.6796E+09	6.4064E+09	8.5059E+09	1.1035E+10	1.4048E+10	1.7587E+10	Pa
G31	5.2832E+08	1.237E+09	2.1479E+09	3.2976E+09	4.7259E+09	6.4701E+09	8.5889E+09	1.1138E+10	1.4165E+10	1.7714E+10	Pa
nu12	0.80727	0.65241	0.54733	0.47301	0.41729	0.3738	0.33785	0.30796	0.28298	0.26347	
nu13	0.28017	0.43893	0.51239	0.53776	0.53814	0.52579	0.50806	0.48957	0.4721	0.456	
nu23	0.27306	0.42824	0.49999	0.52459	0.52548	0.51367	0.49705	0.47994	0.46394	0.44973	
<b>Density</b>											
rho	392.5	785	1177.5	1570	1962.5	2355	2747.5	3140	3532.5	3925	kg m <sup>-3</sup>
<b>Thermal Conductivity</b>											
K1	1.4759	3.1621	5.0267	7.0718	9.3105	11.749	14.41	17.308	20.436	23.777	W m <sup>-1</sup> C <sup>-1</sup>
K2	1.4524	3.1164	4.9606	6.9874	9.2092	11.633	14.285	17.177	20.304	23.649	W m <sup>-1</sup> C <sup>-1</sup>
K3	0.61893	1.3944	2.3165	3.3991	4.6636	6.1362	7.8588	9.8682	12.206	14.895	W m <sup>-1</sup> C <sup>-1</sup>
<b>Specific Heat</b>											
cp	434	434	434	434	434	434	434	434	434	434	J kg <sup>-1</sup> C <sup>-1</sup>
<b>Generated Material</b>											
Include	<input checked="" type="checkbox"/>										
<b>Logs</b>											
RVE log											
Solver logs											

**Figure D2:** The volume fraction for the truss lattice is varied from 5% to 50%, with fixed geometric parameters. This parametric variation results in an effective material for each RVE, which behaves as an orthotropic material with the properties shown here. This procedure can be used for the plate-like geometries as well, resulting in the material properties reported in Part 2.

#### D.3.1. Young's modulus

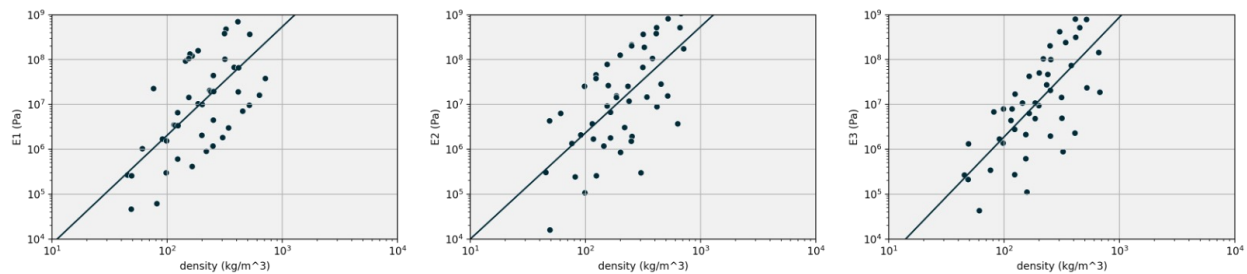


**Figure D3:** Young's moduli in all three material directions as a function of density. [MO] not only spans several orders of magnitude in both density and stiffness, but the scaling exponent is robustly determined to be ~2.4.

As described in Appendix 3, cellular solids tend to have clear scaling laws for the mechanical properties of the effective material, often given in terms of the density. The scaling of MetaCORE Young’s moduli in Figure D4 are generally between that of an isotropic foam and the compliant direction of honeycomb, with a relative modulus scaling according to the relative density like

$$\frac{E^*}{E_s} \sim \left(\frac{\rho^*}{\rho_s}\right)^{2.4}$$

The explanation for this result is currently qualitative. Truss-like cellular structures that are bending-dominated exhibit a scaling

exponent of 2, while stretching-dominated structures exhibit an exponent of 1. Plate-like cellular structures that are bending dominated exhibit a scaling exponent of 3, while stretching-dominated exhibit an exponent of 1. The intermediate behavior of MetaCORE is due to the complex interaction between bending and stretching that *origami*-inspired architectures display, but a prediction for the exact exponent remains elusive.

The functional dependence of the modulus on the *origami* angle parameters is also of some interest. For a fixed ratio of wall thickness to lengths  $L_1$  and  $L_2$ , the elastic moduli obey a more complicated relationship than a simple scaling law, but it can still be understood intuitively.

### D.3.2. Shear Modulus

The shear modulus has a similar scaling relationship, although it remarkably appears

to behave like a stretching-dominated solid, with an exponent close to 1. The functional dependence on density of the three shear moduli are shown in Figure D4.

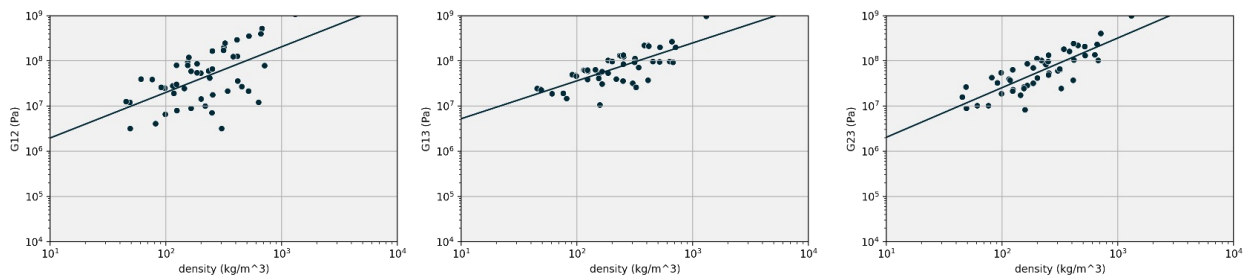


**Figure D4:** Shear moduli as a function of density. A scaling exponent near 1 is found for all three directions.

### D.3.3. Poisson’s ratio

The calculated Poisson’s ratio from *origami* mathematics relies on assumptions about rigid body rotation and constraints on folding, while the calculated Poisson’s ratio from RVEs are found via linear FEA analysis of the ratio of strains. How well do these two metrics compare? The data shows that

the agreement is quite good (Figure D5). In fact, Poisson’s ratio for RVE calculations is weakly dependent on wall thickness  $t$ , but the agreement is quite good in general. While the zero-thickness predictions for *origami*-based RVEs requires the finite thickness corrections to produce reasonable results, the zero thickness Poisson’s ratio predictions can be used to track qualitative (and in some cases

quantitative) functional dependence on the geometric parameters.

### D.3.4. Nonlinear properties

The homogenization analyses described above predict only the linear properties of

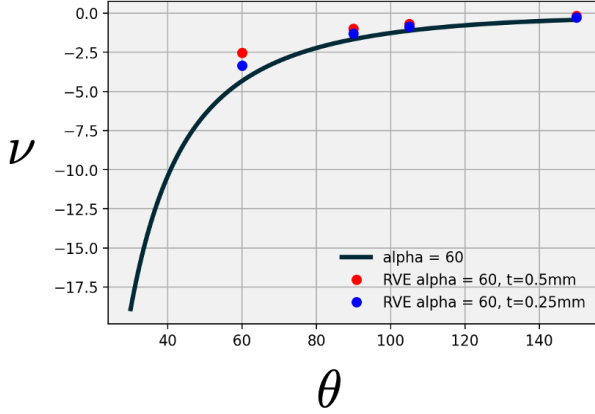


**Figure D5:** Poisson's ratio in the {12} plane as a function of the dihedral angle. Predictions from the equation in Part 2 are shown as a solid line, simulations with finite thickness are shown as dots. There is excellent agreement over a wide range of parameters. Note that [MO] is auxetic in this plane, so Poisson's ratio is negative everywhere.

a cellular solid. To capture the nonlinear behavior of MetaCORE we need to introduce nonlinear constitutive relationships. Based on the experimental results for compression of MetaCORE, we model the nonlinear constitutive response of the material by a multilinear kinematic hardening law (Figure D6). For low strain the material responds according to the Young's moduli, but for larger strains the large deformations of the cellular material leads to a plateau in the stress, before densification causes a diverging stress response at large strain. The multilinear kinematic hardening law defines a yield stress  $\sigma_Y$  whose value depends on internal material variables, which in this case is the plastic strain. Thermomechanical properties are not accounted for in this model. To account for the orthotropy of the material we invoke

a version of the Hill Yield Criterion that defines the equivalent stress in terms of the multilinear kinematic yield stress

$$\sigma_{eq} = \sqrt{\sigma M \sigma^T} = \sigma_Y$$

When the equivalent stress in the material is equal to the yield stress the material will fail. The equivalent stress is defined in terms of a stress-energy composed of current stress state  $\sigma$  and the plastic compliance matrix  $M$  is given by the convoluted system of variables and parameters

$$M = \begin{pmatrix} G + H & -H & -G & 0 & 0 & 0 \\ -H & F + H & -F & 0 & 0 & 0 \\ -G & -F & F + G & 0 & 0 & 0 \\ 0 & 0 & 0 & 2L & 0 & 0 \\ 0 & 0 & 0 & 0 & 2N & 0 \\ 0 & 0 & 0 & 0 & 0 & 2M \frac{1}{G_{23}} \end{pmatrix}$$

Where

$$F = \frac{1}{2} \left( \frac{1}{R_2^2} + \frac{1}{R_3^2} - \frac{1}{R_1^2} \right)$$

$$G = \frac{1}{2} \left( \frac{1}{R_3^2} + \frac{1}{R_1^2} - \frac{1}{R_2^2} \right)$$

$$H = \frac{1}{2} \left( \frac{1}{R_1^2} + \frac{1}{R_2^2} - \frac{1}{R_3^2} \right)$$

$$L = \frac{3}{2} \left( \frac{1}{R_{12}^2} \right)$$

$$N = \frac{3}{2} \left( \frac{1}{R_{23}^2} \right)$$

$$M = \frac{3}{2} \left( \frac{1}{R_{13}^2} \right)$$

And  $R_i = \frac{\sigma_i}{\sigma_Y}$  ,  $R_{ij} = \sqrt{3} \frac{\tau_{ij}}{\sigma_Y}$

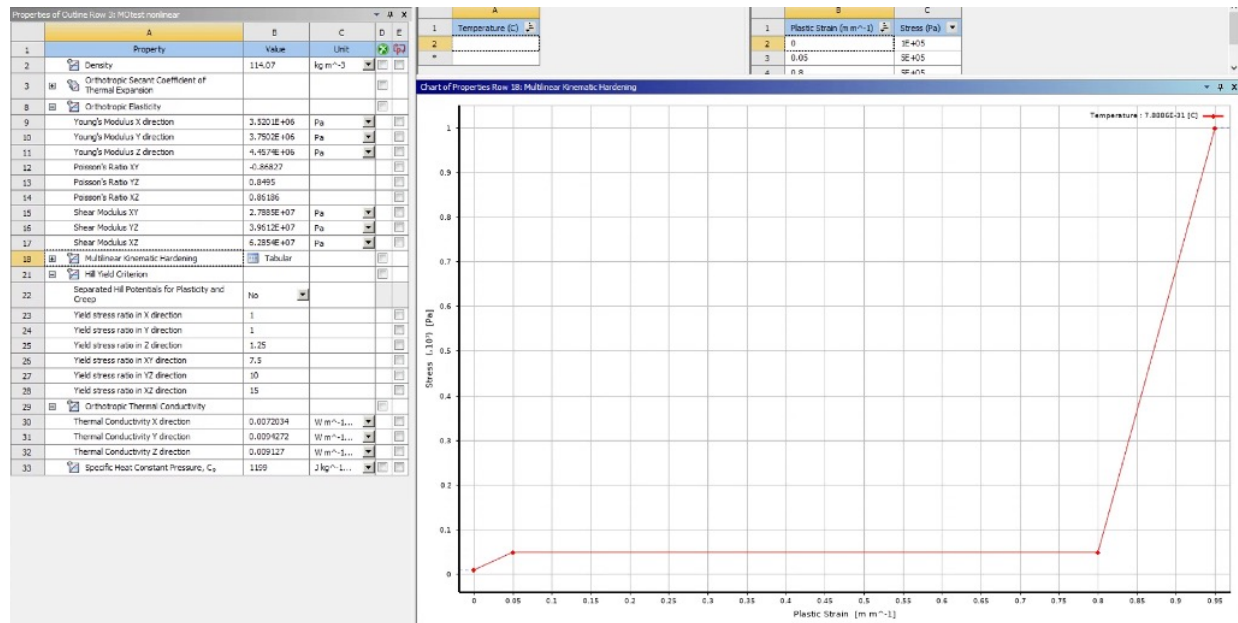


**Figure D6:** Screenshots of an effective material card representing MetaCORE used when modeling structures in FEA.

This model allows us to define a generic yield surface for an orthotropic solid that has six independent plastic yield stresses, which must all be determined from experiment or estimated using first principles.

### D.4. Laminates

The elastic properties described above specifically refer to the principal axes of the material. When an orthotropic material is subjected to uniaxial loading along a direction that is not along a principal axis, or when multiaxial loading conditions of any kind are introduced, then the effective response can change dramatically depending on the orientation of the load. We visualize the properties of orthotropic solids both in and out of plane by using some straightforward but tedious linear algebra.

When constructing a composite laminate, a three-dimensional solid is sliced into 2D

sheets, layered one on top of the other, and consolidated into a solid laminate. Because MetaCORE's unit cell has a complex geometry, arbitrary layup angle is not possible. Nevertheless, classical laminate theory can still inform us about the directional dependence of 2D sheets of MetaCORE. The compliance matrix defined for anisotropic solids is with respect to the principal directions of the RVE. For a lamina, assuming plane stress conditions reduces the problem to a 2D situation where the relationship between in-plane stresses and strains are now given by

$$\begin{pmatrix} \epsilon_{11} \\ \epsilon_{22} \\ \epsilon_{12} \end{pmatrix} = \begin{pmatrix} S_{11} & S_{12} & S_{16} \\ S_{12} & S_{22} & S_{26} \\ S_{16} & S_{26} & S_{66} \end{pmatrix} \begin{pmatrix} \sigma_{11} \\ \sigma_{22} \\ \sigma_{12} \end{pmatrix}$$

The plane stress assumption (i.e.,  $\sigma_{33} = 0$ ) reduces the general stress-strain relationship to a smaller system of two in-plane principal

strains and a single shear strain. We show the general compliance matrix but note that for orthotropic laminates  $S_{16} = S_{26} = 0$ . In physical terms this means that there is no coupling between uniaxial stretching and shear.

To measure the compliance in-plane at an angle  $\beta$  with respect to the original principal axes, a new compliance matrix  $\bar{S}$  needs to be defined. For an orthotropic laminate the elements of  $\bar{S}$  are given by

$$\bar{S}_{11} = S_{11} \cos^4 \beta + (2S_{12} + S_{66}) \sin^2 \beta \cos^2 \beta + S_{22} \sin^4 \beta$$

$$\bar{S}_{12} = S_{12}(\sin^4 \beta + \cos^4 \beta) + (S_{11} + S_{22} - S_{66}) \sin^2 \beta \cos^2 \beta$$

$$\bar{S}_{22} = S_{22} \cos^4 \beta + (2S_{12} + S_{66}) \sin^2 \beta \cos^2 \beta + S_{11} \sin^4 \beta$$

$$\bar{S}_{66} = 2(2S_{11} + 2S_{22} - 4S_{12} - S_{66}) \sin^2 \beta \cos^2 \beta + S_{66}(\sin^4 \beta + \cos^4 \beta)$$

### D.5. In-plane behavior of single ply orthotropic materials

We can use the information developed in the previous section to compare how lamina of MetaCORE behave in-plane, and how the different cross-sections behave. For a sample of MetaCORE made from APET, with  $\theta=105^\circ$ ,

$\alpha=60^\circ$ ,  $L_1=L_2=6$  mm, and a wall thickness of 0.5 mm, an RVE analysis yields  $E_1=21$  MPa,  $E_2=26$  MPa,  $E_3=27$  MPa,  $G_{12}=60$  MPa,  $G_{23}=87$  MPa,  $G_{13}=131$  MPa,  $\nu_{12}=-0.675$ ,  $\nu_{23}=0.8$ , and  $\nu_{13}=0.8$ . Using the formulae above we may visualize the Young's and shear moduli in-plane for three different cross-sectional planes (Figure D7):

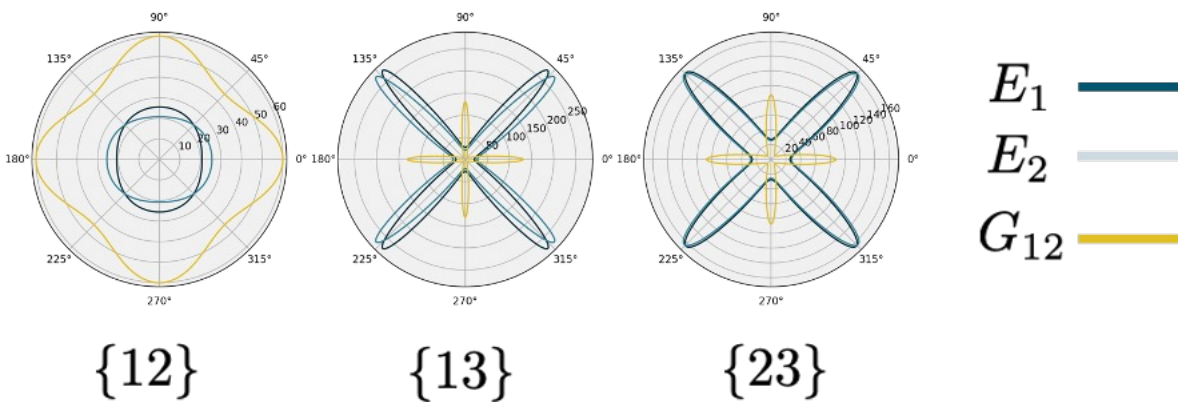


**Figure D7:** Polar plots of Young's and shear moduli in the {12}, {13}, and {23} planes for  $\theta=105^\circ$ ,  $\alpha=60^\circ$ ,  $L_1=L_2=6$  mm, and a wall thickness of 0.5 mm. Interesting notes include the shear modulus exceeding the Young's modulus in the {12} plane, a phenomenon that cannot occur in conventional isotropic solids.

The most interesting case is potentially the {12} plane, since the shear modulus is actually larger than the Young's moduli. The other planes have large stiffnesses bisecting the principal axes, which can be justified by

looking at the material and observing that the facets are primarily oriented along these lines. Changing the geometry to a different set of angles and lengths ( $\theta=105^\circ$ ,  $\alpha = 80^\circ$ ) the polar plots change:

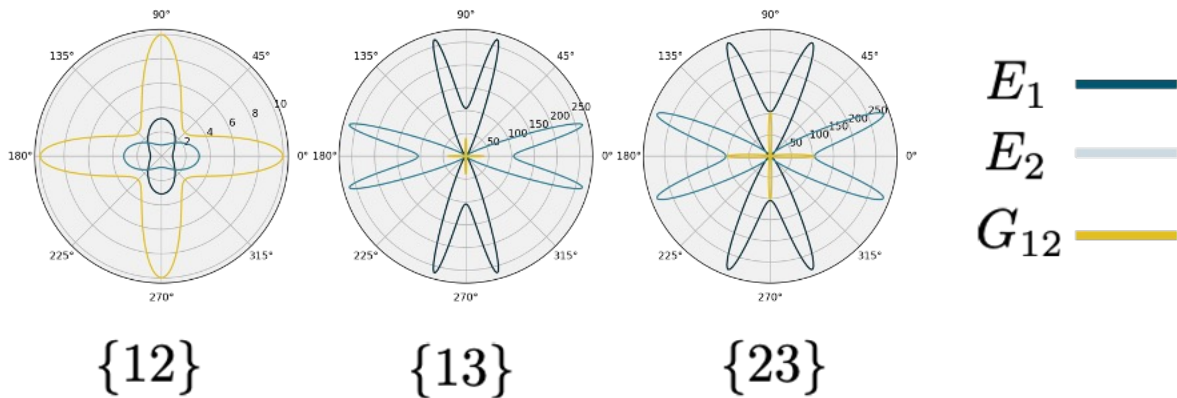


**Figure D8:** Polar plot of Young's and shear moduli in the {12}, {13}, and {23} planes. Interesting notes include the shear modulus exceeding the Young's modulus in the {12} plane, a phenomenon that cannot occur in conventional isotropic solids.

The Poisson's ratio can also be visualized according to the directional dependence.

Examples are shown below.

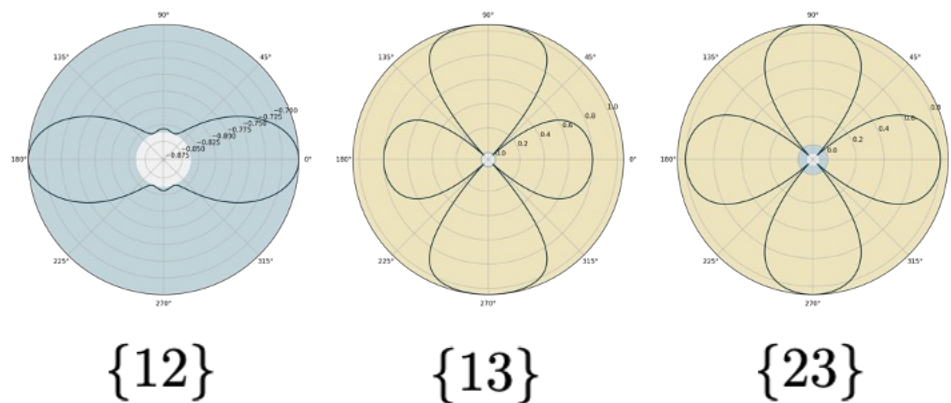


**Figure D9:** Polar plot of Poisson's ratio in three different planes for  $\theta=105^\circ$ ,  $\alpha=60^\circ$ ,  $L_1=L_2=6$  mm, and a wall thickness of 0.5 mm. Blue shading denotes auxetic, tan denotes meiotic. Note that the {12} plane is always auxetic, with only small variability with angle, while the other two planes have large variability that localizes sharply at certain angles. Extreme values of Poisson's ratio can lead to stress and delamination, so understanding these values is important.

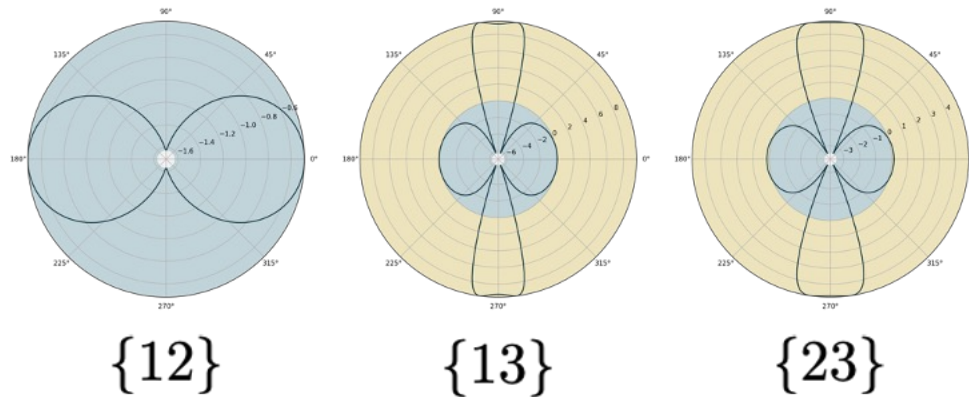


**Figure D10:** Polar plot of Poisson's ratio in three different planes for  $\theta=105^\circ$ ,  $\alpha=80^\circ$ ,  $L_1=L_2=6$  mm, and a wall thickness of 0.5 mm. Blue shading denotes auxetic, tan denotes meiotic. Interestingly enough, the behavior changes from auxetic to meiotic as a function of angle when examining the {13} and {23} plane.

### D.6. 3D anisotropy

In addition to studying 2D lamina of MetaCORE, we can also look at full 3D representations of the anisotropy. This is not always the most useful tool since 3D renders are difficult to appreciate when presented as static figures (Figure D9). Nevertheless, it can give a general sense for the anisotropy of the material response.

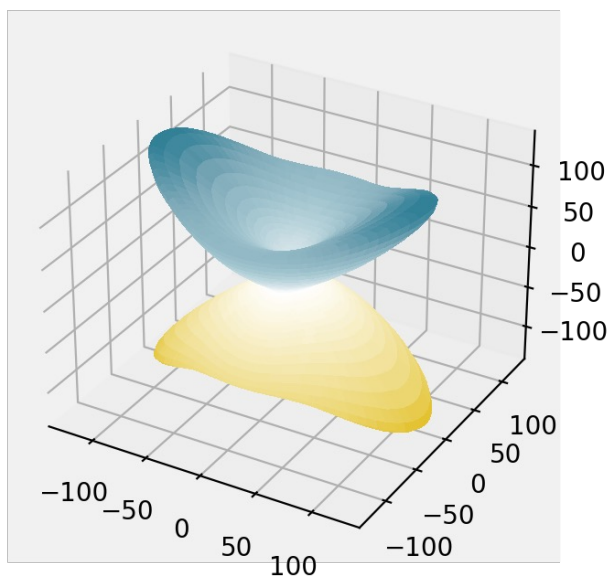


**Figure D11:** 3D plot of the Young's modulus for [MO] with  $\theta=105^\circ$ ,  $\alpha=60^\circ$ ,  $L_1=L_2=6$  mm, and a wall thickness of 0.5 mm. Axis units are in MPa.

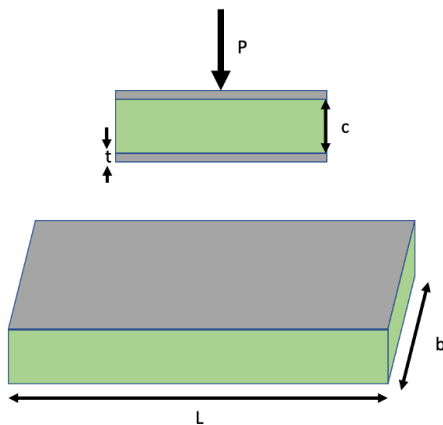
## Appendix E: Sandwich panels

### E.1. Introduction

Sandwich panels are used in a variety of applications to reduce the weight of structural components without lowering stiffness or strength. To design a new panel, details about the materials and their configuration, as

well as loading and failure conditions need to be understood. This appendix addresses some of these details, such as geometry, loading conditions, stiffness and strength calculations, panel failure modes, and optimality.

### E.2. Geometry of a sandwich panel



Geometrical parameters:

1.  $b$  – width of a rectangular sandwich beam
2.  $c$  – core thickness
3.  $d$  – distance between centroids of faces ( $d = c + t$ )
4.  $L$  – span of a sandwich beam
5.  $t$  – thickness of the faces

**Figure E1:** Schematic of a sandwich panel. **Top:** plan view of panel showing central load  $P$  (other loading conditions are shown in subsequent table). Core thickness is  $c$ , and face thickness is  $t$ . **Bottom:** orthographic view of sandwich panel, with length (also called span)  $L$  and width  $b$ .

	Face	Cellular or foamed core	Solid core
Density	$\rho_f$	$\rho_c^*$	$\rho_s$
Young's modulus	$E_f$	$E_c^*$	$E_s$
Shear modulus	-	$G_c^*$	-
Yield strength	$\sigma_{yf}$	$\tau_c^*$	$\tau_c$

These characteristics are for a sandwich beam where both the faces and the core are isotropic. It is more complicated when the core is orthotropic, such as for honeycomb or MetaCORE, or if the face is a fiber reinforced plastic (FRP) material with directional dependence. The calculations are all similar, but slightly more involved.

### E.3. Sandwich panel stiffness: equivalent flexural rigidity

When loaded in bending, a sandwich panel behaves like a beam with an effective moment of inertia. This moment of inertia is determined using the parallel axis theorem, and is represented by three separate terms

$$(EI)_{eq} = \frac{E_f b t^3}{6} + \frac{E_c b c^3}{12} + \frac{E_f b t (c + t)^2}{2}$$

These terms are associated with the bending of the faces about their respective centroids, the bending of the core about its centroid, and the bending of the skins about the centroid of the sandwich. Usually, the faces are much thinner than the core, and are much stiffer than the core, so this term may be approximated as

$$(EI)_{eq} \approx \frac{E_f b t c^2}{2}$$

Note that this approximate flexural rigidity is proportional to the stiffness of the faces, with no dependence on the core stiffness, and the flexural rigidity depends quadratically with the core thickness. Thus, the most efficient way to increase the stiffness of the panel is to increase the thickness of the core.

### E.4. Sandwich panel stiffness: Equivalent shear rigidity

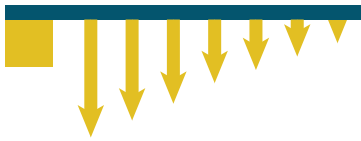
Since a sandwich panel has finite thickness, the effect of shear rigidity of the core can come into play, and the equivalent shear rigidity of the sandwich panel is given as follows

$$(AG)_{eq} = \frac{b(c + d)^2 G_c^*}{c}$$

This term is generally much smaller than the flexural rigidity, and thus its effects can often be neglected, but there are conditions under which it must be accounted for, such as short panels with very soft core materials. These conditions are discussed in detail in Section E.6.

### E.5. Loading conditions

While the flexural and shear rigidity of a panel are intrinsic characteristics, meaning they are determined entirely by the geometry and material composition, the loading conditions on a panel will ultimately affect what forces and deflections are measured. Several common loading conditions are summarized below, along with the maximum shear force, bending moment, and geometric constants. The constants  $B_1$ ,  $B_2$  are geometric factors that enter the force-displacement relationship and are defined by the particular loading and boundary conditions.

Loading type	Max shear force	Max bending moment	$B_1$	$B_2$
<b>Cantilever</b> (one end fixed, end load) 	$P$	$PL$	3	1
<b>Cantilever</b> (one end fixed, distributed load) 	$P$	$PL/2$	8	2
<b>Three-point bend</b> (simply supported, central load) 	$P/2$	$PL/4$	48	4
<b>Three-point bend</b> (simply supported, distributed load) 	$P/2$	$PL/8$	384/5	8
<b>Three-point bend</b> (fixed ends, central load) 	$P/2$	$PL/8$	192	8
<b>Three-point bend</b> (fixed ends, distributed load) 	$P/2$	$PL/12$	384	8
<b>Hydrostatic load</b> 	$P$	$PL/3$	15	3

## E.6. Deflection

When a sandwich beam is deformed, a portion of the response arises due to bending, and a portion arises due to shear. The deflection  $\delta$  of the beam is a linear combination of the bending and shear components, so it may be written as

$$\delta = \delta_{bend} + \delta_{shear} = \frac{PL^3}{B_1(EI)_{eq}} + \frac{PL}{B_2(AG)_{eq}}$$

Note that each deflection contribution is a result of Hooke's law for the loading condition, using the effective rigidity for the type of deflection that is occurring. The overall stiffness of this sandwich panel is given by

$$K = \frac{P}{\delta} = \frac{1}{\frac{L^3}{B_1(EI)_{eq}} + \frac{L}{B_2(AG)_{eq}}}$$

Note that the stiffness  $K$  is the quantity measured during a loading experiment (it is extrinsic), while the flexural and shear rigidities are quantities that are independent of measurement (they are intrinsic). The stiffness  $K$  will change when the length of the panel  $L$  changes.

Since there are two terms in the stiffness that depend on  $L$ , it is natural to discuss which is generally more important. By setting the two terms in the denominator of  $K$  equal, there is a length scale  $L_c$  that emerges for  $\delta_{bend} + \delta_{shear}$

$$L_c \sim \sqrt{\frac{B_1(EI)_{eq}}{B_2(AG)_{eq}}}$$

For thin faces this length scale simplifies to

$$L_c \sim \sqrt{\frac{B_1}{2B_2}} \sqrt{\frac{E_f}{G_c^*}} \sqrt{tc}$$

For three-point bending, with a steel skin (0.4 mm thick,  $E_f=200$  GPa) and foam core ( $G_c^*=100$  MPa,  $c=6$  mm),  $L_c \sim 0.17$  m. For a panel of this length bending and shear deflections are equal. If  $G_c^* = 1$  GPa instead, then  $L_c \sim 0.05$  m.

We write the total deflection in terms of the critical length scale

$$\frac{\delta}{\delta_{bend}} = \left(1 + \left(\frac{L}{L_c}\right)^2\right)$$

Or, alternatively

$$\frac{\delta}{\delta_{shear}} = \left(1 + \left(\frac{L}{L_c}\right)^2\right)$$

This metric is useful for quantitatively determining what size of panel is appropriate for neglecting either bending or shearing deformations (Figure E2)

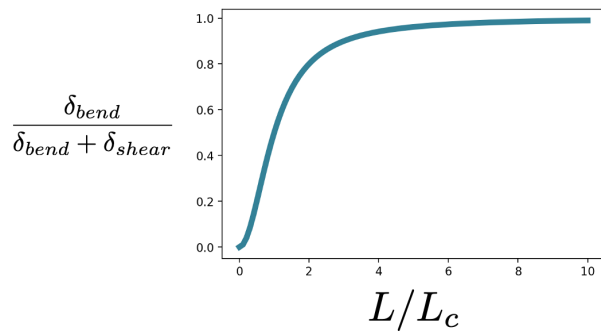


**Figure E2:** As a rule of thumb for using approximations that neglect shear deformation, the length of the panel should be at least 5 times the critical length to achieve less than 5% error in the predicted deflection

## E.7. Failure modes

There are several potential mechanisms of failure for any composite material. We denote the stress at failure as  $\sigma_f$  and discuss several common modes of failure below under the loading conditions for three-point bending.

### E.7.1. Face yielding

$$\sigma_f = \sigma_{yf}$$

When the normal stress in the face is equal to the yield stress of the face material face yielding occurs. For non-isotropic faces this yield strength is directionally dependent, and the loading conditions will affect it.

The load at which faces fail is given as

$$P = 4bc\sigma_{yf} \frac{t}{L}$$

### E.7.2. Face wrinkling

Under a bending load, one of the faces is in tension and the other is in compression. When the normal stress in the compressive face exceeds the local instability limit, face wrinkling occurs. This instability arises as an interaction between the buckling mode of the skin and the core. The competition between the bending energy of the skin and the compressive energy in the core give rise to a natural length scale which can be seen as wrinkling. The failure load associated with wrinkling for isotropic materials is given as

$$P = 2.28bc \left(\frac{t}{L}\right) E_f^{1/3} E_c^{2/3}$$

This formula requires that we know the effective core modulus. For an isotropic foam

this effective modulus can be written as

$$E_c^* \sim E_s \left(\frac{\rho_c^*}{\rho_s}\right)^2$$

This means that for foams

$$P = 2.28bc \left(\frac{t}{L}\right) E_f^{1/3} E_s^{2/3} \left(\frac{\rho_c^*}{\rho_s}\right)^{4/3}$$

For MetaCORE

$$E_c^* \sim E_s \left(\frac{\rho_c^*}{\rho_s}\right)^{12/5}$$

Here we have set the scaling exponent 2.4 to its equivalent fraction. This implies that face wrinkling occurs for MetaCORE as

$$P = 2.28bc \left(\frac{t}{L}\right) E_f^{1/3} E_s^{2/3} \left(\frac{\rho_c^*}{\rho_s}\right)^{8/5}$$

### E.7.3. Core failure

If the shear stress in the core is large compared to the normal stress then failure occurs when the shear strength of the core material is exceeded. For a foam-like material, the failure load is given by

$$P = 2bcC_{11} \left(\frac{\rho_c^*}{\rho_s}\right)^{3/2} \tau_c$$

Here  $C_{11}$  is a constant of proportionality, which we will assume is approximately one. For MetaCORE, the failure load is given by

$$P = 2bcC_{11} \left(\frac{\rho_c^*}{\rho_s}\right) \tau_c$$

### D.7.4. Bond failure

Delamination of the skin-core bond is the hardest mechanism to accurately diagnose, and in many cases the adhesive is stronger than the core material itself. However, if there is a crack between the interface this crack may propagate under load. For a sandwich beam subjected to a moment  $M$  and bent through an angle  $\theta$ , the energy stored is  $U = (M/2) \theta^2$ . If there is a crack of size  $2a$  contained in the interface between the core and the skin, then the crack has an area  $2ba$ . As this crack grows, there is a strain energy release rate  $T = M^2/(2bEI_{eff})$ . If this strain energy release rate exceeds the toughness of the adhesive  $T_c$ , then the beam will fail. Substituting known quantities lets us write a failure load condition

$$P = 4b \frac{t}{L} c \left( \frac{T_c E_f}{t} \right)^{1/2}$$

### E.7.5. Other modes

There are many other possible failure modes, including core compression, core buckling, intra-cell dimpling, and panel buckling. The most common and relatively straightforward failure modes have been considered here, but depending on loading conditions, environmental concerns, and indenter size, other failure modes may have to be considered on a case-by-case basis.

### E.8. Strength

The strength of a sandwich panel is determined by considering all of the possible failure modes and determining which of them leads to the lowest force at failure. The most common modes to consider are face wrinkling, face yielding, and core shear failure. We will calculate failure mode boundaries and plot a failure mode map for both legacy panels and MetaCORE panels.

Under three-point bending, we wish to see what failure mode will dominate the panel strength for a particular geometric configuration. For face yield, face wrinkling, and core shear, we determine three separate transition regions that depend on the materials used for the panel, as well as the geometric parameter  $t/L$  and the relative core density  $\rho/\rho_s$ .

The transition boundary on a failure mode map is given by setting the loads at failure equal to one another and then defining a transition equation. For sandwich panels this process yields the following transition equations:

Skin yield - Skin wrinkle	$\frac{t}{L} = 0.57 \frac{E_f^{1/3} E_c^{*2/3}}{\sigma_{yf}}$
Skin yield - Core shear	$\frac{t}{L} = 0.5 \frac{\tau_c^*}{\sigma_{yf}}$
Core shear - Skin wrinkle	$\tau_c^* = E_f^{1/3} E_c^{*2/3}$

These equations will always be correct for the three failure modes that we consider here, but the useful form of these equations require us to convert the effective properties into the functional relationship between the solid properties and the relative density. This will change depending on the type of materials considered. For a traditional foam the transition equations become:

Skin yield - Skin wrinkle	$\rho_c^*/\rho_s = \left( \frac{\sigma_{yf}}{0.57 E_f^{1/3} E_c^{2/3}} \right)^{3/4}$
Skin yield - Core shear	$\frac{t}{L} = 0.5 \frac{\tau_c}{\sigma_{yf}} (\rho_c^*/\rho_s)^{3/2}$
Core shear - Skin wrinkle	$\frac{t}{L} = 0.88 \frac{\tau_c}{E_f^{1/3} E_c^{2/3}} \left( \frac{\rho_c^*}{\rho_s} \right)^{1/6}$

These boundaries can be plotted on a failure mode map that cross-references the relative density and the dimensionless thickness  $t / L$  (Figure E3).

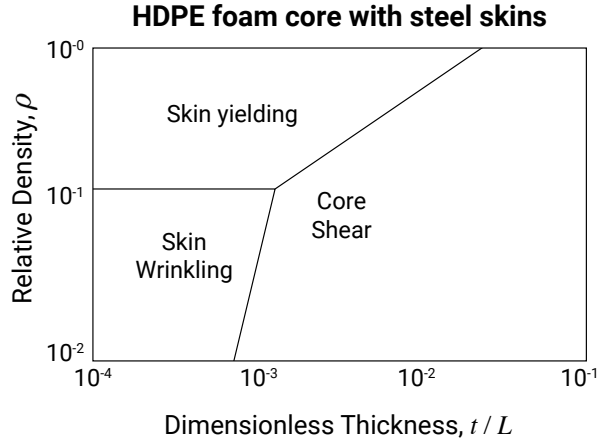


**Figure E3:** The failure mode map for galvanized steel skins and an HDPE foam core.

For MetaCORE this result is slightly different because both the compressional modulus and shear strength of MetaCORE scale differently than a conventional foam:

Skin yield - Skin wrinkle	$\rho_c^* / \rho_s = \left( \frac{\sigma_f}{0.57 E_f^{1/3} E_c^{2/3}} \right)^{5/8}$
Skin yield - Core shear	$\frac{\rho_c^*}{\rho_s} = \frac{2\sigma_f t}{\tau_c L}$
Core shear - Skin wrinkle	$\frac{t}{L} = 0.88 \frac{\tau_c}{E_f^{1/3} E_c^{2/3}} \left( \frac{\rho_c^*}{\rho_s} \right)^{-3/5}$

This change in scaling leads to a qualitative change in the failure mode map (Figure E4).

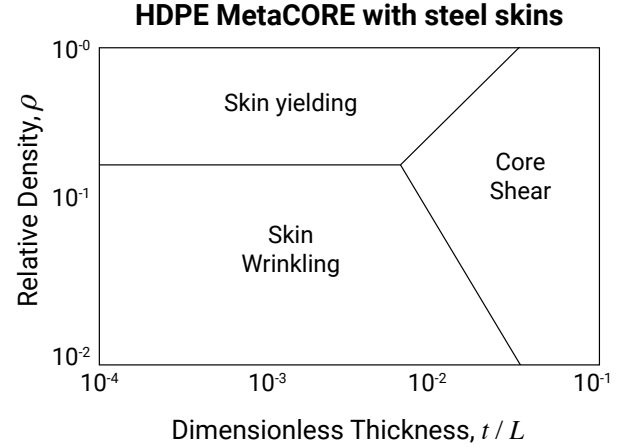


**Figure E4:** The failure mode map for galvanized steel skins and an MetaCORE. Note the smaller region where core shear is the primary culprit for failure, owing to MetaCOREs large shear strength. The larger design space for skin yielding is also an advantage, since the skins tend to be the strongest element in the panel.

## E.9. Optimization

### E.9.1. Weight

To minimize the weight of a sandwich panel for a given stiffness  $K=P/\delta$  we define the mass as the objective function to be minimized

$$M = (2\rho_f t + \rho_c^* c) bL$$

the core density is allowed to vary then there is a set of optimal values for the core density, face thickness, and core thickness. The optimal panel dimensions for an isotropic foam with isotropic skins are given by

$$\frac{c}{L} = 3.6 \left\{ \frac{B_2}{B_1^2} \left( \frac{\rho_f}{\rho_s} \right)^2 \frac{E_s K}{E_f^2 b} \right\}^{1/5}$$

$$\frac{t}{L} = 0.46 \left\{ \frac{1}{B_1 B_2^2} \left( \frac{\rho_f}{\rho_s} \right)^4 \frac{1}{E_f E_s^2} \left( \frac{K}{b} \right)^3 \right\}^{1/5}$$

$$\frac{\rho_c^*}{\rho_s} = \left\{ \frac{B_1}{B_2^3} \left( \frac{\rho_s}{\rho_f} \right) \frac{E_f}{E_s^3} \left( \frac{K}{b} \right)^2 \right\}^{1/5}$$

While apparently unwieldy, these equations can be used to determine the optimal geometry and foam density for maximizing strength and stiffness to weight ratios in a panel.

### **E.9.2. Example: Are legacy sandwich panels optimal?**

As an example, consider the legacy semi-trailer panels (e.g. DuraPlate). For a stiffness per width of  $K/b \sim 1,700$  N (as given in technical data sheets),  $E_f \sim 200$  GPa (galvanized steel faces),  $E_s \sim 1$  GPa (HDPE foam core),  $c \sim 6$  mm,  $t \sim 0.4$  mm,  $\rho_s \sim 960$  kg/m<sup>3</sup> (density of HDPE),  $\rho_f \sim 7,800$  (density of steel). Under three-point bending  $B_1=48$ ,  $B_2=4$ . These values yield  $c/L \sim 0.087$ ,  $t/L \sim 0.000078$ ,  $\bar{\rho} \sim 0.08$ . For  $L \sim 2.7$  m this would yield a core about an inch thick, with skins 0.2 mm thick. The legacy panels are far from optimal.

## Appendix F: Cylindrical structures

### F.1. Introduction

Thin structures of any kind generally prove difficult to analyze. Thin-walled cylinders are especially hard to categorize under buckling and crushing loads because of the many ways that such a geometry can fail. Analysis of MetaCORE cylinders further compounds this

difficulty by adding additional surface texture that imbues the component with auxetic behavior. In this Appendix, we review classical modes of buckling and failure in cylinders. We then use these results as a baseline for comparison to MetaCORE cylinders. This approach helps to identify unusual and important phenomenology.

### F.2. Buckling of cylinders

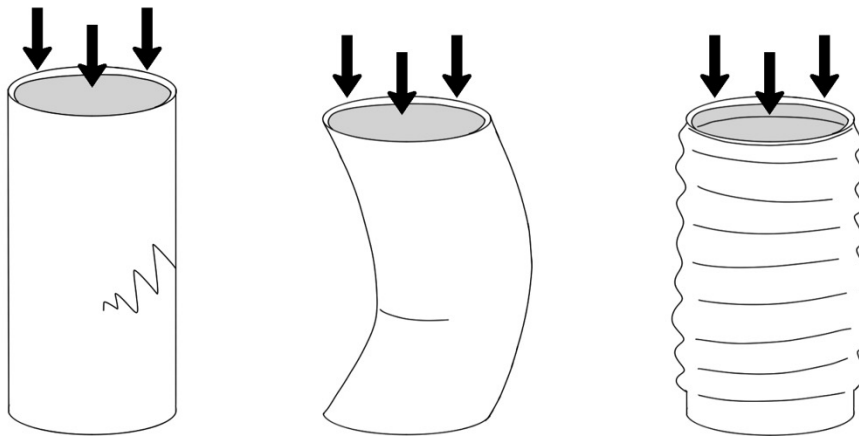


**Figure F1:** Under an axial load a cylinder buckles and deforms in a variety of shapes, depending on the size and thickness. The material itself can fail (left), the cylinder can buckle like a beam or a column (middle), or it can buckle from a “chessboard” instability (right).

Examining the linear instability (or buckling) of a cylinder is the first step to understanding how a crush tube or other curved component will behave under large axial load. For the particular scenario that we consider here, a cylinder of axial length  $L$  and radius  $R$ , with a wall thickness  $h$  is loaded axially with a force  $P$ . The first unstable eigenmode is then determined from the equations that govern shell mechanics. We assume that the material is isotropic with Young’s modulus  $E$ . This is a classical treatment that is covered in many

fundamental engineering textbooks, so we will simply reproduce the results here.

There are three regimes of behavior to consider for determining the classical buckling load. For  $L \gg R$ , the shell appears more like a beam, and the instability that occurs can be approximated as the classic Euler mode for column buckling, with a critical load  $P$  given by

$$P = \frac{\pi^3 R^3 h}{L^2} E$$

This mode is sometimes called global buckling or long-wavelength buckling. The critical stress  $\sigma_c$  at which this load occurs can be found by relating the critical load to the cross-section of the cylinder  $P \approx 2\pi R h \sigma_c$ . For  $L \ll R$  the shell is so short that the curvature effects of the cylinder are almost negligible, and the shell wall buckles like a Euler column with critical load  $P$  given by

$$P = \frac{\pi^2 R h^3}{6L^2(1 - \nu^2)} E$$

Finally, when  $L \sim R$  the shell buckles via a “chessboard” pattern and the critical stress  $\sigma_c$  is given approximately as

$$\sigma_c = \frac{1}{\sqrt{3(1 - \nu^2)}} \frac{Eh}{R}$$

Example plots for the critical stress are shown below, for various values of  $R/h$ . The crossover between regimes isn’t actually sharp, but since this is an asymptotic result on a log-log plot the representation is a reasonable pedagogical simplification.

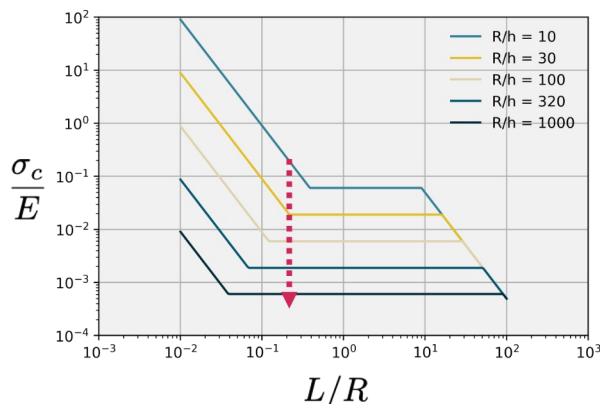


**Figure F2:** The critical buckling stress normalized by the stiffness of the cylinder, plotted as a function of the aspect ratio  $L/R$ . Multiple wall thicknesses are shown as solid lines of different colors. For any given  $L/R$ , lowering the thickness not only lowers the critical stress, but it can cause a crossover from one failure mode to another.

### F.3. Failure mode maps for cylinders

The critical stresses and loads defined above can be used to determine a failure mode map as a function of geometric parameters. Much like the failure modes for sandwich panels (Appendix E), determining the likely mode of failure for the crush tube will guide the design of the overall component. For cylinders, the buckling mode is highly imperfection sensitive, so the most robust design should choose an aspect ratio and wall thickness as close to the “triple point” on the failure map as possible (i.e., the point where all three failure mode boundaries intersect).

#### F.3.1. Isotropic thin-walled cylinders

For isotropic materials we can use the critical loads defined above to create a failure mode map (compare to the sandwich panel failure mode maps in Appendix E.8.).

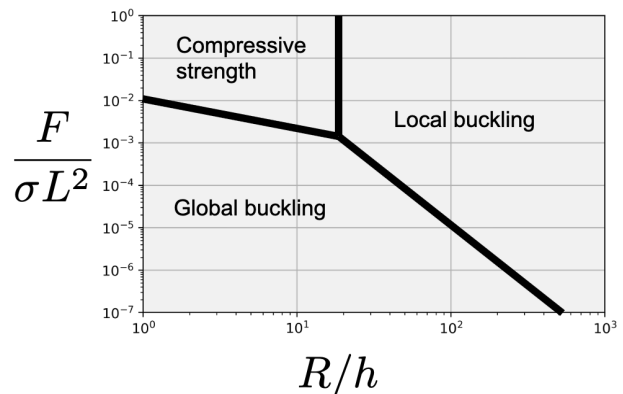


**Figure F3:** Failure mode map for an aluminum cylinder. The optimal design space straddles the boundaries of all three failure modes.

#### F.3.2. Composite thin-walled cylinders

Cylinders created from fiber-reinforced materials are even more complicated than isotropic materials, since there is an inherent directional dependence to the material (Figure F4). However, the calculations can be done,

and a failure mode map created. In the case of a unidirectional fiber-reinforced material, the optimal space for design changes due to the existence of fiber orientation. Figure F5 shows how fiber orientation expands the failure mode boundaries away from the

isotropic case, indicating that the optimal geometry can be adjusted simply by changing the orientation of the fibers.

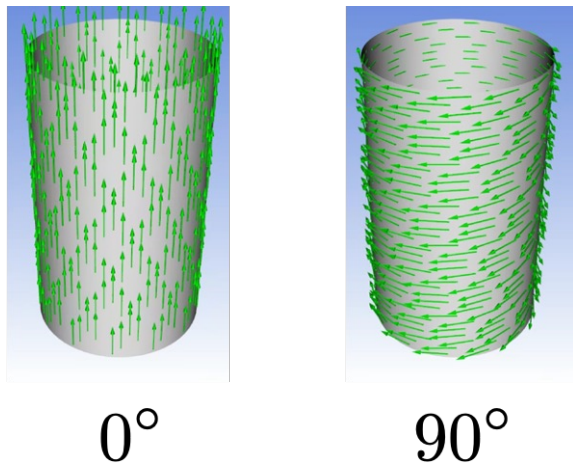


**Figure F4:** Graphical representation of fiber orientation in a cylinder.

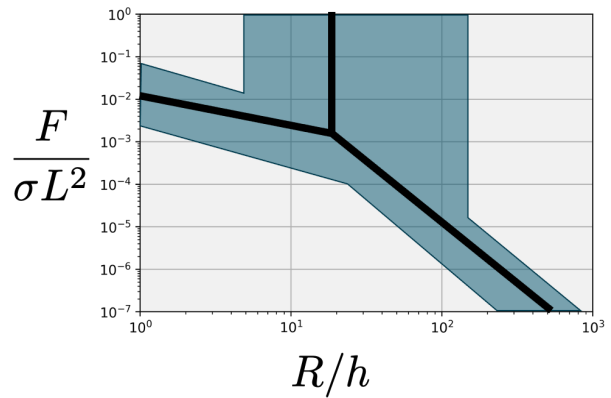


**Figure F5:** Failure mode map for composite cylinder. The blue region indicates an expanded area of optimality that arises from the orientation of the fibers. If a particular load, wall thickness, or aspect ratio of cylinder is required for design considerations, the fiber orientation can be adjusted to ensure that this geometry is closer to the optimal point in design space.

### F.3.4. MetaCORE cylinders

While MetaCORE also buckles and deforms like a composite cylinder, since it behaves like an orthotropic solid, there are some key nonlinear geometric aspects that need to be considered as well. For example, MetaCORE cylinders have two qualitatively different behaviors depending on the orientation of the pattern when crushed. This orientation can be treated similarly to the fiber direction in a composite cylinder, which helps explain the different behaviors.

For the orientation of [MO] with its x-axis parallel to the cylinder's central axis ( $0^\circ$  in fiber nomenclature), the crushed MetaCORE collapses in on itself. For the  $90^\circ$  orientation

the cylinder crushes straight down (Figure F6 (B)). This can be explained by recalling that MetaCORE as an orthotropic solid has a negative in-plane Poisson's ratio, and that this ratio is directionally dependent.

Using the derived material cards for MetaCORE and assigning the appropriate element directions in FEA software (Figure F6 (C), left), we see the effects of auxetic behavior (Figure F6 (C), right). While MetaCORE has a host of nonlinear behaviors associated with large deformation, this "self-stabilizing" behavior arising from a predictable orientation-dependent Poisson's ratio is a key element to designing the proper layup for cylindrical MetaCORE.

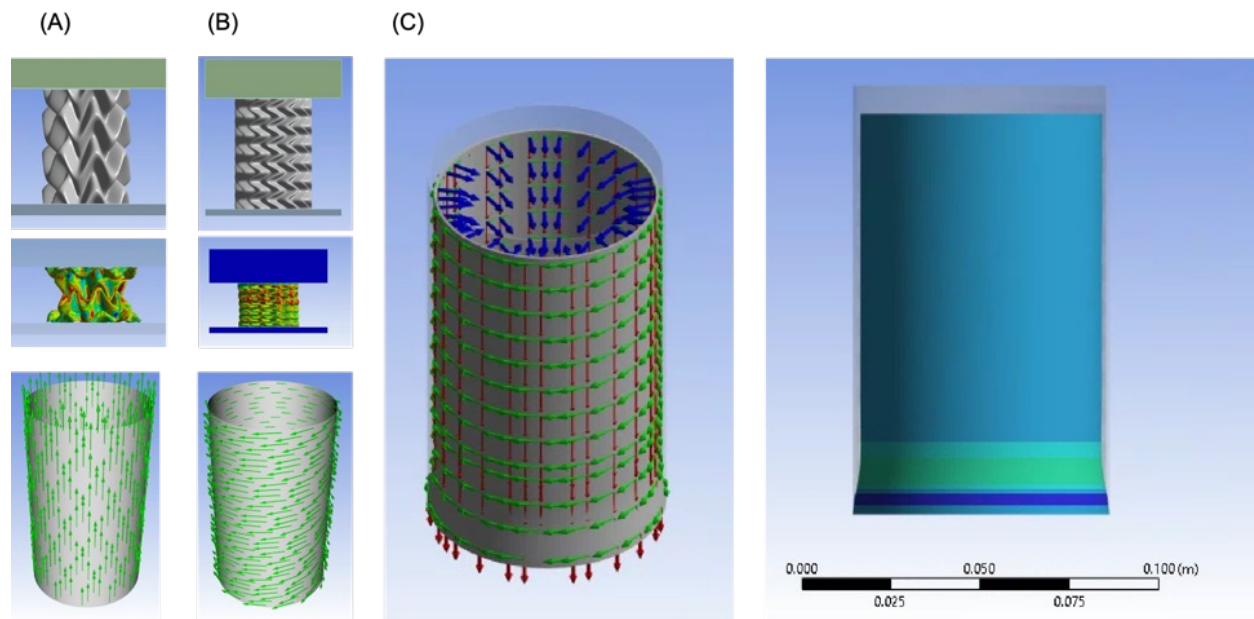


**Figure F6:** (A) crushing of MetaCORE cylinder with pattern in the  $0^\circ$  orientation. The structure collapses inward in a self-stabilizing fashion. (B) Crushing of MetaCORE cylinder with pattern in  $90^\circ$  direction. The cylinder crushes without noticeable self-stabilization. (C) Using a material card and orienting the fiber directions appropriately, stress analysis shows the effect of a negative Poisson's ratio on the cylinder as a whole; it is this effect that leads to self-stabilization

## F.4. Off-axis indentation and impact

Thin shells exhibit complicated mechanical behavior, due in large part to the tendency for stresses to focus during loading. While a full discussion is outside the scope of this Appendix, a comparison between thin and thick shells is relevant for understanding the response of MetaCORE cylinders compared to simple cylinders. If a ball-point indenter impacts a cylindrical shell (Figure F7), the stress response changes qualitatively depending on the shells thickness. For thick shells the stress is localized to the point of impact, with a diffuse distribution of stress through the whole body. For thin shells the stress propagates throughout the whole body in concentrated lines, eventually forming “kinks” or “crumples” or other singularities that focus the stress.

Since MetaCORE is a thin-walled structure but arranged with large undulations, it is unclear *a priori* if it should behave like a thin or thick walled cylinder. Since we assume in many cases that MetaCORE can be reduced to an effective material, we can homogenize the undulations and simply simulate a thick-walled cylinder with the appropriate material card (Figure F8).

Under various indentation conditions (Figure F9), we see the effective material representation of MetaCORE behaves largely like those seen in experiments (Part 4). It is important to note that the MetaCORE material breaks the general intuition for stress localization in thick cylinders, since the MetaCORE material itself has unconventional orthotropic properties. Moreover, the undulations in the full geometry cause delocalized stresses to spread throughout the body of the cylinder under indentation.

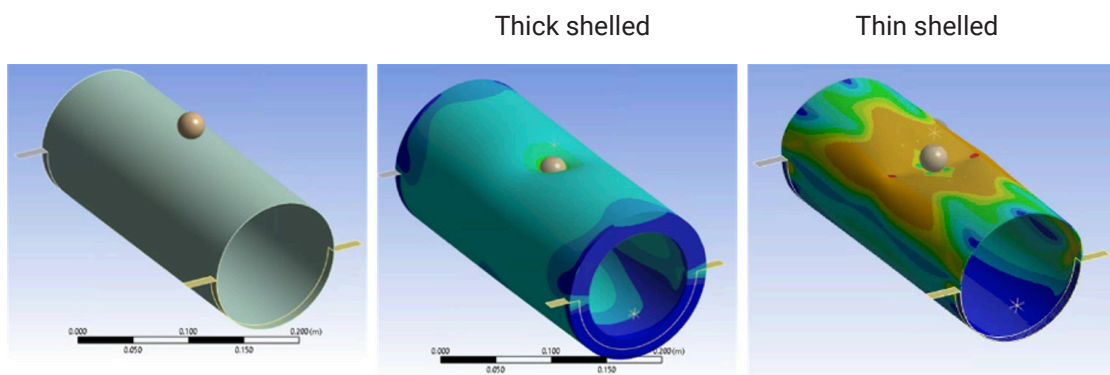


**Figure F7:** Off-axis indentation of aluminum cylinders with a ball bearing shows the difference in stress concentrations experienced by thick and thin walled structures. First panel shows the neutral state. The second and third panels show the stressed states with colors corresponding to the magnitude of stress.

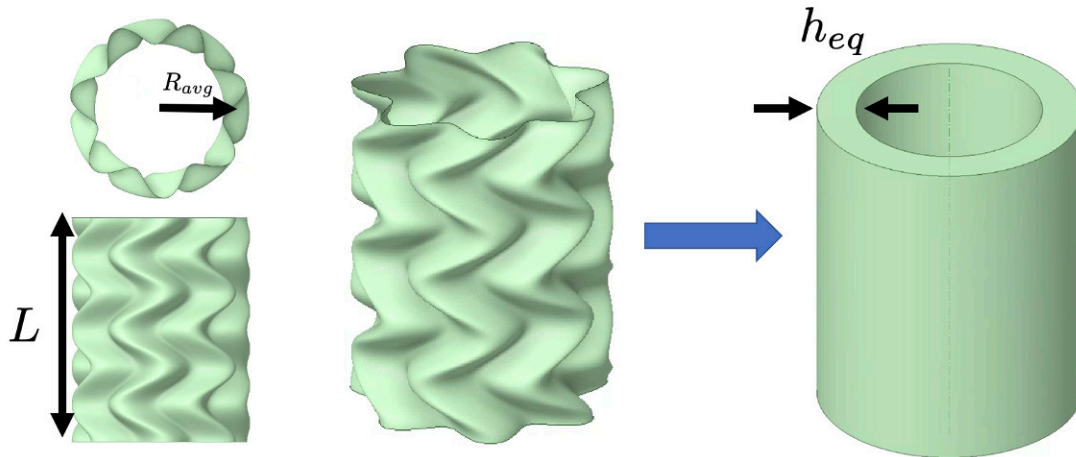


**Figure F8:** A MetaCORE cylinder and the appropriate homogenization. By using a thick walled geometry we can assign the MetaCORE material card and use a computationally simple loading set up that captures the effective properties of the whole system.

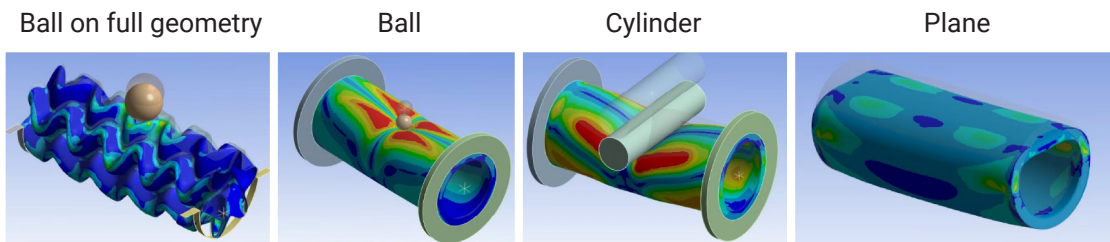


**Figure F9:** FEA results comparing indentation of a full MetaCORE mesh and the homogenized thick walled cylinder assigned a MetaCORE material card. By using a thick walled geometry with the MetaCORE material card we have a computationally simple loading set up that captures the effective properties of the whole system.